A review of the geologic sections and the faunal assemblages of Aurelian Mammal Age of Latium (Italy) in the light of a new chronostratigraphic framework

F. Marra, S. Nomade, A. Pereira, C. Petronio, L. Salari, G. Sottili, J.-J. Bahain, G. Boschian, G. Di Stefano, C. Falguères, et al.

Manuscript Details

Manuscript number	JQSR_2017_644
Title	A review of the geologic sections and the faunal assemblages of Aurelian Mammal Age of Latium (Italy) in the light of a new chronostratigraphic framework
Article type	Research Paper

Abstract

The Aurelian Mammal Age for peninsular Italy was introduced on the basis of faunal assemblages mainly recovered at sites along the Via Aurelia west of Rome. These sites exposed a set of sedimentary deposits currently attributed to the Aurelia and to the Vitinia Formations correlated with MIS 9 and MIS 7, respectively. In the present paper we reconstruct the geologic-stratigraphic setting in the western sector of Rome within the wider context of glacio-eustatically controlled, geochronologically constrained aggradational successions defined for this region. We present a chronostratigraphic study based on dedicated field surveys, that, combined with five new 40Ar/39Ar ages and eighteen trace-element and EMP glass analyses of volcanic products, allow us to revise age and correlation with the Marine Isotopic Stages for 10 sites out of 12 previously attributed to the Aurelia Formation and the Torre in Pietra Faunal Unit. In particular, we demonstrate a MIS 13/MIS 11 age for several sections along the Via Aurelia between Malagrotta and Castel di Guido. Based on this new geochronological framework, the first occurrences of Canis lupus and Vulpes vulpes in Italy are antedated to MIS 11, within the Fontana Ranuccio Faunal Unit of the Galerian Mammal Age, consistent with the wider European context. This contribution is intended as the groundwork for a revision of the Middle Pleistocene Mammal Ages of the Italian peninsula, according to the improved chronostratigraphy of the geologic sections hosting the faunal assemblages.

Keywords	Aurelian Mammal Age; Latium; Middle Pleistocene; biostratigraphy; chronostratigraphy; tephrostratigraphy; aggradational successions

Corresponding Author	fabrizio marra
Corresponding Author's Institution	Istituto Nazionale di Geofisica e Vulcanologia
Order of Authors	fabrizio marra, sebastien nomade, Alison Pereira, Carmelo Petronio, Leonardo Salari, Gianluca Sottili, Jean-Jacques Bahain, Giovanni Boschian, Giuseppe Di Stefano, Christophe Falguéres, Fabio Florindo, Mario Gaeta, Biagio Giaccio, Matteo Masotta
Suggested reviewers	Ralf-Dietrich Kahlke, Juan Manuel López-García, Paola Petrosino, Francesco Zarlenga

- We provide precise chronostrtatigraphic framing to several archaeologic sites in the area of Rome
- We provide new geochronologic constraints to the faunal assemblages of the Aurelian Mammal Age
- We revise the chronology of Castel di Guido, Malagrotta and Riano archaeological sites
- We revise the depositional context of La Polledrara di Cecanibbio archaeological site
- We revise the first occurrences of *Canis lupus* and *Vulpes vulpes* in Italy

A review of the geologic sections and the faunal assemblages of Aurelian Mammal Age of Latium (Italy) in the light of a new chronostratigraphic framework

F. Marra[1], S. Nomade[2], A. Pereira[2,3,4,5], C. Petronio[6], L. Salari[6], G. Sottili[6], J.-J. Bahain[5], G. Boschian[7], G. Di Stefano[6], C. Falguères[5], F. Florindo[1], M. Gaeta[6], B. Giaccio[8], M. Masotta[9]

1. Istituto Nazionale di Geofisica e Vulcanologia, Via di Vigna Murata 605, 00143 Roma, Italy
2. Laboratoire des Sciences du Climat et de L'Environnement, UMR8212, IPSL-CEA-CNRS-UVSQ and Université Paris-Saclay, Domaine du CNRS Bât. 12, Avenue de la Terrasse, 91198 Gif-Sur-Yvette, France.
3. Sezione di Scienze Preistoriche e Antropologiche, Dipartimento di Studi Umanistici, Università degli Studi di Ferrara, C.so Ercole d'Este I, 32, Ferrara, Italy
4. Ecole française de Rome, Piazza Farnese, IT-00186, Roma, Italy
5. Département Hommes et environnements, Muséum national d'Histoire naturelle, UMR 7194 du CNRS, 1 rue René Panhard, 75013 Paris, France.
6. Dipartimento di Scienze della Terra, Sapienza, Università di Roma, P.le Aldo Moro 5, 00185, Roma, Italy
7. Dipartimento di Biologia, Università di Pisa, 56126 Pisa, Italy
8. Istituto di Geologia Ambientale e Geoingegneria - C.N.R., Montelibretti (Rome), Italy
9. Dipartimento di Scienze della Terra, Università di Pisa, 56126 Pisa, Italy

corresponding author: Fabrizio Marra, fabrizio.marra@ingv.it

Keywords: Aurelian Mammal Age, Latium, Middle Pleistocene, biostratigraphy, chronostratigraphy, tephrostratigraphy, aggradational successions

Abstract

The Aurelian Mammal Age for peninsular Italy was introduced on the basis of faunal assemblages mainly recovered at sites along the Via Aurelia west of Rome. These sites exposed a set of sedimentary deposits currently attributed to the Aurelia and to the Vitinia Formations correlated with MIS 9 and MIS 7, respectively. In the present paper we reconstruct the geologic-stratigraphic setting in the western sector of Rome within the wider context of glacio-eustatically controlled, geochronologically constrained aggradational successions defined for this region. We present a chronostratigraphic study based on dedicated field surveys, that, combined with five new $^{40}Ar/^{39}Ar$ ages and eighteen trace-element and EMP glass analyses of volcanic products, allow us to revise age and correlation with the Marine Isotopic Stages for 10 sites out of 12 previously attributed to the Aurelia Formation and the Torre in Pietra Faunal Unit. In particular, we demonstrate a MIS 13/MIS 11 age for several sections along the Via Aurelia between Malagrotta and Castel di Guido. Based on this new geochronological framework, the first occurrences of *Canis lupus* and *Vulpes vulpes* in Italy are antedated to MIS 11, within the Fontana Ranuccio Faunal Unit of the Galerian Mammal Age, consistent with the wider European context. This contribution is intended as the groundwork for a revision of the Middle Pleistocene Mammal Ages of the Italian peninsula, according to the improved chronostratigraphy of the geologic sections hosting the faunal assemblages.

1. Introduction

The Aurelian Mammal Age (AMA) is based on the faunal assemblages mainly recovered at several sites along the Via Aurelia west of Rome (Gliozzi et al., 1997, Figure 1). These sites exposed a set of continental to transitional sedimentary deposits that were attributed by the authors to the Aurelia and to the Vitinia Formations. Deposition of these successions was correlated with Marine Isotopic Stage (MIS) 9 and MIS 7, respectively, based on rather weak geochronological markers pointing out to an age around 350 - 300 ka for the former one (Conato et al., 1980). Within the AMA, two faunal units (FU) corresponding to the Early and to the Middle Aurelian were defined: Torre in Pietra FU and Vitinia FU, correlating to MIS 9 and MIS 7, respectively (Gliozzi et al., 1997). Representative local fauna for the Late Aurelian was recognized only later on (Melpignano FU and Ingarano FU; Petronio et al., 2007).

Gliozzi et al. (1997) and Petronio et al. (2011), proposed that the beginning of the AMA was approximately in correspondence with MIS 10 and characterized by the appearance of the taxa representing the core of the present day mammal fauna, considered to mark the early Aurelian or Torre in Pietra FU (MIS 10-9). In particular, the faunal renewal in this region was characterized by the disappearance of the cervid species *Megaceros savini*, *Megaceroides verticornis*, *Cervus elaphus acoronatus*, which were replaced by *Megaloceros giganteus*, along with the spread of the quasi endemic subspecies of *Cervus elaphus eostephanoceros* and *rianensis*, and by the first occurrence (FO) of several carnivorous species, including *Mustela putorius*, *Ursus spelaeus, Vulpes vulpes*, *Canis lupus*, *Felis silvestris,* and *Panthera spelaea*. However, the Italian FO's of these latter species postdate those reported in the literature of the new Millennium for western Europe, where a MIS 12 lower boundary for the AMA is generally assumed (e.g., Barishnikov, 2002).

The middle Aurelian faunal assemblages constituting the Vitinia FU (MIS 8.5-7) were characterized by appearance of a subspecies of fallow deer, *Dama dama tiberina*, and of a small sized equid with slender limbs, *Equus hydruntinus* (Di Stefano and Petronio, 1997; Marra et al., 2014a).

Table 1 reports all the outcrops of the sedimentary successions known in the Latium region to host the faunal assemblages attributed to the AMA (Palombo, 2004, and references therein). Until 2014 the only section, among those listed in Table 1, with secure radio-isotopic constraints demonstrating the correlation with the corresponding MIS was the Vitinia section (Karner and Marra, 1998). Precise geochronologic constraints were more recently provided by means of $^{40}Ar/^{39}Ar$ dating to Torre in Pietra lower and upper levels, confirming these archaeological layers within MIS 9 and MIS 7, respectively (Villa et al., 2016), and to

Polledrara di Cecanibbio, now securely dated to the end of MIS 9 (Pereira et al. 2017). Furthermore, significant revisions of the previous attributions were recently proposed by Marra et al. (2014a, 2015a, 2016a).

In the present contribution we aim at reconstructing the geologic-stratigraphic setting in the western sector of Rome along the Via Aurelia within the wider context of glacio-eustatically controlled, geochronologically constrained aggradational successions defined for this region (Marra et al., 2016b). We present a chronostratigraphic study based on dedicated field surveys that, combined with five new $^{40}Ar/^{39}Ar$ ages, and eighteen trace-element, EMP glass and petrographic analyses of volcanic products, provides the systematically re-designed chronological picture resumed in Table 1. According to this renewed scenario (10 sites out of 12 previously attributed to the Aurelia Fm and the Torre in Pietra FU have been assigned to different units), a review and a preliminary revision of the FUs of the AMA is provided in this paper, along with an updated chronostratigraphic framework of the geologic sections hosting the faunal assemblages. Future work will deal with the paleontological and palethnological implications of this revised chronologic picture.

1.1 Geological Setting

The study area is located on the Tyrrhenian Sea margin of central Italy (Figure 1a), which, since the early Middle Pleistocene, was characterized by continental conditions in consequence of a progressive regional uplift accompanying the development of a NW-SE chain of ultra-potassic volcanic districts (Karner et al., 2001a; Marra et al., 2016c), constituting the Roman Magmatic Province (Conticelli and Peccerillo, 1992). The volcanic products, mainly pyroclastic-flow and air-fall deposits, are intercalated within the sedimentary successions deposited by the Tiber River and its tributaries in fluvial and lacustrine environments during Middle and Upper Pleistocene. The geologic evolution of this sector was therefore driven by the interplay among volcanism, tectonics, and glacio-eustacy (Luberti et al., 2017, and references therein).

2. Methods:

2.1 Aggradational successions

The methodological approach used to provide age constraints to the sedimentary deposit relies on the concept of aggradational succession deposited in response to sea-level rise during the glacial terminations (Marra et al., 2008; 2016b), combined to biochronologic

constraints provided by the embedded fossil record, as introduced in Marra et al. (2014a). A suite of sedimentary successions in the near-costal and in the coastal area of Rome has been defined, whose ages have been constrained by means of $^{40}Ar/^{39}Ar$ dating of interbedded volcanic layers and paleomagnetic investigation of clay intervals, allowing for their their precise and accurate correlation with the MISs (Karner and Marra, 1998; Marra et al., 1998; Florindo et al., 2007; Marra et al., 2008; 2016b). Detail on the methodological approach can be found in the work mentioned above.

2.2 $^{40}Ar/^{39}Ar$ dating

Five samples were analyzed by $^{40}Ar/^{39}Ar$ single-crystal dating method: two from Castel di Guido area (CDG 1 and 2), one from Casal de'Pazzi (CdP), one from Riano (RI), and one from Torre in Pietra (A2). Ages are calculated according to the age of 1.193 Ma for the ACs (Nomade et al., 2005), and reported with 2σ analytical uncertainties throughout the paper. Results for all the dated crystals are shown as probability diagrams (Deino and Potts, 1990), and corresponding inverse isochrones. Detail of the dating procedure and all the analytical details and procedural blanks are presented in supplementary dataset (Supplementary File 1 and Tables S1 to S5).

2.3 Geochemical analyses

Electron Microprobe glass geochemistry (EMP) can be applied only on unaltered materials. For this reason, only a few samples containing fresh glass shard incorporated in pumice fragments have been analyzed here with this method. In order to identify the strongly weathered pyroclastic flow deposits cropping out at the investigated localities we have integrated petrographic analyses in thin section with a method relying on ratio of immobile elements (e.g., Zr, Nb, Y) that has been recently introduced (Marra et al., 2011), and applied in several archaeological and tephrostratigraphic contexts (e.g., Marra and D'Ambrosio, 2013; Marra et al., 2014b; 2015b). Analytical procedures and full data are reported in Supplementary File #1, Supplementary Table S6, and Supplementary dataset #1.

2.4 Paleontology

A review of the literature reporting descriptions, images, ostaeological data, as well as regional syntheses on the major vertebrate deposits and fauna assemblages attributed to the AMA was performed. This review aims at evaluating the distribution of different taxa. In many cases (Cava Rinaldi, Via Aurelia km 19.3, Malagrotta, Via Flaminia km 8.2, Riano, Sedia del

Diavolo, Prati Fiscali, Monte Sacro, Batteria Nomentana, Vitinia, Cerveteri-Migliorie San Paolo) fossil remains were directly re-examined, because they were stocked in the Paleontology Museum Department, at Università Sapienza in Rome.

The reviewed faunal lists for all the sections hosting the faunal assemblages previously included in the FU's of the AMA are reported in Table 2.

3. Results

3.1 Volcanic stratigraphy

Field investigations performed for the present study have shown that the volcanic deposits cropping out in the investigated area are mainly associated with the eruptive activity of the Monti Sabatini district in the time span 546±3 - 285±2 ka (Karner et al., 2001b; Sottili et al. 2004, 2010; Marra et al., 2014b), and with the deposits of the Vico I Perod (Perini et al., 2004), including the regional tephra marker Vico α (418-412 ka, Cioni et al., 1993; Marra et al., 2014b). We describe the main eruptive units providing chronostratigraphic constraints to the sedimentary successions and to the hosted faunal assemblages of MIS 13 through MIS 8.5 in this area. A composite cross-section reconstructing the stratigraphic relationships among the investigated sites along Via Aurelia between Castel di Guido and Malagrotta is shown in Figure 2. Photographs of representative rock samples are presented in Figure 3. Each volcanic unit is detailed below starting with the oldest one.

Tufo Giallo della Via Tiberina (TGVT - 546±3 ka)

It is a complex eruption cycle (Masotta et al., 2010; Marra et al., 2014b) starting with a Plinian fallout deposit (FAD 3) followed by a basal, diluted ash-flow (Lower TGVT), passing to a large, massive, ash-and-pumice flow (Upper TGVTa-b). It was closed by stratified deposit (UTGVT-c) and by a final lithic breccia (UTGCT-d). The TGVT crops out at km 15.9 of Via Aurelia (Figure 2b) in the investigated area, where a sample (CDG-2) was collected and dated by $^{40}Ar/^{39}Ar$ to 550±6 ka (Figure 4). This particular outcrop displays a bedded deposit with alternating, decimeter-thick layers of ash and vesicular, grey and yellow scoriae with abundant leucite crystals (Figure 3a).

Tufo Giallo di Prima Porta (TGPP - 516±1 ka)

This unit is emplaced at the climax of a marked erosive phase during MIS 13.2 lowstand (Marra et al., 2017a) and displays varying elevation throughout the investigated area (Figure

2a). Due to the concomitant erosive phase, the deposit shows partial re-working and re-deposition, particularly in distal settings, where lateral transition to sub-primary lahar deposit, characterized by incorporation of abundant sedimentary material occurs. In most of the investigated sections the TGPP pyroclastic-flow is constituted by a very fine-sized, ash-supported deposit, which looks like a yellow sand with sparse, tiny, white leucite crystals (e.g., MG2-Casal Bruciato, CDG-1, Figure 3f-g-i), whereas in a few places it appears like a pale yellow, diluted ash conglobating accidental lithic clasts (e.g.: Malagrotta; Figure 3d), mainly diatomite-rich lacustrine sediments and occasional gastropod shells (e.g.: MG1-Casal Bruciato, Figure 3e). These latter features are probably the reason of its frequent misinterpretation as a sedimentary deposit ("tufite"; e.g., Cassoli et al., 1982; Anzidei et al., 1993).

Four samples of the TGPP pyroclastic-flow deposit collected in Castel di Guido (CDG-3, CDG-5, Figure 3h-j), Casal Bruciato (MG1, Figure 3e), and in Malagrotta (MG5D, Figure 3d) have been analyzed for trace-element composition in this study to compare 8 samples previously analyzed in Marra et al. (2017a) (Figure 5b).

Grottarossa Pyroclastic Sequence (GRPS - 510±4 ka)

The GRPS is a succession of four main units separated by paleosoils (GRPS a -d, Karner et al., 2001b) and include a widespread holocrystalline lithic-rich layer originated by a source area located in the eastern Sabatini sector (Marra et al., 2014b). Dark grey, often laminar, clast-supported, mm-sized lapilli and scoriae deposits, rich in leucite and pyroxene crystals interbedded with thin ashy layers have been interpreted as pyroclastic-flows deposits (e.g., Marra et al., 2014b). $^{40}Ar/^{39}Ar$ age of 510±4 ka, combined with stratigraphic evidence from Cava Rinaldi of intervening sedimentation above the TGPP dated 516±1 ka, show that the GRPS was emplaced at the onset of sea-level rise of MIS 13.1 (Marra et al., 2017a; see Figure 6). According to these paleo-climatic constraints, the GRPS at km 19.3 of Via Aurelia (sample BAR-1, Figure 3n) is emplaced within a fluvial channel with an erosive contact above a thin bed of fluvial-lacustrine sediments, overlying the TGPP pyroclastic-flow deposit which, in turn, is emplaced at the base of the paleo-incision (Figure 2a). Consistently, at the summit of Castel di Guido hill, in correspondence of a morphologic height, the GRPS (sample CDG8, Figure 3k) shows a planar contact above a paleosoil developed on top of the TGPP (Figure 2b).

Tufi Terrosi con Pomici Bianche (TTPB - 498±2 - 461±2 ka)

It is a complex, long lasting eruption cycle emplacing a thick suite of Plinian fallout deposits, constituted by three main units (Fall A, Fall B, Fall C; Sottili et al., 2004) dated between 498±2

and 461±2 ka (Marra et al., 2017a). In the investigated area, West of Rome, pumice Fall A crops out in Cava Rinaldi where it provides geochronologic constraints to the final aggradation of the Valle Giulia Formation (Marra et al., 2017a; Figure 6), whereas Fall B and Fall C are exposed on the western flanks of the hill where the La Polledrara di Cecanibbio museum site is located (Figure 9a).

Tufo Rosso a Scorie Nere Eruption Cycle (TRSN - 452±2 - 447±7 ka)

The TRSN unit opens with a widespread Plinian fall deposit (Fall D; Sottili et al., 2004) followed by the main pyroclastic-flow deposit characterized by the typical Scorie Nere (i.e., black scoriae) in a zeolitized, often welded, reddish ash matrix. The TRSN pyroclastic-flow deposit is emplaced in the late stages of the regressive phase associated with MIS 12, and it locally occurs within marked paleo-morphologies, where it is partially eroded and covered by a thick succession of reworked volcanoclastic deposits rich in black and white pyroclastic sand, constituted by abundant femic and leucite crystals. It is the case of the outcrop at km 16.6 of Via Aurelia (Figure 2b), where a 4 m thick horizon corresponding to the "leucititic tuff" included by Cassoli et al. (1982) in the stratigraphic scheme of Malagrotta (sample MG4, Figure 3m), is present above the primary TRSN pyroclastic-flow deposit.

In contrast, a more or less complete succession of fallout deposits emplaced in the late stages of the eruption cycle (Fall E and Fall F, 450±7 and 447±7 ka; Marra et al., 2014b) is usually preserved in the morphologic heights, like in the case of the Polledrara and Castel di Guido hills. The loose, basal portion of the pyroclastic-flow deposit constituted by decimetric black pumices crops out on the Castel di Guido hill (sample CDG-6, Figure 3l) and in locality La Bottaccia (sample BOT-1) (Figure 2b). At this latter location the pumice-rich basal portion grades upwards into a fine grained, massive, light brown, leucite-rich pyroclastic deposit.

Vico α (418±2 - 412±2 ka)

The Vico α widespread Plinian fallout deposit records the first large-scale eruptive episode of the Vico Volcano (Cioni et al., 1987). In proximal settings, the Vico α stratigraphy consists of a basal Plinian fallout deposit, up to 1 m thick, topped by a sequence of pinkish ashy beds; the sequence is closed by a ~2 m thick Plinian scoriae fallout deposit (Cioni et al., 1987). Overall, the Vico α sequence, as described in proximal settings, exhibits a strong, vertical compositional zoning (i.e., from rhyolite to latite; pumice bulk compositions), with the basal Plinian fallout made up of white, sanidine-bearing pumice and the upper subunit made up of grey, leucite-bearing scoriae (Cioni et al., 1987; Perini et al., 2004). In distal settings, including

the investigated area to the West of Rome, the Vico α unit consists of a primary or sub-primary ~30 cm thick deposit of moderately to highly vesicular whitish pumice. Notably, the Vico α rhyolitic glass composition (Marra et al., 2014b) represents a singularity within the context of the ultrapotassic Roman Province.

Tufo di Bracciano (TdB 307±4, 316±2, 325±2 ka)

The TdB pyroclastic unit crops out over a wide area (some hundreds km^2) to the west of Lake Bracciano (Fig. 1), as far as the Tyrrhenian coastal plain. In the western Monti Sabatini area it usually tops the volcanic succession; facies analyses and borehole data suggest a source area located in the W sector of present-day Bracciano depression (Sottili et al., 2010).

The TdB succession opens with a Plinian fall deposit topped by a massive, several meter-thick greenish-grey, matrix supported pyroclastic-flow deposit containing poorly vesicular, greenish-grey, leucite- and dark mica bearing scoria lapilli and blocks.

Dating of this product produced scattered results on different samples, ranging 307±5 ka, 316±6 ka (Sottili et al., 2010), along with age of 325±2 ka proposed by correlation with TdB of the mudflow deposit of La Polledrara di Cecanibbio (Marra et al., 2016a). This is probably a consequence of the large presence of cognate lithic clasts within the pyroclastic-flow deposit of TdB, displaying very variable dimensions and heterogeneous nature, including leucititic lava blocks, and abundant tuff and flysch fragments. However, when calibrated for a different standard age (i.e., 0.186 Ma for the Alder Creek sanidine; see Marra et al., 2017a for a discussion), the age of the La Polledrara deposit (i.e.: 322.6±2 ka) is indistinguishable from that of 316±6 ka yielded by the TdB.

A pumice fragment collected in the basal fallout deposits in Anguillara (TB1) didn't yield analyzable glass. Textural and mineralogical features of this pumice and of a scoria sample collected in the pyroclastic-flow deposit (TB2) have been analyzed at the SEM.

Tufo Giallo di Sacrofano (TGS - 285±2 ka)

The TGS caldera-forming event emplaced a complex pyroclastic unit cropping out all around the present Sacrofano caldera (Fig. 1). The main unit consists of a few tens of meter-thick, massive, yellowish zeolitised tuff (sillar) containing leucite+sanidine-bearing whitish pumice lapilli (Sottili et al., 2010). It frequently crops out on the top of the hills in the investigated area west of Rome, like in Polledrara di Cecanibbio and Castel di Guido. In northern Rome the TGS is a fundamental chronostratigraphic marker of the Via Mascagni succession, providing

link with MIS 8.5 for the sections of the Aniene Valley (Sedia del Diavolo, Ponte Mammolo) hosting the earliest European direct evidence of *Homo neanderthalensis* (Marra et al., 2017b).

3.2 New $^{40}Ar/^{39}Ar$ age constraints

Torre in Pietra (Sample TiP-A2)

Thirteen sanidine crystals extracted from a fluvial sediment were measured (see table S1 supplementary dataset). The probability diagram obtained is, as expected, multimodal. Two major eruptions are identified, the main mode is represented by eight of the thirteen crystals (Figure 4) analyzed and is centered around 453 ka. The youngest recorded eruption found is made of only three crystals and presents a weighted mean age of 391±3 ka (2σ analytical uncertainties) with a probability of 0.36 (Figure 4). The inverse isochron obtained for the largest population is not precise ($^{40}Ar/^{36}Ar$ ratio of 294±73 ka) but demonstrates, within uncertainties, a $^{40}Ar/^{36}Ar$ ratio close to the atmospheric one of 298.56 (Lee et al., 2006).

Castel di Guido 1 (Sample CDG 1)

The nine crystals dated for this primary fallout deposit displayed statistically the same age, highlighting the primary origin of this deposit (see table S2 supplementary dataset). This juvenile population of crystals allows to calculate a weighted mean age of 516±4 ka (2σ) with a probability of 0.24 (Figure 4). The inverse isochron demonstrate a $^{40}Ar/^{36}Ar$ ratio close to the atmospheric one (i.e., 296±9 ka) confirming the absence of excess argon in these crystals.

Castel di Guido 2 (Sample CDG 2)

For this primary volcanic layer eleven crystals were measured (see table S3). The probability diagram obtained is more complex than CDG 1 (Figure 4). The main mode is composed of nine crystals out of the eleven. Excluding the two obvious xenocrystals we were able to calculate a weighted mean age of 550±6 ka (2σ) for this volcanic deposit (Figure 4).

Casal de'Pazzi (Sample CdP)

Twelve crystals collected from the uppermost fluvial layer were analyzed (see table S4). The probability diagram is multimodal with two major modes centered at 304±8 ka (probability of 0.91) and around 355 ka for the youngest and oldest population of crystals, respectively (Figure 4). The inverse isochron initial $^{40}Ar/^{36}Ar$ intercept obtained for the youngest population is very imprecise and does not allow to draw any conclusion concerning the presence of excess argon.

Riano (Sample RI)

Nine sanidine crystals were dated for this tephra layer (see table S5). The probability diagram demonstrates only one mode suggesting the primary volcanic nature of the deposit (Figure 4). The weighted mean age of the main population of crystals is 406±5 ka (2σ) with a probability of 0.93. The inverse isochron is precise and demonstrate the absence of argon excess (Figure 4).

3.3 EMP interstitial glass analyses

We have analyzed two large pumice clasts of TRSN collected in Castel di Guido (CDG6) and in La Bottaccia (BOT-1), and selected pumice fragments from the pyroclastic-flow deposit containing the faunal remains in Castel di Guido (CDG-S1), and from a pumice layer (CDG-36) underlying this deposit, recovered during archaeological excavations. A pumice fragment from a volcanic deposit collected in the archaeological excavation at Castel di Guido (CDG7), another pumice collected in the basal fallout of TdB in Anguillara (TB), and two samples of selected pumice fragments picked up from the pyroclastic-flow deposits of La Polledrara (POL 112-01, POL 12-03), did not yield analyzable glass.

Samples CDG6 and BOT-1 yielded comparable compositions that plot in the TAS diagram between the initial fallout deposit (Fall D) and the pyroclastic-flow deposit of TRSN (Figure 5a). Sample CDG-S1 yielded rhyolitic composition, quite atypical for the Monti Sabatini products and remarkably similar to that of the most differentiated products of Vico α (Marra et al., 2014b; Perini et al., 2004). Specifically, the sample CDG-S1 matches the most evolved composition of the distal tephra of Vico found in Sulmona Basin (Regattieri et al., 2015; this study), which documents a wide composition spectrum ranging from trachyte to rhyolite, with some well clustered glass populations (Fig. 10). Finally, sample CDG-36 yielded trachytic composition, much similar to those of Fall A/B from literature (Fig. 5a) (Sottili et al., 2004; Marra et al., 2014b).

3.4 Petrographic analyses

In order to compare the mineralogical assemblages of the pumice samples which did not yield analyzable glass with those for which EMP glass geochemical composition was determined, we have observed these samples in thin section either at the optical microscope and at the scanning electromicroscope (SEM). Aimed at providing further evidence for correlation of the deposits yielding indistinguishable radiometric ages, particular care has been deserved to the

comparison of the juvenile volcanic fraction occurring in the samples collected at La Polledrara di Cecanibbio (POL 12-10/03), represented by dark grey scoria lapilli, with the analogous fraction occurring in the Tufo di Bracciano pyroclastic-flow deposit (sample TB2).

CDG-7

This sample shows a clastic texture made up of: i) abundant, millimeter sized scoria clasts, characterized by similar texture and paragenesis; ii) sub-millimeter sized, lithic clasts; iii) millimeter to sub-millimeter sized, frequently rounded crystals belonging to different mineralogical phases, and iii) relatively scarce matrix. The scoria clasts are scarcely vesiculated and contain rare leucite, clinopyroxene and mica phenocrysts. The groundmass occurring in the scoria clasts is characterized by leucite microcrysts showing star-like habit (an idiosyncratic feature of Pozzolane Rosse pyroclastic-flow deposit; Marra et al., 2015b) and orange glass almost totally turned in zeolite and/or halloysite. Lithic clasts are mainly represented by quartz and quartz-feldspatic, mica-bearing, crystalline rocks of metamorphic origin. Quartz, sanidine, microcline, plagioclase, leucite (mostly transformd into analcime), clinopyroxene, garnet and phlogopite crystals have been distinguished among the mineralogical phases. The occurrence of relatively abundant quartz, feldspars and crystalline rocks, combined with the textural and mineralogical features of the scoria clasts indicate that the CDG-7 sample was likely originated from the reworking of a distal deposit of the Pozzolane Rosse eruption.

CDG-S1

The analyzed CDG-S1 sample is formed by lapilli clasts characterized by variable texture and mineralogical assemblage. The following lithotypes have been distinguished: i) porphyritic, scarce vesicular scoria containing millimeter-sized clinopyroxene phenocrysts and relatively coarse grained groundmass made up of pseudo-abundant leucite (i.e., analcime), and clinopyroxene; ii) lava lithics showing a porphyritic texture and made up of sub-millimeter sized leucite and clinopyroxene phenocrysts and groundmass with abundant leucite, almost totally turned in analcime, and clinopyroxene; iii) granular lithic clasts made up of Ba-rich feldspar, clinopyroxene and garnet; iv) lithics with clastic texture characterized by relatively large (>500 mm) quartz crystals; v) pyroclastite characterized by a glassy matrix with eutaxitic texture, quartz, K-feldspar, mica and highly vesicular glassy pumices. The latter are rhyolitic in composition and are certainly attributable to the leucite-free juveniles occurring in the Vico α deposit. The presence of leucite-bearing scoria is consistent with the

compositional zoning of this complex eruptive succession, which in the late stages is characterized by phono-tephritic to latitic compositions (Perini et al., 2004), suggesting that CDG-S1 may represent a sub-primary product.

TB 1

The light grey pumice collected in the fallout deposit shows porphyritic, scarcely vesicular texture, with leucite (partially transformed in analcime), sanidine, aegerine-augite, mica and magnetite phenocrysts. The groundmass is relatively coarse grained and made up of leucite and scarce mica, feldspar and clinopyroxene. Garnet- and plagioclase-bearing microgranular enclaves also occur.

TB2

The black scoria lapilli of the pyroclastic-flow deposit are porphyritic, medium vesicular, with leucite (partially transformed in analcime), clinopyroxene, mica and magnetite phenocrysts. The clinopyroxene occurs either as homogeneous, diopside-rich phenocrysts, or as chemically reversely zoned crystals characterized by an aegerine-augite core and a diopside rich-rim. The groundmass of the TB black scoria is made up of scarce glass associated with leucite, clinopyroxene and magnetite (Fig. 9 d').

POL12-01/POL 12-03

The POL-12-01/03 samples are relatively fine grained, matrix supported clastic rocks characterized by abundant volcanic components and occasional (POL 12-01) diatomites. The main volcanic components are represented by loose crystals and sub-millimeter, dark grey scoria clasts. The loose crystals are leucite, turned in analcime, clinopyroxene and mica associated with scarce sanidine and apatite. The submillimeter sized scoria clasts are fine grained, scarcely vesicular and made up of abundant leucite, turned in analcime, associated with clinopyroxene and magnetite. The association of volcanic materials with diatomites suggests that the POL12-01 sample belongs to a partially reworked volcanic deposit (lahar). In particular, texture and the mineral phases occurring in the POL12-03 scoria clasts (Fig. 9b') are almost identical to those of the groudmass of the black scoria occurring in the TdB deposit (Fig. 9d'). Moreover, the juveniles in the TdB pyroclastic-flow deposit are also characterized by relatively abundant mica phenocrysts, thus representing a favorable source for the abundant loose mica crystals observed in the POL12-01 sample.

These observations strongly support the hypothesis that the TdB eruption may be a possible source for the lahar incorporating the fossil remains of La Polledrara di Cecanibbio.

3.5 Trace-element discrimination diagrams

Results of geochemical analyses for trace-element composition are summarized in the discrimination diagrams of Figure 5b-b'. Four TGPP samples analyzed in this work (CDG3, CDG5, MG1, MG5E, enclosed by the red line in Figure 5b) plot close to the compositional field (grey rectangle in Figure 5b) defined by eight samples of this unit previously analyzed in Marra et al. (2017a). These geochemical data support the correlation based on macroscopic petrographic features. However, two other samples of different units also plot close (CDG2) or even within (BAR-1) the TGPP compositional field, suggesting that this discrimination diagram should be used with caution to distinguish the different Monti Sabatini products. The black pumice sample BOT-1 displays composition very similar to the TRSN control sample analyzed in Marra et al. (2014b). Finally, POL-12-03 and CDG-S1B yielded much offset compositions, plotting in the lower part of the Zr/Y vs Nb/Y diagram, outside of the MS and Vico compositional fields. However, trace-element composition of these partially reworked samples cannot provide reliable attribution.

The attributions proposed in Figure 5 for the pyroclastic-flow deposits of Castel di Guido and Malagrotta based on the combined lithological, petrological, and geochemical features, and on stratigraphic correlations, will be the subject of further investigation, by means of $^{40}Ar/^{39}Ar$ dating in the frame of a work in progress by Boschian et al..

4. Discussion: chronostratigraphy and biostratigraphy of the geologic sections and associated faunal assemblages

Results of the integrated field investigations, geochronologic and geochemical analyses are summarized in the stratigraphic sections for the archaeological sites shown in Figure 2 and in Figures 6 through 11. The revised chronostratigraphy of the investigated sections and the description of the paleontological assemblages are discussed in chronological order, starting from the oldest one, and based on the aggradational succession and corresponding MIS in the following sub-sections.

4.1. MIS 15 - Santa Cecilia Formation

The progressive continentalization of the Tyrrhenian Sea margin of central Italy since the end of the Santernian, led to the emplacement of the delta of the Paleo Tiber River in Ponte Galeria, to the south-west of Rome (Figure 1), around 0.8 Ma (Marra and Florindo, 2014). These coastal to continental deposits constitute the Ponte Galeria Formation (Ambrosetti and Bonadonna, 1967; Conato et al., 1980; Milli et al., 2016), which is composed of three main aggradational successions, named Ponte Galeria 1, Ponte Galeria 2 and Santa Cecilia Formations, deposited during sea-level rise of MIS 19, MIS 17 and MIS 15, respectively (PG1, PG2, and SC; Marra et al., 1998).

4.1.1 Cretone

A scanty faunal assemblage, including *Palaeoloxodon antiquus*, *Bos primigenius*, *Dama* sp., *Cervus* sp., was recovered in association with several choppers and some flakes in a clayey deposit of the Cretone lacustrine basin by Manni et al. (2000), who attributed it to the Late Galerian/Early Aurelian. This site was included among those of the Torre in Pietra FU in Palombo (2004). More recently, Marra et al. 2016a determined an age ≥544±11 ka for the Cretone site through the $^{40}Ar/^{39}Ar$ dating of the pyroclastic-flow deposit at the top of the lacustrine succession hosting the fossils. The faunal assemblage recovered by Manni et al. (2000) is therefore part of the Isernia FU (Marra et al., 2014a) (Table 1). It should be noted that large part of the sedimentary succession found in the Cretone basin spans a long period covering MIS 13 through MIS 5 (Marra et al., 2016a). As a consequence, the overall lacustrine succession should not be associated with the site reported in Palombo (2004), which should be intended as referring only to the specific lacustrine horizon described by Manni et al. (2000).

4.2 MIS 13 - Valle Giulia Formation

The Valle Giulia Formation introduced by Marra and Rosa (1995) designates the fluvial deposits of the Paleo-Tiber River emplaced during MIS 13. Later on, several geochronologic constraints were provided, demonstrating the strict link between deposition of the aggradational succession and two consecutive peaks of the $\delta^{18}O$ curve during MIS 13 (Figure 6; Marra et al., 2017a). In particular, the age of 533±2 ka of Tufo del Palatino, emplaced at the top of the basal gravel layer of the Valle Giulia Formation constrains occurrence of glacial termination VI (Figure 6b). Ages of several volcanic deposits intercalated within the fluvial-lacustrine to brackish succession cropping out at Cava Rinaldi in the Fosso Galeria valley

(Figure 6a), spanning 516±1 - 496±9 ka, provided constraints to the late aggradational phase during the MIS 13.1 highstand (Marra et al., 2014a; 2017a).

4.2.1 Cava Rinaldi

From the faunal assemblages of Cava Rinaldi (Table 2) Capasso Barbato and Minieri (1987) classified a molar tooth of bear as *Ursus spelaeus*. Until recently this species was considered a taxon characteristic of the Early Aurelian. In contrast, the Cava Rinaldi section is a type-section of the Valle Giulia Formation (Marra et al., 2017a), correlated with MIS 13 sea-level rise (Figure 6a). The fossil remain was recovered in the "basal layer of the upper tuffitic formation, overlying the deposits of the Ponte Galeria Formation", corresponding to the TGPP pyroclastic-flow deposit (Figure 6a), dated to 516±1 ka by Marra et al. (2017a) using a sample collected at this location.

4.2.2 Via Aurelia

A complex picture arises from literature concerning several archaeological sites located between kms 19 - 20 of Via Aurelia, due to the common reference to the nearby locality of Castel di Guido (Figure 2b). In particular, two distinct archaeological excavations were carried on in 1980 (Radmilli and Boschian, 1996, and references therein) and in 1982 (Anzidei and Sebastiani, 1984) at two sites, located ca. 70 m a.s.l. (i.e., on the hill facing the Via Aurelia at km 20, hereby referred as Castel di Guido), and ca. 58 m. a.s.l. (i.e., at the foot of the hill cut by the Via Aurelia at km 19.3) (Figure 2). Later on, two new excavations were conducted at km 18.9 and at km 18.7-19.0 of Via Aurelia (Figure 2) in 1989 (Anzidei et al., 1993). Moreover, several papers published description and classification of fossils remains hosted in different repositories, attributed to surface collection in the area of Castel di Guido (e.g. Radmilli et al., 1979; Capasso Barbato and Petronio, 1981; Capasso Barbato and Minieri, 1987), and treated the remains as part of the same, homogeneous faunal assemblage (i.e., Torre in Pietra FU). The detailed geologic study conducted in this work highlights a different scenario, showing that the sedimentary deposits of the aggradational successions correlating with MIS 13 (Valle Giulia Fm), crop out extensively in this area, with only a few sedimentary deposits attributed to the younger San Paolo Formation (MIS 11) (Figure 2a). In contrast, no sedimentary deposit ascribable to MIS 9 has been found so far in all the investigated sections along Via Aurelia (Figure 2b).

4.2.3 Via Aurelia km 18.7-19 (Collina Barbattini) and km 18.9

Vertebrate fossils and lithic tools recovered at two excavation sites located on the opposite sides of Via Aurelia between km 18.7 and 19 (Figure 2) were described by Anzidei et al. (1993). These authors report that all the archaeological material was found within a deposit filling a paleomorphology, excavated in the underlying fluvial-lacustrine succession (inset c in Figure 2a). We have observed this erosional surface at km 19.3 of Via Aurelia and noted that it is composed of different erosive levels, overlain by partially reworked pyroclastic material of the GRPS-a. Moreover, the TGPP pyroclastic-flow deposit crops out immediately below the erosive surface. These morphostratigraphic features allowed us to recognize the exposed deposit as the basal portion of the aggradational succession of the Valle Giulia Formation in this area, which is emplaced at the beginning of the ingressive phase associated with MIS 13.1 sea-level rise (Figure 6c; Marra et al., 2017a).

The primary pyroclastic-flow deposit of the GRPS-a crops out above a pedogenized layer overlying the TGPP in Castel di Guido, while the sample dated at 516±4 ka collected on the hill west of Castel di Guido (CDG1 in Figure 2) is interpreted as the fallout deposit of this unit, based on its age and depositional features.

The biochronology of mammals recovered in the above-mentioned sites (Table 2) is mainly compatible with the revised chronostratigraphy attributing the sediments to MIS 13. In contrast, we noticed the incongruent datum regarding the presence of *Arvicola terrestris* (= *A. italicus*) and *D. dama*. In fact, the first one has never been found in Italy before MIS 5 (Kotsakis et al., 2003), while the modern species of fallow deer spreads in Europe during MIS 8.5 (Di Stefano and Petronio, 1997; Marra et al., 2014a).

4.2.4 Via Aurelia km 19.3

The re-examination of the remains hosted at the Paleontology Museum of Università Sapienza in Rome, whose provenance was referred to the surroundings of Via Aurelia km 19, was performed for the present study. Among the recovered taxa (Table 2), we attribute the hippopotamus remain to *H. antiquus*, based both on morphological and morphometric criteria:

i- parallel grooves in canines (Caloi et al., 1980a; Petronio, 1995)

ii- large size of the 3rd metacarpal bone and the tibial fragment, never reported in *H. amphibius* (see Mazza, 1995).

Although the stratigraphic position of these fossils is unclear, the reference to km 19 and the stratigraphic scheme reported by Capasso Barbato and Petronio (1981) strictly adhere to the description of the stratigraphy of the lower portion of the hill at km 19.3 of Via Aurelia made

in Barbattini et al. (1982), from which these authors collected several fossils in the years 1976-78, as well as to the stratigraphy at km 19.3 reported in Anzidei and Sebastiani (1984) (see inset c in Figure 2). Consistent with these observations, the presence of *H. antiquus*, whose last occurrence (LO) is in the Fontana Ranuccio FU (MIS 11, Pereira et al., submitted), accounts for the widespread occurrence of the MIS 13 deposits of the Valle Giulia Formation in the road cuts affecting the hillsides in this area (Figure 2a), allowing us to reject a MIS 9 age for them.

4.2.5 Malagrotta

Field observations (Figure 2) enabled us to recognize the occurrence of the TGPP pyroclastic-flow deposit at the base of the sedimentary succession hosting the lithic artifacts (Cassoli et al., 1982) and the fossil remains (Caloi and Palombo, 1980, Table 2) in Malagrotta. $^{40}Ar/^{39}Ar$ dating of this deposit is in project within a study by Boschian et al.

The stratigraphic scheme reported in Caloi and Palombo (1980) clearly evidences that the described fossil assemblage was included within the pyroclastic-flow deposit of 516±1 ka (Marra et al., 2017a) (see inset e in Figure 2a). A different, more complete stratigraphic scheme was provided in Cassoli et al. (1982), in which they report the occurrence of artifacts within the clay layers above the pyroclastic-flow deposit, suggesting that the collection of the fossils occurred in a slightly offset location (see Figure 2e-f). Moreover, Cassoli et al. (1982) describe a paleosoil at the top of the clay layers, covered by more sedimentary deposits rich in reworked pyroclastic material since they use the word "tufite" for some of them, which in turn are overlain by a more than 2m-thick "leucititic tuff". Unfortunately, the term "tufite" was commonly used by numerous authors to indicate both fully sedimentary as well as primary volcanic deposits, as the study conducted for the present work as repeatedly ascertained. It is therefore impossible to establish the actual lithologic features of the products that are described in the previous literature and are no more visible in outcrop, as in the case of the upper portion of the Malagrotta section described by Cassoli et al. (1982). Through field data, we identified and safely correlated with the Valle Giulia Formation only the lowest part of the section, still exposed, which includes the strata hosting the fossils and the lithic industry. However, we have correlated to the Valle Giulia Formation also the upper portion of the section, that is currently not exposed, according to the identification of the partially reworked deposits of the TRSN, cropping out in Via Aurelia at km 16.6 (sample MG4, Figure 2, 3), not far from Malagrotta, correlating the "leucititic tuff" at the top of the succession described in Cassoli et al. (1982) (Figure 2f).

Among the several taxa recovered from the pyroclastic-flow deposit of Malagrotta, Caloi and Palombo (1980) reported *Canis lupus*, whose FO in the peninsular Italy was considered to occur during MIS 9. However, we do not consider classification of *Canis lupus* based on a small molar fragment a reliable clue, and we rather attribute it to *Canis* sp., in agreememnt with considerations reported in Caloi and Palombo (1980) about the size of the lower carnassial, which is "smaller, or equal at the least, than that attested in the Rissian wolves". Capasso Barbato and Minieri (1987) reported the presence of *Vulpes vulpes*, also considered a MIS 9 marker for this region (Gliozzi et al., 1997), within the uppermost travertine layers occurring above the "leucititic tuff" at the top of the sedimentary succession of Malagrotta described by Cassoli et al. (1982). Remarkably, a travertine layer caps the leucititic pyroclastic deposit above the TRSN at km 16.6 of Via Aurelia, like in Cassoli et al. (1982) stratigraphy of Malagrotta. Based on the stratigraphic continuity of the succession and according to the overall stratigraphic setting in this area, a MIS 11 age for the travertine is proposed. Therefore, the FO of *Vulpes vulpes* must be backdated within the Fontana Ranuccio FU, as already observed for the red fox remains from Bristie 1 and Visogliano (Trieste Karst; Petronio et al. 2006; Sardella et al. 2006; Masini and Sala 2007).

4.2.6 Via Flaminia km 8.2

Kotsakis et al. (1979) describe the remains of a steppe elephant and a deer found at Km 8.2 of the Via Flaminia, attributing them to *Mammuthus chosaricus* and *Cervus elaphus rianensis*. A second skull of *M. chosaricus* was recovered by one of the authors of this paper (CP) in a nearby site located 200 meters north of the first locality, along the Fosso della Crescenza valley. Based on re-examination of the deer antler, showing features similar to a late form of *C. elaphus acoronatus*, we attribute it to *Cervus elaphus* ssp..

Previous work interpreted the deposit cropping out at km 8.2 of Via Flaminia as a fluvial terrace onlapping on the older TRSN pyroclastic-flow deposit. However, field surveys in this area, including the nearby site of Cava Nera Molinario where the same succession is exposed, evidenced a completely different stratigraphic setting (Figure 7). The deposits cropping out at km 8.2 of Via Flaminia represent indeed a type-section of the Valle Giulia Formation (Marra et al., 2017a). Here, the Tufo del Palatino pyroclastic-flow deposit (TP; 533±2 ka, Marra et al., 2017a) rests directly above the basal gravel layer of the Valle Giulia Formation, and is covered by a succession of fluvial-lacustrine sediment in which the fossils described in Kotsakis et al. (1979) were recovered. The pyroclastic-flow deposit of TRSN (452±2 ka, Karner et al., 2001b)

fills a marked paleo-incision cutting through the underlying deposit of the Valle Giulia Formation (Figure 7).

At Cava Nera Molinario remains of *Cervus elaphus eostaphanoceros* were also recovered within the Valle Giulia Formation, but in a lower stratigraphic position with respect to *C. elaphus* ssp. recovered at km 8.2 of Via Flaminia. Indeed, re-interpretation of the stratigraphic scheme provided in Blanc et al. (1955) (Figure 7) shows that the antler of the cervid occurred below the TP, within the upper portion of the basal gravel of the Valle Giulia Formation. The sedimentary succession cropping out at Cava Molinario was previously correlated with MIS 11 and the faunal assemblage recovered there, as opposed to that of km 8.2, was attributed to the Fontana Ranuccio FU (Palombo, 2004, and references therein). According to later revision by Marra et al. (2014a), the Fontana Ranuccio FU spans the interval comprising MIS 13 and MIS 11, therefore only a revision of age applies to Cava Nera Molinario, whereas a more significant revision is provided here to the site at km 8.2 of Via Flaminia, previously considered to correlate with MIS 7, and to the biochronology of the fossil remains, which were included into the Torre in Pietra FU of the AMA (Palombo, 2004).

According to the revised chronology of the deposit, the morphology and systematics of elephants remains found in the site should be classified as *Mammuthus trogontherii-chosaricus*.

4.3 MIS 11 - San Paolo Formation

4.3.1 Riano

The diatomitiferous lacustrine deposits of the Riano basin in which three complete skeletons of *Cervus elaphus rianensis* were recovered in anatomical connection (Accordi and Maccagno, 1962) have been considered for decades as one type-section hosting a characteristic faunal assemblage of the AMA (Palombo, 2004). Consequently, the lacustrine succession exposed near the town of Riano by quarry excavations for exploitation of TGVT was attributed to the Aurelia Formation and MIS 9 (Conato et al., 1980).

A primary pyroclastic-fall deposit sampled in the middle of the outcropping lacustrine deposits (Figure 8a, c) and dated in the frame of this study, yielded age of 406±5 ka (Figure 4), evidencing that the exposed sedimentary succession correlates instead with MIS 11 and is therefore part of the San Paolo Formation. Trace element composition of the volcanic deposit evidences a Monti Sabatini provenance, and strong geochemical affinity with the products erupted between 450 - 380 ka, despite the undistinguishable radiometric age of the large

Pozzolane Nere eruption cycle (407±3 ka, Marra et al., 2009) from the Colli Albani volcanic district (Figure 5b').

Stratigraphic setting of the Riano basin displays striking similarity with that of the fluvial-lacustrine succession of Rignano Flaminio, recently correlated with MIS 11 based on coupled chronostratigraphic and paleontological evidence (Petronio et al., 2017; Figure 8d). At Rignano, the presence of *Cervus elaphus eostephanoceros*, among other taxa, indicates a time interval limited to MIS 13 and MIS 11. The occurrence of the TRSN pyroclastic-flow deposit, dated to 452±2 ka, at the base of the sedimentary deposits hosting the faunal assemblage allowed Petronio et al. (2017) to provide an age within MIS 11.

Stratigraphy of Riano reported by Accordi and Maccagno (1962) (Figure 8c) shows that the remains of *C. e. rianensis* occur in the uppermost part of the lacustrine succession (asterisks in the picture of Figure 8a and in the stratigraphic sketch of Figure 8c), few meters above the pyroclastic layer we dated at 406±5 ka. Figure 8b shows that this age corresponds to the terminal phase of aggradation of the San Paolo Formation. It is therefore inferred that the occurrence of *C. e. rianensis* postdates that of *C. e. eostephanoceros*, which is found in the lower part of the fluvial-lacustrine succession of Rignano, corresponding to an earlier aggradational phase of the San Paolo Formation.

4.3.2 Castel di Guido (Via Aurelia km 20)

A rich Acheulean industry and paleontological assemblages were recovered following excavations conducted since 1980 at the archaeological site of Castel di Guido (Radmilli and Boschian, 1996, and references therein). The stratigraphic/depositional contexts of the site were described in detail by Boschian and Saccà (2010). The large majority of the archaeological remains were found above an erosional surface, or in rare cases some centimeters within the overlying sediment, represented by a 0 to 20 cm-thick layer of sand incorporating sparse "mud-balls". The paleo-morphology was filled by a 1.5–1.9 m thick layer of homogeneous, whitish fine sediment, lacking sedimentary structures, apart from a concentration of coarse pumice clods at its top (Figure 9c). In thin section, a sample of the deposit revealed the occurrence of abundant diatoms, incorporated within pyroclastic material, suggesting a partially reworked origin. Sala and Barbi (1996) provided a complete list and the classification of the fossil remains recovered above the paleosurface at Castel di Guido during the excavations performed in the years 1980-1990 (Table 2). Among other, discriminating for attribution to MIIS 9 were the species *Canis lupus* and *Panthera spelaea*

(Capasso Barbato and Minieri 1987).

Re-examination of photographs, stratigraphic sketches, and samples collected during the original excavations, combined with a new dedicated field survey, allowed us to reconstruct the stratigraphy of the site reported in the cross-section of Figure 9a and summarized in Figure 2. The field survey has evidenced the presence of the Monti Sabatini volcanic succession spanning 516-452 ka, cropping out on the southern flank of the hill where the archaeological site of Castel di Guido is located. From bottom to top, it comprises the TGPP (ca. 63 m a.s.l.), the GRPS and the Fall A pumice (ca. 65 m), white lacustrine muds (between 63 and 68 m), and the TRSN (ca. 70 m a.s.l.) (Figure 9a). Moreover, petrographic analyses of sample CDG-7, collected from a semi-lithified pyroclastic deposit occurring ca, 68 m a.s.l. in the archaeological excavation, allowed us to attribute it to a partially reworked Pozzolane Rosse (456±4 ka, Marra et al., 2009) distal fallout deposit. Finally, the peculiar rhyolitic EMP glass composition of the small pumice fragments extracted from the pyroclastic deposit of Castel di Guido (Figure 5a) evidences its correlation with the Vico α deposits (418-412 ka, Marra et al., 2014b) (Figure 10), which are intercalated in the Monti Sabatini volcanic succession, and at La Polledrara occur in very similar stratigraphic position (i.e., filling a paleoincision eroding the TRSN deposit; see Figure 9a).

Based on the combined morpho-stratigraphic, geochronologic, geochemical and petrographic feature of the Castel di Guido succession (Figure 9a), we interpret the deposit immediately above the paleo-surface as a partially reworked, sub-primary Vico α deposit, which incorporated diatomitic lacustrine deposits. More in general, we correlate the ca. 2 m thick succession exposed by the excavation with the late aggradational deposits of the San Paolo Formation (see also Figure 2), in which the Vico α fallout products are typically intercalated (Marra et al., 2016b). Therefore, we attribute the age of 412±2 ka to the deposit above the paleosurface of Castel di Guido, revising the previously assigned collocation within MIS 9 to the faunal assemblages incorporated within it, or resting above the underlying paleo-surface, recovered at this site, and attributing it to MIS 11. This implies a significant revision of the FO for *Canis lupus*, which should be backdated within the Fontana Ranuccio FU. Direct $^{40}Ar/^{39}Ar$ dating of the deposit in the fram of an ongoing project by Boschian et al. may clarify this issue.

The fragmentary remains attributed to cave lion, *P. spelaea*, as well as those referred to *Panthera* cf. *spelaea* from Collina Barbattini, have to be reviewed considering the possible attribution to *Panthera fossilis*, a lion-like pantherine felid that occurs in Italy in the Isernia FU (MIS 15) and in continental Europe from MIS 19-17 to MIS 9-7 (see Marciszak et al., 2014; Sabol, 2014).

4.4 MIS 9 - Aurelia Formation

4.4.1 La Polledrara di Cecanibbio

The sequence of La Polledrara di Cecanibbio was discovered in 1984 and excavated during more than thirty years (Anzidei et al., 2004; 2012, and references therein). More than 600 artifacts were discovered so far, including both lithic and bone tools, along with more than 20.000 vertebrate fossils. The paleontological assemblage of this site (Table 2) is mainly composed of *Bos primigenius* and *Palaeoloxodon antiquus* remains, and include *Canis lupus*, *Vulpes vulpes*, *and Felis silvestris* which were considered exclusive of MIS 9 (Anzidei et al., 2012, and references therein). All archaeological and paleontological remains are embedded within a graded, fining upward volcanic mudflow (lahar) very rich in centimetric to decimetric pyroclastite fragments, mainly pumice clods (Figure 9a-b; Marra et al., 2016b). However, it is worth mentioning that fossils and industries at the base of the lahar (displaying either fluitation evidence and fresh fracturing) were transported or incorporated by the mudflow, whereas at the top three *Palaeoxodon antiquus* skeletons were found in anatomical connection (Santucci et al., 2016), likely trapped after trampling above it (Pereira et al., 2017). The mudflow was dated by Pereira et al. (2017) to 325±2 ka by $^{40}Ar/^{39}Ar$ on single crystal. This age was obtained on sanidine crystals extracted from pumices embedded in the mudflow. The age and probability diagrams obtained on the pumices sampled in two different locations confirm the homogeneous origin of the volcanic material transported by the mudflow, which Marra et al. (2016b) tentatively correlated with the eruption of TdB, despite the slightly different radiometric ages yielded by the latter, ranging 316±6 to 307±5 ka (Sottili et al., 2010). However, the occurrence of large white pumices is not observed in the main pyroclastic-flow deposit of TdB, characterized by leucite-bearing, grey scoria juveniles with trachytic composition (Figure 5a), whereas white pumice only occurs in the initial, Plinian fallout deposits at the base of the eruptive unit (see Figure 9d). However none of the pumices from these two samples yielded analyzable glass. In contrast, petrographic observation at SEM evidenced that the scoria of the TdB pyroclastic-flow deposit and those occurring in the lahar of La Polledrara have the same textural/mineralogical features (POL 12-03, TB2, Figure 9b', d'; see section 3.4). A possible explanation is that the pumice dated by Pereira et al. (2017) represents an inclusion in the distal, sub-primary pyroclastic-flow deposit of TdB in La Polledrara, incorporated as rip-up clasts from the TdB basal fallout deposit, upon which it flew.

Notably, a markedly different interpretation of the depositional context of this site was provided until recently in the literature (e.g.: Anzidei et al., 2012, and references therein). Taking into account the chronostratigraphic scheme derived by sequence stratigraphic subdivision of the Roman Pleistocene deposits by Milli et al. (2016), the La Polledrara site was interpreted as developed during MIS 9, in the final phase of the Transgressive Systems tract of the PG6 sequence (= Aurelia Formation aggradational succession, Karner and Marra, 1998). The deposit hosting the fossils was described by Anzidei et al. (2012) as volcanoclastic fine to very fine sand and mud sediments of fluvial ephemeral channels and of palustrine and marshy environments, emplaced during the final filling phase of the upper portion of an incised valley caused by repeated flood events, and its successive transformation into a palustrine-lacustrine basin. Based on interpretation provided in Anzidei et al. (2012), the deposits of the PG6 sequence in the examined area derived from the primary and contemporaneous re-sedimentation of a volcanic unit known in the literature as "Tufi Stratificati Varicolori di La Storta" (Mattias and Ventriglia, 1970; Corda et al., 1978).

In contrast to interpretations above, the deposit hosting part of the fossils clearly displays the textural and depositional features of a sub-primary pyroclastic-flow deposit (lahar) (Figure 9b), which was emplaced within a small paleo-incision mainly during one sudden depositional event. It is indeed characterized by a very fine ash matrix incorporating large pumice clods, up to 10 cm in diameter at the base, and a few heterogeneous volcanic blocks, whereas progressively finer pumice is embedded in the upper portion of the deposit (Pereira et al., 2017). A feature equivalent to a bimodal, gravel and clay class granulometry, clearly incompatible with a high-energy fluvial deposit, capable of transporting the large *Elephas* bones occurring in the lowest part of the deposit. Moreover, the deposit is massive, lacking any bedding or stratification, and mineralogical and geochemical analyses (Castorina et al., 2015) have shown that it is entirely composed of sub-primary, siliceous volcanic material. Finally, no vegetal remain or pollen occur within the sediment. However, thin section observation performed in this study evidenced the occurrence of occasional diatoms within the pyroclastic deposits, which likely derive from erosion and incorporation of a sedimentary substrate above which the lahar flew. The same occurrence has been observed in the sub-primary pyroclastic-flow deposit of Castel di Guido.

Age of the volcanic deposit (≤325±2 ka) evidences its emplacement after the completion of highstand of MIS 9, occurred by 330 ka. Therefore, it lacks direct link to the fluvial-lacustrine succession that was deposited in response to sea-level rise during glacial termination IV (see Figure 11). According to this evidence, a fluvial cross-bedded sediment underlying the lahar

deposit (Figure 9a) contains a heterogeneous population of crystals with a youngest age of 359 ±6 ka (Pereira et al., 2017), consistent with deposition at the onset of glacial termination IV, similar to the lowest portion of the Aurelia Formation in Torre in Pietra (see Figure 11). This thin layer represents the only sedimentary deposit of the Aurelia Formation in this area, and overlies another primary volcanic deposit whose $^{40}Ar/^{39}Ar$ age of 411±5 ka (Pereira et al., 2017) allows correlation with the Vico α eruption unit, which supersedes the discarded unit name of Tufi Stratificati Varicolori di La Storta (Marra et al., 2014b; Luberti et al., 2017). Indeed, a scarce eruptive activity characterized the Monti Sabatini district after the late stages of the TRSN Eruption Cycle (452±2 - Fall F 447±7 ka), represented by the airfall deposits of the Sant'Abbondio Succession, dated between 389-379 ka (Marra et al., 2014b). The stratigraphy at Polledrara di Cecanibbio reflects well this chronostratigraphic picture, as shown in the scheme of Figure 9. A continuous succession of eruptive deposits spanning 494 - 447 ka, encompassing Fall B, Fall C, TRSN, Fall E, and Fall F, crops out on the western flanks of the hill at the top of which the archaeological site is located (Figure 9a). A marked hiatus ontop of this succession is evidenced by the occurrence of the TGS pyroclastic-flow deposit (285±2 ka, Sottili et al., 2010), directly above the partially eroded fallout deposits of Fall E-Fall F. The mudflow correlated with the TdB pyroclastic-flow deposit fills a paleoincision excavated in the older volcanic succession during the two consecutive glacial maxima (i.e.: MIS 12 and MIS 10), as evidenced by occurrence of the Vico α fallout deposits beneath a very reduced succession of fluvial sediments of the Aurelia Formation. A palustrine basin formed after the emplacement of the mudflow deposit, in which large vertebrates got bogged down. Later on, this area was covered by the TGS pyroclastic-flow (285±2 ka), and successively re-exhumed by erosion during the sea-level fall of the last three glacial maxima, which originated the saddle between the two hilltops, where the archaeological site is located.

4.4.2 Torre in Pietra lower level

In the stratigraphic sequence of the site two faunal associations occur, one within the lower levels (n, m) including the Lower Palaeolithic industry, and the other one in the upper level (layer d) including Mousterian industry (Caloi and Palombo, 1978, Malatesta, 1978; Palombo 2004; Petronio et al., 2011; Villa et al., 2016). The faunal assemblage recovered within the lower level of Torre in Pietra is considered the local fauna for the homonym faunal unit and, among others includes: *Canis lupus*, *Megaloceros giganteus*, *Vulpes vulpes*, *Ursus spelaeus*, *Panthera spelaea.*

Geochronologic constraints to the sedimentary succession cropping out in Torre in Pietra were provided in Villa et al. (2016) (Figure 11a). In this paper we present a previously unpublished $^{40}Ar/^{39}Ar$ age on a sample (TIP-A2) collected in the mid of the lower portion of the succession (Figure 11a), which despite its reworked feature, reinforces the chronostratigraphic interpretation by Villa et al. (2016), and confirms previous assumption (Marra et al., 2016b) on the early aggradational phase (AU-1) of the Aurelia Formation (Figure 11c). Indeed, the absence of any crystal younger than 391±4 ka within this reworked volcanic layer supports the inferences made previously about the lack of significant volcanic activity at the Monti Sabatini district in the interval 380 - 325 ka (Marra et al., 2014b). In light of one youngest crystal yielding 335±8 ka in sample TIP-B0, collected within a coarse sedimentary layer within the second aggradational unit of the Aurelia Formation (AU-2, Figure 11a), supposed to mark the occurrence of glacial termination V (Villa et al., 2016), occurrence of older crystal ages in TIP-A2 evidences the early deposition of the AU-1 succession in Torre in Pietra, consistent with an age of ~350 ka for the first aggradation phase of the Aurelia Formation (Marra et al., 2016b).

Therefore, as already remarked in Villa et al. (2016), an age close to 354±5 ka should be attributed to the lithic industry and the faunal assemblage occurring at the base of the Torre in Pietra succession (AU-1). Notably, this age is ~30 ka older with respect to that of the fossils and the artifacts occurring within the 325 ka-old pyroclastic-flow deposit at Polledrara. Indeed, the AU-1 succession correlates MIS 10, while the TdB post-dates the MIS 9 peak (Figure 11).

In the stratigraphic sequence of the site two faunal associations occur, one within the lower levels (n, m) including the Lower Palaeolithic industry, and the other one in the upper level (layer d) including Mousterian industry (Caloi and Palombo, 1978, Malatesta, 1978; Palombo 2004; Petronio et al., 2011; Villa et al., 2016).

4.5 MIS 8.5 - Via Mascagni succession

The Via Mascagni succession was firstly introduced by Marra et al. (2008) who correlated with sub-stage 8.5 a minor aggradational succession unconformably overlying fluvial-lacustrine deposits of the Aurelia Formation in the Aniene Valley in northern Rome. Strict geochronologic constrains to these aggradational successions in this area are provided by the pyroclastic-flow deposits of Tufo Lionato (365 ± 5 ka) and TGS (285 ± 2 ka), intercalating at the base of the lower one and above the upper one, respectively (Figure 12). They allow to constrain deposition of the Via Mascagni succession during MIS 8.5, 295 - 285 ka (Figure 11c).

As noted by Marra et al. (2014a) the deposits of the Via Mascagni succession records the FOs of *Equus hydruntinus* and *Dama dama tiberina*, and the hosted faunal assemblages are therefore included, along with those of the following MIS 7 deposits of the Vitinia Formation (Vitinia FU). Stratigraphy of the sections of the Via Mascagni succession located along the Aniene Valley and their chronostratigraphic constraints have been described in detail by Marra et al. (2017b) and are summarized in Figure 12. These comprehend: Sedia del Diavolo ("upper gravel"), Monte delle Gioie and Ponte Mammolo. Based on bibliographic review data we include in the Via Mascagni succession also the following sections.

4.5.1 Prati Fiscali

This toponym corresponds to the road where the Monte delle Gioie outcrop is located. Although it is uncertain whether the faunal assemblage described above is collected at the same site or in a slightly different location, the occurrence of *H. hydruntinus* constraints it within the Vitinia FU and the deposit in which it occurred is very likely the same gravel layer where the assemblage referred to Monte delle Gioie was recovered.

4.5.2 Monte Sacro

Also this toponym corresponds to the larger area where Monte delle Gioie is located. Consistently, a faunal assemblage of the Vitinia FU (Table 2) is reported by Petronio et al. (2011) from this locality.

4.5.3 Batteria Nomentana

According the close location of this toponym to Sedia del Diavolo and to the sampling site of the sample of TGS dated by Karner et al. (2001b) in Via Cheren (see also Marra et al., 2017b), remains of *Dama dama tiberina* (Di Stefano and Petronio 1997; Di Stefano et al., 1998) were recovered in this locality, suggesting a provenance from the deposits of the Via Mascagni succession.

4.5.4 Vigna San Carlo

This site is located along Via Portuense in a sector where fluvial-lacustrine deposits occur above the Tufo Lionato pyroclastic-flow deposit in the outcrops where ancient Roman quarries for exploitation of this volcanic rock where located (Mara et al., 2017c). Based on the similarity with the stratigraphic setting of the sections exposing the Via Mascagni succession

in the Aniene Valley, where the aggradational deposits of MIS 8.5 directly overly the Tufo Lionato, we attribute the faunal assemblage of Vigne Torte to this stage.

4.5.5 Cerveteri-Migliorie di San Paolo

Capasso Barbato et al. (1983) described the faunal remains from Migliorie di San Paolo locality west of Rome (Figure 1) hosted in the Paleontological Museum at the Earth Science Department at La Sapienza University of Rome (Table 2). Later on, Di Stefano and Petronio (1997) determined the fallow deer remains as *D. d. tiberina*, and Petronio et al. (2011) included the faunal assemblage into the Vitinia FU and attributed the site to MIS 7. However, stratigraphic scheme of the site in Capasso Babato and Petronio (1981) reports the deposit hosting the fossil as a small sedimentary succession unconformably overlying the TRSN pyroclastic-flow deposit (452±2 ka), preventing discrimination between MIS 8.5 and MIS 7.

4.6 MIS 7 - Vitinia Formation

4.6.1 Vitinia Upper levels

The type-section of the homonymous Formation and FU is located in Vitinia, on the flanks of Fosso di Malafede valley to the south of Rome. Here, a pyroclastic layer dated 253±8 ka (Karner and Marra, 1998) provides strict link with glacial termination III and MIS 7.5 to the deposits (Marra et al., 2016b; Figure 11c) and to the embedded fossil remains. The aggradational succession of the Vitinia Formation unconformably overlies the Tufo Lionato pyroclastic-flow deposits and thin remainders of the eroded Aurelia Formation, or a more than 20 m thick gravel layer attributed to the Santa Cecilia Formation (Marra and Florindo, 2014) (Figure 12). From the "upper levels" of the sedimentary succession Petronio et al. (2011) reported the following taxa: *Palaeoloxodon antiquus*, *Stephanorhinus hemitoechus*., *Cervus elaphus rianensis*, *Bos primigenius*, *Canis lupus*, *Vulpes vulpes*, *Dama dama tiberina*.

4.6.2 Torre in Pietra upper level

The upper part of the sedimentary succession of Torre in Pietra is characterized by a basal coarse deposit of gravel and sand (level d) in which a rich lithic industry was recovered (Malatesta, 1978). Villa et al. (2016) have constrained deposition of this upper sedimentary succession within the interval 270 - 210 ka, corresponding to MIS 7.5 though MIS 7.1, thanks to a $^{40}Ar/^{39}Ar$ age of 208±2 ka yielded by a partially reworked volcanic layer above level d (Figure 11a, c). An age spanning 270-240 was estimated for the basal level d, also consistent with U-Th ages on cement layers and dentine sections ranging 270-235 ka (Villa et al., 2016).

4.6.3 Saccopastore

Marra et al. (2015a) have correlated with the aggradational successions of MIS 9 and MIS 7 the stratigraphic section of Saccopastore, described in detail by Segre (1948), thanks to the geochronologic and geometric constraints shown in Figure 12. In particular, these authors recognized the occurrence of three aggradational sub-cycles above the basal gravel layer of the Aurelia Formation, correlating the occurrence of three consecutive peaks of sea-level rise at around 270 ka, 245 ka, and 220 ka (Figure 11c). Through this correlation corroborated by the identification of *D. dama tiberina* remains, Marra et al. (2017b) proposed ages of ca. 245 and 220 ka, respectively, for two skulls of *H. neanderthalensis* (Bruner and Manzi, 2006) recovered within the gravel beds of the second and the third sub-cycle, back-dating the deposit with respect to previous estimation of 125 to 80 ka (Manzi et al., 2001, and references therein), based on attribution to the MIS 5 interstadial which was not supported by any geochronologic constraint, nor chronostratigraphic evidence. However, such much older, controversial age may be verified by new paleoanthropological investigations that will be undertaken in the future.

4.6.4 Casal de' Pazzi

Consistent with previous interpretation (e.g., Anzidei et al., 2001) correlation with MIS 7 of the sedimentary succession exposed by excavations for the Casal de' Pazzi Museum has been proposed in Marra et al. (2017b) (Figure 12). In particular, Marra et al. (2017b) correlated the deposit of Casal de' Pazzi with the initial stages of aggradation of the Vitinia Formation around 270 ka, based on morpho-stratigraphic considerations. Consequently, the fragment of human parietal (Manzi et al., 1990) recovered within the basal deposits of the MIS 7 aggradational succession of Casal de' Pazzi, has been suggested to represent the oldest direct evidence of *H. neanderthalensis* in Europe (Marra et al., 2017b).

The $^{40}Ar/^{39}Ar$ age on single sanidine crystals extracted form a fluvial deposit (cross-bedded and graded gravels) and sampled stratigraphically above the archaeological layer of Casal de'Pazzi allowed us to refine these observations. The youngest population of crystals with an age of 304±9 ka (Figure 4) proves that sanidines younger than the MIS 9 sedimentary succession are present within the fluvial sediments of the Casal de'Pazzi sequence. These new data, combined with the occurrence of the sedimentary deposit below the base level of the older Via Mascagni succession (MIS 8.5), reinforce the hypothesis that the faunal assemblage and the hominin remain belong chronologically to the next aggradational phase (i.e., MIS 7).

4.7 MIS 5 - Epi-Tyrrhenian Formation

In revising the previous attribution to MIS 5 of the Saccopastore sedimentary deposits and the hosted Neanderthal fossils Marra et al. (2015a) have remarked on the scarcity of sedimentary deposits correlated with MIS 5 in the greater area of Rome, with respect to a large record of aggradational deposits correlated with MIS 19 through MIS 7, hosting a wide range of faunal assemblages encompassing the Galerian and Aurelian Mammal Ages (Marra et al., 2014a). Indeed, these authors regarded the complete erosion of the deposit of the penultimate glacio-eustatic cycle during the regressive phase associated with the Last Glacial as a reliable occurrence, due to morpho-structural causes.

4.7.1 Fosso del Cupo

As a matter of fact, the correlation of only one outcrop in this region previously attributed to MIS 5 (Evangelista and Porcari, 1988) has been confirmed based on morpho-structural investigation (Ceruleo et al., 2016). It is a site described by Ponzi (1866-67) in the small valley of Fosso del Cupo, near Montecelio village not far from the town of Tivoli. Ponzi (1866-67) reported the occurrence of several vertebrate remains (Table 2) and a small set of lithic artifacts from the abovementioned locality.

5. Conclusions and remarks on the renewed chronologic framework for the Aurelian Mammal Age

The different chronostratigraphical interpretation of the continental deposits from the Late Galerian to Middle Aurelian (MIS 13 to MIS 7) and the reappraisal of many taxa collected in the Roman area, involve some problems for the systematic and biochronology of the Mammal groups. In particular, the recognition of widespread deposits of the Valle Giulia Formation (MIS 13) and San Paolo Formation (MIS 11) along the Via Aurelia, where sites referred to the Torre in Pietra FU are located, requires a careful review of the exact stratigraphical position of several of those sites, since their importance for the origin and the distinction of the FUs and the AMA.

This is the case of *Ursus spelaeus* recovered in Cava Rinaldi and Collina Barbattini (MIS 13), *Canis lupus* referred to Castel di Guido site and *Vulpes vulpes* recovered from the uppermost travertine layers of Malagrotta (MIS 11). Indeed, the FOs of these species must be backdated within the Fontana Ranuccio FU, consistent with biochronologic data from

the European continent. In particular, Schreve and Bridgland (2002) reported the occurrence of U. *speleus* remains in the terraced deposits of Lower Thames (England) correlated with MIS 11, while Barishnikov (2002) reported the occurrence of *V. vulpes* in the Urup FU, at the MIS 12-11 transition in the Caucasus. Finally, the FO occurrence of *Canis lupus* during MIS 11 in Western Europe is attested at Lunel Viel, France (Salari et al. 2017, with references).

Also consistent with the European early appearances, Sardella et al. (2007) suggested a transitional character to the Fontana Ranuccio FU (MIS 13/11) for the faunal assemblage of Visogliano (northern Italy) which included *V. vulpes* and *F. silvestris*. In contrast, the different remains attributed to *Panthera spelaea* in some sites along Via Aurelia and referred to MIS 13-11 should be reviewed considering the possible attribution to *Panthera fossilis* (see Marciszak et al., 2014; Sabol 2014).

Based on the considerations above, the Torre in Pietra FU can be considered still valid only for the first occurrences of *Mustela putorius*, *Megaloceros giganteus* and probably *Felis silvestris.* In fact, even if the wild cat is reported from Visogliano mammal assemblage (Sardella et al. 2006; Masini and Sala 2007), the origin of *F. silvestris* in the Italian peninsula is debated (Yamaguchi et al. 2004; Iurino et al. 2014). However, the new chronological picture outlined in this paper suggests that a wider faunal renewal in this region occurred at the onset of MIS 11, contextual to the evidence from Europe. This is consistent with the general global climatic-environmental change associated to the mid-Brunhes event, which undergone the establishment of the longer (~100 ka) and larger amplitude of the glacial-intergalcial cycles, leading a larger contrasts between climatic conditions during glacial and interglacial periods and major change in terrestrial ecosystems (e.g. Head and Gibbard, 2015).

The re-examination of the chronostratigraphy of the sites correlated with MIS 9, MIS 7 and MIS 5 in this region, permitted us to confirm the absence of *D. dama tiberina* in the deposits older than MIS 8.5 (Via Mascagni succession), while this fallow deer widely occurs with *E. hydruntinus* in almost all the sites referred to MIS 8.5 and MIS 7 (Sedia del Diavolo, Batteria Nomentana, Vitinia, Torre in Pietra u.l., Saccopastore). In the only site so far referred to MIS 5, Fosso del Cupo (Ceruleo et al., 2016), the presence of *D. dama dama* has been reported. Therefore, the two occurrences above should be considered distinctive of the Vitinia FU, encompassing MIS 8-5 and MIS 7, while in the first part of the Late Aurelian (MIS 5), besides many taxa occurring in the previous FUs, *E. hydruntinus* is less frequent and the fallow deer *D. d. dama*, derived from *D. d. tiberina*, appears (Di Stefano and Petronio 1997; Petronio et al., 2007).

Regarding the red deer subspecies, we confirm that *C. elaphus eostephanoceros* is a marker of Fontana Ranuccio FU, showing peculiar features that makes it easily distinguishable from both *C. elaphus acoronatus* and *C. elaphus rianensis.* In contrast, the biochronologic value of *C. elaphus rianensis*, endemic form of Latium, must be revised. This subspecies, showing still archaic, but less peculiar features (for some aspects more similar to the acoronate deer), is documented from 404 ka until 250 ka, while its occurrence in older deposits (Caloi et al., 1998; Petronio et al., 2011) should be considered as no more reliable.

These preliminary considerations based on the renewed chronologic framework outlined in the present work will be necessarily expanded and examined in detail within a forthcoming plaleontologic study.

Conclusion and final remarks

The renewed chronologic picture outlined by the chronostratigaphic study presented in this paper sensibly modifies previously defined FOs of several species upon which the FUs of the AMA for peninsular Italy were instituted. In particular, previous FO of *Ursus spelaeus*, *Canis lupus*, and *Vulpes vulpes*, which were dated at MIS 10/9 (330 ka), are now placed back within MIS 13 - MIS 11 (516-410 ka), consistent with ages of the FO's documented in the European continent.

Remarkably, the most abundant faunal assemblage of the Early Aurelian, constituting the local fauna for the Torre in Pietra Faunal unit, was recently geochronologically constrained at 355 ka (Villa et al., 2016). This age largely pre-dates the highstand of MIS 9 and, also given the fluvially-reworked feature of the deposit conglobating the faunal remains, supports the notion highlighted in this paper that the faunal renewal was favored by the enhanced sea-level oscillation and climatic change occurred during MIS 12/11.

Besides challenging the criteria which guided the institution and the sub-division of the local FU's for the Middle Pleistocene in Italy, the geochronology data presented here confirm the occurrence of a broad faunal renewal between 410 and 355 ka, and in some cases support the validity of local subspecies (e.g., *Dama dama tiberina* and *Dama dama dama*) to provide biochronologic markers for this time span.

Therefore, a thorough revision dealing with the paleontological implications of the new chronology for the faunal assemblages of the Galerian and the Aurelian Mammal Ages for the Italian peninsula is in order, and will be the subject of future work.

A key point highlighted in the present work is that most of faunal records of this area occur in depositional contexts interbedded with age-constrained pyroclastic deposits that "sealed" the

incipient to deeply incised fluvial valleys. This is the case of the Polledrara di Cecanibbio, Malagrotta and, very likely, Castel di Guido. Further works are in progress, aimed at investigating the detailed volcanic chrostratigraphy and the taphonomical aspects of the paletnological contexts of Castel di Guido and Malagrotta (Boschian et al., in progress). In this perspective, future works should be focused on a full description of the geological and volcanological evolution of the study area in order to better constrain the complex interplay among constructional and destructional volcanic activity, erosion, pedogenesis and secondary volcaniclastic sedimentation (e.g., lahar emplacement) and their relevance to faunal records preservation.

Acknowledgments

Sample POL 12-03 and photo in Figure 9a are part of the material collected under authorization by *Soprintendenza del Lazio e dell'Etruria Meridionale* for the geochronologic study at La Polledrara di Cecanibbio museum by Pereira et al. (2017). Samples CDG-S1, CDG-7 and CDG-36 and photos in Figure 9b are part of the archive material from original excavations performed in Castel di Guido since the year 1980 (Radmilli and Boschian, 1996, and references), stored at Dipartimento di Scienze Archeologiche of Pisa University.

FIGURES CAPTION

Figure 1 - a) Regional geologic scheme and b) location map of the investigated sites.

Figure 2 - a) Composite cross-section showing stratigraphy reconstructed in the present study along Via Aurelia and interpretation of literature sketches for specific sites. b) Location of sections and sampling.

Figure 3 - Photographs of representative rock samples.

Figure 4 - 40Ar/39Ar data.

Figure 5 - a) TAS diagram of EMP glass compositions. b-b') Zr/Y *vs*. Nb/Y discrimination diagrams. Compositions of the samples analyzed in this work are compared to those of the eruptive products of the Monti Sabatini and Colli Albani volcanic district provided in the literature (Marra et al., 2014b; 2015b; 2017a; Masotta, 2012)

Figure 6 - Stratigraphy of the Valle Giulia Formation in Cava Rinaldi (a) and in the northern Rome's sections (b). The volcanic deposits providing geochronologic constraints for correlation with MIS 13 (c) are shown. Legend: TGPP: Tufo Giallo di Prima Porta; GRPS: Grottarossa Pyroclastic Sequence; TP: Tufo del Palatino.

Figure 7 - Stratigraphy and geochronologic constraints of Via Flaminia km 8.2 and Cava Nera Molinario sections.

Figure 8 - a, c) Stratigaphy and geochronologic constraints of Riano section and (d) comparison to Rignano. Age constraints providing correlation with glacial termination V and MIS 11 for the San Paolo Formation are shown ($\delta^{18}O$ record by Lisiecki and Raymo, 2005).

Figure 9 - a) Stratigraphy of La Polledrara di Cecanibbio and Castel di Guido reconstructed through the integration of dedicated field surveys in the surrounding areas with literature and archive data from the archeological sites (yellow boxes: 1 from Pereira et al., 2017; 2: original data by G. Boschian). b) Photographs of the pyroclastic flow deposits of La Polledrara (b), Castel di Guido (c) and of Tufo di Bracciano in Anguillara (c), showing position of the samples analyzed for geochemistry and mineralogy in this work. b') and d') SEM microphotographs of samples POL 12-03 and TB.

Fig. 10. Total alkali versus silica classification diagram and representative bi-plots for the glass in sample CDG-S1 from Castel di Guido section compared with Vico α glass compositions. A straightforward correlation is evidenced in the different compositional diagrams.

Figure 11 - Stratigraphy and geochronologic constraints of the Torre in Pietra (a), modified from Villa et al., 2016, and Polledrara di Cecanibbio (b), modified from Marra et al., 2016b, sections. c) Aggradational phases of Aurelia Fm, Via Mascagni succession, Vitinia Fm (yellow boxes) and their geochronologic constraints (vertical red bars: ages in ka of intercalated volcanic deposits) providing correlation with the marine isotope stages (MIS) ($\delta^{18}O$ record by Lisiecki and Raymo, 2005) and the relative sea-level curve (RSL, by Grant et al., 2014).

Figure 12 - Cross-section along the Aniene River Valley, correlating the geologic sections of the Aurelia, Via Mascagni, and Vitinia aggradational successions (modified from Marra et al., 2017b). Geochronologic and biostratigraphic constraints are also shown.

Table 1 - Revised chronology for the sites of the Aurelian Mammal Age (AMA).
Sections confirmed within the FU in the recent literature are reported in regular fonts, while those revised and attributed to different FUs are in italics (reference for the revision of these sections is reported in Table 1). Sections whose age is assessed in this paper are reported in bold, those that have been revised here with respect to previous attribution are in bold italics. The last three columns report the revised attribution to the geologic formation and to the associated MIS, and the corresponding age for the deposit. When the fossils recovered at the site are embedded within, or closely constrained by a dated volcanic deposit the corresponding $^{40}Ar/^{39}Ar$ age (with the associated analytical uncertainties at 2σ) is given; otherwise, the time span of emplacement for the corresponding aggradational phase, according to criteria illustrated in this work, is reported.

Table 2 - Faunal lists reporting all the vertebrate taxa recovered at the investigated sites correlated with the MISs according to the chronostrotagraphic revision presented in this paper. Names of the taxa are reported according to the cited literature, while updated and re-determined names are reported in brackets, when appropriate.

REFERENCES

Accordi, B., Maccagno, A.M., 1962. Researches in the Pleistocene of Riano (Roma). Geol. Romana 1, 25-32.

Ambrosetti, P., 1965. Segnalazione di una fauna con *Elephas antiquus* rinvenuta nella zona di Ponte Galeria (Roma). Boll. Soc. Geol. Ital. 84(1), 3-11.

Ambrosetti, P., Bonadonna, F.P., 1967. Revisione dei dati sul Plio-Pleistocene di Roma. Atti Accademia Gioenia di Scienze Naturali in Catania 18, 33-70.

Anzidei, A.P., Caloi, L., Giacopini, L., Montero, D., Palombo, M.R., Sebastiani, R, Segre, A.G., 1993. Saggi di scavo nei depositi pleistocenici del km 18,900 della Via Aurelia e di Collina Barbattini (Castel di Guido - Roma). Archeologia Laziale 11, 81-90.

Anzidei, A.P., Biddittu, I., Gioia, P., Mussi, M., Piperno, M., 2001. Lithic and bone industries of OIS9 and OIS7 in the Roman area. In: Cavarretta, G., Gioia, P., Mussi, M., Palombo M.R. (Eds), Proceedings of the 1st International Congress The World of Elephants, CNR, Roma, 3-9.

Anzidei, A.P., Arnoldus Huizendveld, A., Palombo, M. R., Argenti, P., Caloi, L., Marcolini, F., Lemorini, L., Mussi, M., 2004. Nouvelles données sur le gisement Pléistocène moyen de La Polledrara di Cecanibbio (Latium, Italie). In: Baquedano, E., Rubio, S. (Eds). Miscelànea en homenaje a Emiliano Aguirre. Zona Archeologica 4. Archeologia. Museo Arqueológico Regional, Madrid, pp. 20-29.

Anzidei, A.P., Bulgarelli, G.M., Catalano, P., Cerilli, E., Gallotti, R., Lemorini, C., Milli, S., Palombo, M.R., Pantano, W., Santucci, E., 2012. Ongoing research at the late Middle Pleistocene site of La Polledrara di Cecanibbio (central Italy), with emphasis on human–elephant relationships. Quaternary International 255, 171–187.

Anzidei, A.P., Sebastiani, R., 1984. Saggi di scavo nel deposito pleistocenico al km 19,300 della Via Aurelia (Castel di Guido). In: Bietti Sestieri A.M. (Ed.), Preistoria e Protostoria nel Territorio di Roma, Lavori e Studi di Archeologia Pubblicati dalla Soprintendenza Archeologica di Roma 3, 86-93.

Barbattini, A., Longo, E., Settepassi, E. 1982. Nuovo giacimento del Paleolitico inferiore in Agro Castel di Guido (Roma). Atti della 23a Riunione Scientifica, Il Paleolitico in Italia, Istituto Italiano di Preistoria e Protostoria, Firenze, 7-9 Maggio 1980, 562-565.

Barishnikov, G.F., 2002. Local biochronology of Middle and Late Pleistocene mammals from the Caucasus. Russian J. Theriol. 1 (1), 61-67.

Biddittu, I., Mallegni, F, Segre, A., 1987. Riss age human remain recovered from Pleistocene deposits in Ponte Mammolo (Rome, Italy). Z. Morphol. Anthropol. 77: 181-191

Blanc, A.C., Lona, F., Settepassi, F., 1955. Una torba ad Abies, malacofauna montana e criosedimenti nel Pleistocene inferiore di Roma - Il periodo glaciale Cassio. Ricerche sul Quaternario Laziale 1. Quaternaria 2, 151-158.

Boschian, G., Saccà, D., 2010. Ambiguities in human and elephant interactions? Stories of bones, sand and water from Castel di Guido (Italy). Quaternary International 214, 3-16.

Bruner, E., Manzi, G., 2006. Saccopastore 1: the earliest Neanderthal ? A new look at an old cranium, *in* Harvati, K., and Harrison, T., eds, Neanderthals Revisited: New Approaches and Perspectives. Dordrecht, 23-36.

Caloi, L., Palombo, M.R., 1978. Anfibi, rettili e mammiferi di Torre del Pagliaccetto (Torre in Pietra, Roma). Quaternaria 20, 315-428.

Caloi, L., Palombo, M.R., 1980. Resti di mammiferi del Pleistocene medio di Malagrotta (Roma). Boll. Serv. Geol. d'Italia 100, 141-188.

Caloi, L., Palombo, M.R., Petronio, C. ,1980a. Resti cranici di Hippopotamus antiquus (=H. major) e Hippopotamus amphibius conservati nel Museo di Paleontologia dell'Università di Roma. Geologica Romana 19, 91-119.

Caloi, L., Palombo, M.R., Petronio, C., 1980b. La fauna quaternaria di Sedia del Diavolo (Roma). Quaternaria 22, 177-209.

Capasso Barbato, L., Minieri, M.R., 1987. Nuovi resti di carnivori del Pleistocene medio dei dintorni di Roma. Geologica Romana 26, 1-15.

Capasso Barbato, L., Petronio, C., 1981. La mammalofauna pleistocenica di Castel di Guido (Roma). Bollettino del Serivizio Geologico d'Italia 102, 95-108.

Capasso Barbato, L., Palmarelli, A., Petronio, C., 1983. La mammalofauna pleistocenica di Cerveteri (Roma). Bollettino del Serivizio Geologico d'Italia 102, 77-94.

Cassoli, P.F., De Giuli C., Radmilli, A.M., Segre, A.G., 1982. Giacimento del Paleolitico inferiore a Malagrotta (Roma), Atti XXIII Riunione Scientifica "Il Paleolitico inferiore in Italia", Istituto Italiano di Preistoria e Protostoria, Firenze , maggio 1980. Firenze

Castorina, F., Masi, U., Milli, S., Anzidei, A.P., Bulgarelli, G.M., 2015. Geochemical and Sr/Nd isotopic characterization of Middle Pleistocene sediments from the paleontological site of La Polledrara di Cecanibbio (Sabatini Volcanic District, central Italy). Quaternary international 357, 253-263.

Ceruleo, P., Marra, F., Pandolfi, L., Petronio, C., Salari, L., 2016. The MIS 5.5 terraced deposit of Fosso del Cupo (Montecelio, Central Italy) and its Mousterian lithic assemblage: re-evaluation of a nineteenth-century discovery. Quaternary International 425, 224-236.

Cioni, R., Sbrana A., Bertagnini, A., Buonasorte G., Landi, P., Rossi, U., Salvati, L., 1987. Laurenzi, M.A., Tephrostratigraphic correlations in the Vulsini, Vico and Sabatini volcanic successions. Periodico di Mineralogia 56, 137-155.

Cioni, R., Laurenzi, M.A., Sbrana A., Villa I.M., 1993. $^{40}Ar/^{39}Ar$ chronostratigraphy of the initial activity in the Sabatini volcanic complex (Italy). Boll. Soc. Geol. It. 112, 251-263.

Conato, V., Esu, D., Malatesta, A., Zarlenga, F., 1980. New data on the Pleistocene of Rome. Quaternaria 22: 131-176.

Conticelli, S., Peccerilllo, A., 1992. Petrology and geochemistry of potassic and ultrapotassic volcanism in central Italy: petrogenesis and inferences on the evolution of the mantle sources, Lithos 28, 221-240.

Corda, L., De Rita, D., Tecce, F., Sposato, A., 1978. Le piroclastiti del sistema vulcanico sabatino: il complesso dei tufi stratificati varicolori de La Storta. Boll. Soc. Geol. Ital. 27, 353-366.

Deino, A., Potts, R., 1990. Single-crystal 40Ar/39Ar dating of the Olorgesailie Formation, Southern Kenya Rift. Journal of Geophysical Research 95, 8453-8470.

Di Stefano, G., Petronio. C., 1997. Origin and evolution of the European fallow deer (*Dama*, Pleistocene), Neues Jahrbuch für Geologie und Paläontologie 203, 57-75.

Di Stefano, G., Petronio, C., Sardella, R., 1998. Biochronology of the Pleistocene mammal Faunas from Rome urban area. Il Quaternario 11(2), 191-199.

Evangelista, P., Porcari, R., 1988. Un ritrovamento di resti fossili di Elephas antiquus nella Campagna Romana presso Guidonia, Atti e Memorie Società Tiburtina Storia ed Arte 61,7-13.

Florindo, F., Karner, D.B., Marra, F., Renne, P.R., Roberts, A.P., Weaver, R., 2007. Radioisotopic age constraints for glacial terminations IX and VII from aggradational sections of the Tiber River delta in Rome, Italy. Earth and Planetary Science Letters 256, 61-80.

Gliozzi, E., Abbazzi, L., Ambrosetti, P.G., Argenti, P., Azzaroli, A., Caloi, L., Capasso Barbato, L., Di Stefano, G., Ficcarelli, G., Kotsakis, T., Masini, F., Mazza, P., Mezzabotta, C., Palombo, M.R., Petronio, C., Rook, L., Sala, B., Sardella, R., Zanalda, E., Torre, D., 1997. Biochronology of selected Mammals, Molluscs and Ostracods from the Middle Pliocene to the Late Pleistocene in Italy. The state of the art. Rivista Italiana di Paleontologia e Stratigrafia 103, 369-388.

Grant, K.M., Rohling, E.J., Bronk Ramsey, C., Cheng, H., Edwards, R.L., Florindo, F., Heslop, D., Marra, F., Roberts, A.P., Tamisiea, M.E., Williams, F., 2014. Sea-level variability over five glacial cycles. Nature Communications 5, 5076, doi:10.1038/ncomms6076

Head, M.J., Gibbard, P.L. 2015. Early-Middle Pleistocene transitions: Linking terrestrial and marine realms. Quaternary International, 389, 7-46.

Indes, Frère, 1869. Lettre du frère Indes, sous directeur de l'école Chrétienne à Rome, à M. de Verneuil sur la formation des tufs des environs de cette ville et sur une caverne à ossements. Bulletin de la Société Géologique de France 26, 11-28.

Iurino, D.A., Bellucci, L., Sardella, R., 2014. Il felino di Ingarano (Pleistocene Superiore, Puglia) e l'origine del gatto selvatico (*Felis silvestris*) nella penisola italiana. Hystrix the Italian Journal of Mammalogy 25(Supplement), 10.

Karner, D.B., Marra, F., 1998. Correlation of fluviodeltaic aggradational sections with 1 glacial climate history: a revision of the classical Pleistocene stratigraphy of Rome. Geol. Soc. Am. Bull. 110, 748-758.

Karner, D.B., Marra, F., Renne, P.R., 2001a. The history of the Monti Sabatini and Alban Hills volcanoes: groundwork for assessing volcanic-tectonic hazards for Rome. Journal of Volcanology and Geothermal Research 107, 185-219.

Karner, D.B., Marra, F., Florindo, F., Boschi, E., 2001b. Pulsed uplift estimated from terrace elevations in the coast of Rome: evidence for a new phase of volcanic activity? Earth and Planetary Science Letters 188, 135-148.

Kotsakis, T., Abbazzi, L., Angelone, C., Argenti, P., Barisone, G., Fanfani, F., Marcolini, F., Masini F., 2003. Plio-Pleistocene biogeography of Italian mainland micromammals. Deinsea 10, 313-342.

Kotsakis, T., Barisone G., 2008. I vertebrati fossili continentali del Plio-Pleistocene dell'area romana, in: Funiciello R., Praturlon A., Giordano G. (Eds.), La Geologia di Roma, Memorie Descrittive della Carta Geologica d'Italia 80, 115-143.

Kotsakis, T., Palombo, M.R., Petronio, C., 1979. *Mammuthus chosaricus* e *Cervus elaphus* del Pleistocene superiore di Via Flaminia (Roma). Geol. Romana 17, 411-445.

Lee, J.Y., Marti, K., Severinghaus, J.P., Kawamura, K., Hee-□Soo, Y., Lee, J.B., Kim, J.S., 2006. A redetermination of the isotopic abundances of atmospheric Ar. Geochimica et Cosmochimica Acta 70, 4507-4512. doi:10.1016/j.gca.2006.06.1563.

Leonardi, G., Petronio, C., 1974. I cervi pleistocenici del bacino diatomitico di Riano (Roma), Mem. Accad. Naz. Lincei 223, 101-208.

Lisiecki, L.E., Raymo, M.E., 2005. A Pliocene-Pleistocene stack of 57 globally distributed benthic $\delta^{18}O$ records. Paleoceanography 20, PA1003. http://dx.doi.org/10.1029/2004PA001071.

Luberti, G.M., Marra, F., Florindo, F., 2017. A review of the stratigraphy of Rome (Italy) according to geochronologically and paleomagnetically constrained aggradational successions, glacio-eustatic forcing and volcano-tectonic processes. Quaternary International, in press. http://dx.doi.org/10.1016/j.quaint.2017.01.044

Malatesta, A., 1978. La serie di Torre del Pagliaccetto ed il bacino di Torre in Pietra. Quaternaria 20, 237-246.

Manni, R., Margottini, S., Palladino, D., Palombo, M.R., Zarattini, A., 2000. Scavo e recupero di resti di *Elephas (Palaeoloxodon) antiquus* Falconer & Cautley nei pressi di Palombara Sabina (Roma). Atti del 2° Convegno Nazionale di Archeozoologia Abaco Forlì, 99–106.

Manzi, G., Salvadei, L., Passarello, P., 1990. The Casal de' Pazzi archaic parietal: comparative analysis of a new fossil evidence from the late Middle Pleistocene of Rome. J. Human Evol. 19, 751-759.

Manzi, G., Palombo, M.R., Caloi, L., Mallegni, F., 2001. Transitions in human evolution and faunal changes during the Pleistocene in Latium (Central Italy). In: Cavaretta, G., Gioia, P., Mussi, M., Palombo, M.R. (Eds.), The World of Elephants, pp. 59-66. Roma.

Marciszak, A., Schouwenburg, C., Darga, R., 2014. Decreasing size process in the cave (Pleistocene) lion Panthera spelaea (Goldfuss, 1810) evolution – A review. Quat. Int. 339-240, 245-257.

Marra, F., D'Ambrosio, E., 2013. Trace-element classification diagrams of pyroclastic rocks from the volcanic districts of Central Italy: the case study of the ancient Roman ships of Pisa, Archaeometry, 55, 6, 993-1019. doi: 10.1111/j.1475-4754.2012.00725.x

Marra, F., Rosa, C., 1995. Stratigrafia e assetto geologico dell'area romana, in: Funiciello R, ed. Memorie Descrittive Carta Geologica d'Italia, 50: 49-118.

Marra, F., Florindo, F., 2014. The subsurface geology of Rome: sedimentary processes, sea-level changes and astronomical forcing. Earth-Science Rev. 136, 1-20.

Marra, F., Florindo, F., Karner, D.B., 1998. Paleomagnetism and geochronology of early Middle Pleistocene depositional sequences near Rome: comparison with the deep sea $\delta^{18}O$ climate record. Earth Planet. Sci. Lett. 159, 147-164.

Marra, F., Florindo, F., Boschi, E., 2008. History of glacial terminations from the Tiber River, Rome: Insights into glacial forcing mechanisms. Paleoceanography 23, 1-17. doi:10.1029/2007PA001543

Marra, F., Karner, D.B., Freda, C., Gaeta, M., Renne, P.R., 2009. Large mafic eruptions at the Alban Hills Volcanic District (Central Italy): chronostratigraphy, petrography and eruptive behavior. J. Volc. Geotherm. Res. 179, 217-232. http://dx.doi.org/10.1016/j.jvolgeores.2008.11.009.

Marra, F., Deocampo, D., Jackson, M.D., Ventura, G., 2011. The Alban Hills and Monti Sabatini volcanic products used in ancient Roman masonry (Italy): an integrated stratigraphic, archaeological, environmental and geochemical approach. Earth Sci. Rev. 108, 115-136. http://dx.doi.org/10.1016/j.earscirev.2011.06.005

Marra, F., Pandolfi, L., Petronio, C., Di Stefano, G., Gaeta, M., Salari, L., 2014a. Reassessing the sedimentary deposits and vertebrate assemblages from Ponte Galeria area (Roma, central Italy): An archive for the Middle Pleistocene faunas of Europe. Earth-Science Review 139, 104-122.

Marra, F., Sottili, G., Gaeta, M., Giaccio, B., Jicha, B., Masotta, M., Palladino, D.M., Deocampo, D., 2014b. Major explosive activity in the Sabatini Volcanic District (central Italy) over the 800-390 ka interval: geochronological - geochemical overview and tephrostratigraphic implications. Quaternary Science Reviews 94, 74-101. doi:10.1016/j.quascirev.2014.04.010

Marra, F., Ceruleo, P., Jicha, B., Pandolfi, L., Petronio, P., Salari, L., 2015a. A new age within MIS 7 for the *Homo neanderthalensis* of Saccopastore in the glacio-eustatically forced sedimentary successions of the Aniene River Valley, Rome. Quaternary Science Reviews 129, 260-274.

Marra, F., D'Ambrosio, E., Gaeta, M., Mattei, M., 2015b. Petrochemical Identification and Insights on Chronological Employment of the Volcanic Aggregates Used in Ancient Roman Mortars. Archaeometry 58(2), 177-200. doi:10.1111/arcm.12154

Marra F., Ceruleo P., Jichac B., Pandolfi L., Petronio C., Salari L., Giaccio B, Sottili G., 2016a, Glacio-eustatic and tectonic forcing on the lacustrine succession of the Cretone basin: chronostratigraphic constraints to Acheulian industry and Middle Pleistocene faunal assemblages of Latium (central Italy), Journal of Quaternary Science 31, 641-658.

Marra, F., Rohling, E.J., Florindo, F., Jicha, B., Nomade, S., Pereira, A., Renne, P.R., 2016b. Independent $^{40}Ar/^{39}Ar$ and 14C age constraints on the last five glacial terminations from the aggradational successions of the Tiber River, Rome (Italy). Earth Planet Sci Lett, 449, 105-117. http://dx.doi.org/10.1016/j.epsl.2016.05.037

Marra, F., Florindo, F., Anzidei, M., Sepe, V., 2016c. Paleo-surfaces of glacio-eustatically forced aggradational successions in the coastal area of Rome: assessing interplay between tectonics and sea-level during the last ten interglacials. Quaternary Science Review 148, 85-100. http://dx.doi.org/10-2016/j.quascierev.2016.07.003

Marra, F., Florindo, F., Jicha, B., 2017a. $^{40}Ar/^{39}Ar$ dating of Glacial Termination VI: constraints on the duration of Marine Isotopic Stage 13. Scientific Reports, in press.

Marra, F., Ceruleo, P., Pandolfi, L., Petronio, C, Rolfo, M.F., Salari, L., 2017b. The Aggradational Successions of the Aniene River Valley in Rome: Age Constraints to Early Neanderthal Presence in Europe. PLoS ONE 12(1): e0170434. doi:10.1371/journal.pone.0170434

Marra, F., D'Ambrosio, E., Gaeta, M., Mattei, M., 2017c. Geochemical fingerprint of Tufo Lionato blocks from the *Area Sacra di Largo Argentina*: implications for the chronology of volcanic building stones in ancient Rome. Archaeometry. DOI:10.1111/arcm.12343

Masini, F., Sala, B., 2007. Large- and small-mammal distribution patterns and chronostratigraphic boundaries from the Late Pliocene to the Middle Pleistocene of the Italian peninsula. Quaternary International 160, 43-56.

Masotta, M., 2012. Magma differentiation in shallow, thermally zoned magma chambers: the example of Sabatini Volcanic District (central Italy). PhD thesis, Sapienza Università di Roma, Roma.

Masotta, M., Gaeta, M., Gozzi, F., Marra, F., Palladino, D.M., Sottili, G., 2010. H_2O – and temperature-zoning in magma chambers: the example of the Tufo Giallo della Via Tiberina eruptions (Sabatini Volcanic District, central Italy). Lithos 118 (1), 119-130. doi:10.1016/j.lithos.2010.04.004

Mattias, P.P., Ventriglia, U., 1970. La regione vulcanica dei monti Sabatini e Cimini. Mem. Soc. Geol. It. 95, 831-849.

Mazza, P., 1995. New evidence on the Pleistocene hippopotamuses of Western Europe.– Geol. Rom., 31, 61–241.

Milli, S., Mancini, M., Moscatelli, M., Stigliano, F., Marini, M., Cavinato, G.P., 2016. From river to shelf, anatomy of a high-frequency depositional sequence: the Late Pleistocene-Holocene Tiber Depositional Sequence. Sedimentology 591(63), 1886-1928.

Nomade, S., Renne, P.R., Vogel, N., Deino, A.L., Sharp, W.D., Becker, T.A., Jaouni, A.R., Mundil, R., 2005. Alder Creek sanidine (ACs-2), A Quaternary $^{40}Ar/^{39}Ar$ dating standard tied to the Cobb Mountain geomagnetic event. Chemical Geology 218, 315-338.

Palombo, M.R., 2004. Le mammalofaune della campagna romana: biocronologia, paleoambienti Escursione pre-congresso 2° Congresso GeoSed, Roma, 29 pp.

Pereira, A., Nomade, S., Falguères, C., Bahain, J-J., Tombret, O., Garcia, T., Voinchet, P., Bulgarelli, A.G., Anzidei, P., 2017. 40Ar/39Ar and ESR/U□series data for the La Polledrara di Cecanibbio archaeological site (Lazio, Italy). Journal of Archaeological Science: Reports, in press.

Pereira, A., Nomade, S., Moncel, M-H., Voinchet, P., Bahain, J-J., Biddittu, I., Falguères, C., Giaccio, B., Manzi, G., Parenti, F., Scardia, G., Scao, V., Sottili, G., Vietti., A., 2017. Geochronological evidences of a MIS 11 to MIS 10 age for several crucial Acheulian sites from the Frosinone province (Latium, Italy): Archaeological implications**.** Submitted to Quaternary Science Reviews.

Perini, G., Francalanci, L., Davidson, J.P., Conticelli, S., 2004. Evolution and genesis of magmas from Vico volcano, Central Italy: multiple differentiation pathways and variable parental magmas: Journal of Petrology 45, 139–182.

Perrone, F., 2016. Il sito di Collina Barbattini nella Biocronologia della Campagna Romana. Unpublished thesis, Università La Sapienza, Rome.

Petronio, C., 1995. Note on the taxonomy of Pleistocene hippopotamuses. Ibex J.M.E. 3, 53–55.

Petronio, C., Petrucci, M., Salari, L., 2006. La volpe nel Pleistocene superiore della Puglia: indicazioni paleoambientali. Bollettino Museo Civico Storia Naturale di Verona 30, 59-78.

Petronio, C., Di Canzio, E., Salari, L., 2007. The Late Pleistocene and Holocene Mammals in Italy: new biochronological and paleoenvironmental data. Palaeontographica Abt. A 279, 147-157.

Petronio, C., Bellucci, L., Martinetto, E., Pandolfi, L., Salari, L., 2011. Biochronology and Palaeoenvironmental Changes from the Middle Pliocene to the Late Pleistocene in Central Italy. Geodiversitas 33, 485-517.

Petronio, C., Ceruleo, P., Marra, F., Pandolfi, L., Rolfo, M.F., Salari L., Sottili, G., 2017. A novel multidisciplinary bio- and geo-chronological approach for age determination of Palaeolithic bone artifacts in volcanic settings: An example from eastern Sabatini, Latium, Italy. Quaternary International 438, 81-89. http://dx.doi.org/10.1016/j.quaint.2017.02.010

Ponzi, G., 1866-67. Sui manufatti in focaja rinvenuti all'Inviolatella nella Campagna Romana e sull'uomo all'epoca della pietra. Atti della Accademia Pontificia de' Nuovi Lincei 20, 41-52.

Ponzi, G., 1873. Oggetti preistorici spediti dal Gabinetto di Geologia e Mineralogia, Roma, p. 14.

Radmilli, A.M., Boschian, G., 1996. Storia della scoperta e degli scavi., in: Radmilli, A.M., Boschian, G. (Eds), Gli scavi a Castel di Guido. Il più antico giacimento di cacciatori del Paleolitico inferiore nell'Agro Romano. Istituto Italiano di Preistoria e Protostoria, Firenze, 19-29.

Radmilli, A.M., Mallegni, F., Longo, E., Mariani, R., 1979. Reperto umano con industria acheuleana rinvenuto presso Roma. Atti Società Toscana Scienze Naturali, Mem. A 86, 203-214.

Regattieri, E., Giaccio, B., Zanchetta, G., Drysdale, R.N., Galli, P., Nomade, S., Peronace, E., Wulf, S., 2015. Hydrological variability over the Apennines during the Early Last Glacial precession minimum, as revealed by a stable isotope record from Sulmona basin, Central Italy. J. Quat. Sci. 30, 19-31.

Sabol, M., 2014. *Panthera fossilis* (Reichenau, 1906) (Felidae, Carnivora) from Za Hájovnou Cave (Moravia, the Czech Republic): a fossil record from 1987-2007. Acta Mus. Nat. Pragae, Ser. B, Hist. Nat. 70, 59-70.

Sala, B., Barbi, G., 1996. Descrizione della fauna, in: Radmilli, A.M., Boschian, G. (Eds), Gli scavi a Castel di Guido. Il più antico giacimento di cacciatori del Paleolitico inferiore nell'Agro Romano. Istituto Italiano di Preistoria e Protostoria, Firenze, 49-90.

Salari, L., Achino, K.F., Gatta, M., Petronio, C., Rolfo, M.F., Silvestri, L., Pandolfi, L., 2017. The wolf from Grotta Mora Cavorso (Simbruini Mountains, Latium) within the evolution of *Canis lupus* L., 1758 in the Quaternary of Italy. Palaeogeography Palaeoclimatology Palaeoecology 476, 90-105.

Salari, L., Ceruleo, P., Pandolfi, L., Petronio, C., Marra, F., 2015. Una nuova età nel MIS 7 per la fauna di Saccopastore (bassa valle dell'Aniene, Roma). Atti 8° Convegno Nazionale di Archeozoologia, Lecce 11-14 novembre 2015.

Santucci, E., Marano, F., Cerilli, E., Fiore, I., Lemorini, C., Palombo, M.R., Anzidei, A.P., Bulgarelli, G.M., 2016. Palaeoloxodon exploitation at the Middle Pleistocene site of La Polledrara di Cecanibbio (Rome, Italy). Quaternary international 406, 169-182.

Sardella, R., Palombo, M.R., Petronio, C., Bedetti, C., Pavia, M., 2006. The early Middle Pleistocene large mammal faunas of Italy: An overview. Quaternary International 149, 104-109.

Schreve, D.C., Bridgland, D.R., 2002. Correlation of English and German Middle Pleistocene fluvial sequences based on mammalian biostratigraphy. Netherlands Journal of Geosciences / Geologie en Mijnbouw 81 (3-4), 357-373.

Segre, A.G., 1948. Sulla stratigrafia dell'antica cava di Saccopastore presso Roma. Rendiconti Accademia Nazionale Lincei (Cl. Scienze FMN) 4 (s. 8), 743-751.

Sottili G., Palladino D.M., Zanon V., 2004. Plinian activity during the early eruptive history of the Sabatini Volcanic District, Central Italy. J. Volcanol. Geotherm. Res. 135, 361-379.

Sottili, G., Palladino, D.M., Marra, F., Jicha, B., Karner, D.B.,and Renne, P., 2010. Geochronology of the most recent activity in the Sabatini Volcanic District, Roman Province, central Italy, Journal of Volcanology and Geothermal Research 196, 20-30.

Villa, P., Soriano, S., Grün, R., Marra, F., Nomade, S., Pereira, A., Boschian, G., Pollarolo, L., Fang, F., Bahain, J.J., 2016. The Acheulian and early Middle Paleolithic in Central Italy: Stability and Innovation. PLoS ONE 11(8): e0160516. doi:10.1371/journal.pone.0160516.

Yamaguchi, N., Driscoll, C.A., Kitchener, A.C., Ward, J.M ., Macdonald, D.W., 2004. Craniological differentiation between European wildcats (*Felis silvestris silvestris*), African wildcats (*F. s. lybica*) and Asian wildcats (*F. s. ornata*): implications for their evolution and conservation. Biological Journal of the Linnean Society 83, 47-63.

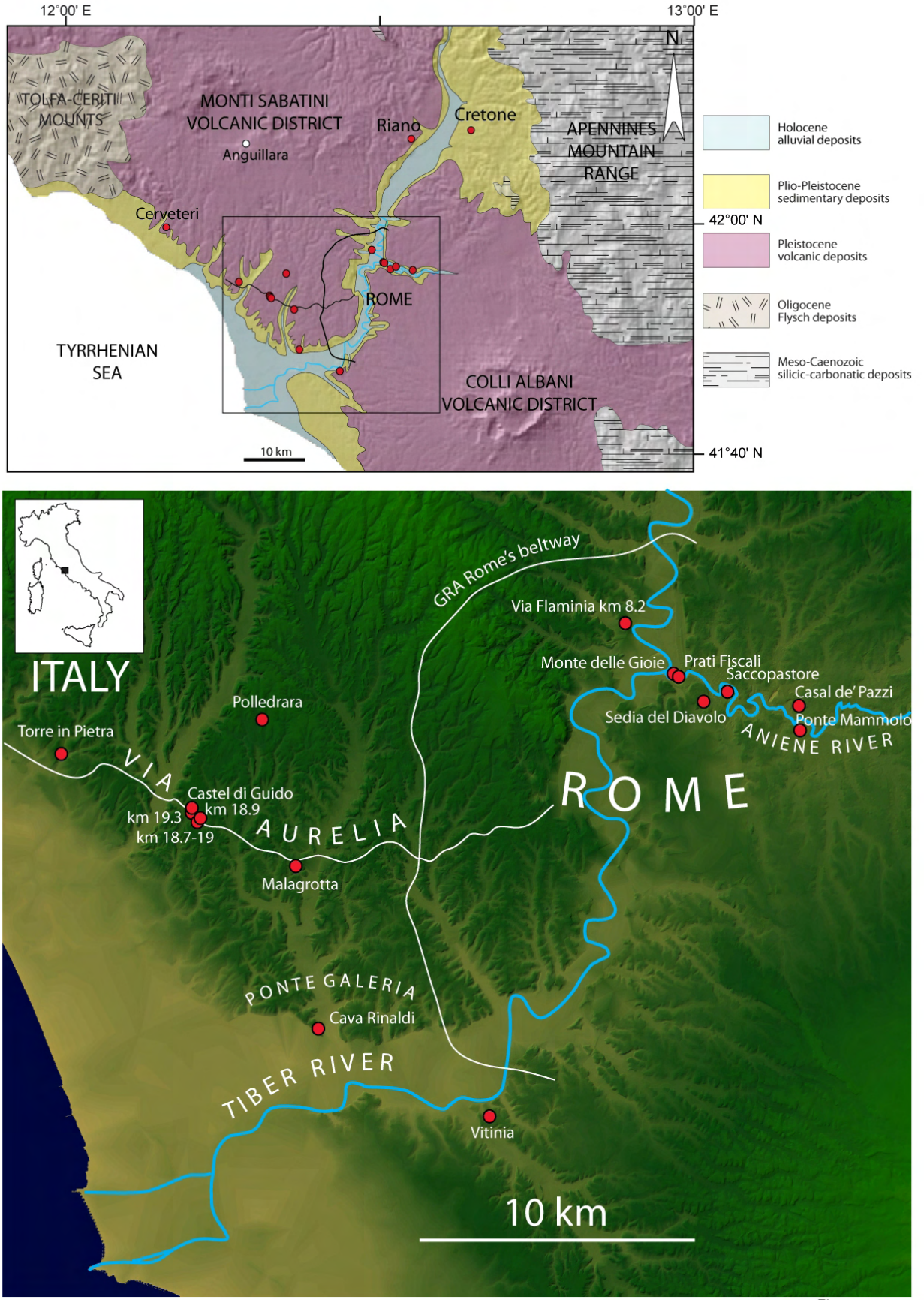
12°00' E
13°00' E
N
TOLFA-CERITI MOUNTS
MONTI SABATINI VOLCANIC DISTRICT
Anguillara
Riano
Cretone
APENNINES MOUNTAIN RANGE
Cerveteri
ROME
TYRRHENIAN SEA
COLLI ALBANI VOLCANIC DISTRICT
10 km
42°00' N
41°40' N
Holocene alluvial deposits
Plio-Pleistocene sedimentary deposits
Pleistocene volcanic deposits
Oligocene Flysch deposits
Meso-Caenozoic silicic-carbonatic deposits
ITALY
GRA Rome's beltway
Via Flaminia km 8.2
Monte delle Gioie
Prati Fiscali
Saccopastore
Casal de' Pazzi
Sedia del Diavolo
Ponte Mammolo
ANIENE RIVER
Polledrara
Torre in Pietra
VIA
Castel di Guido
km 18.9
km 19.3
km 18.7-19
AURELIA
ROME
Malagrotta
PONTE GALERIA
Cava Rinaldi
TIBER RIVER
Vitinia
10 km

Figure 1

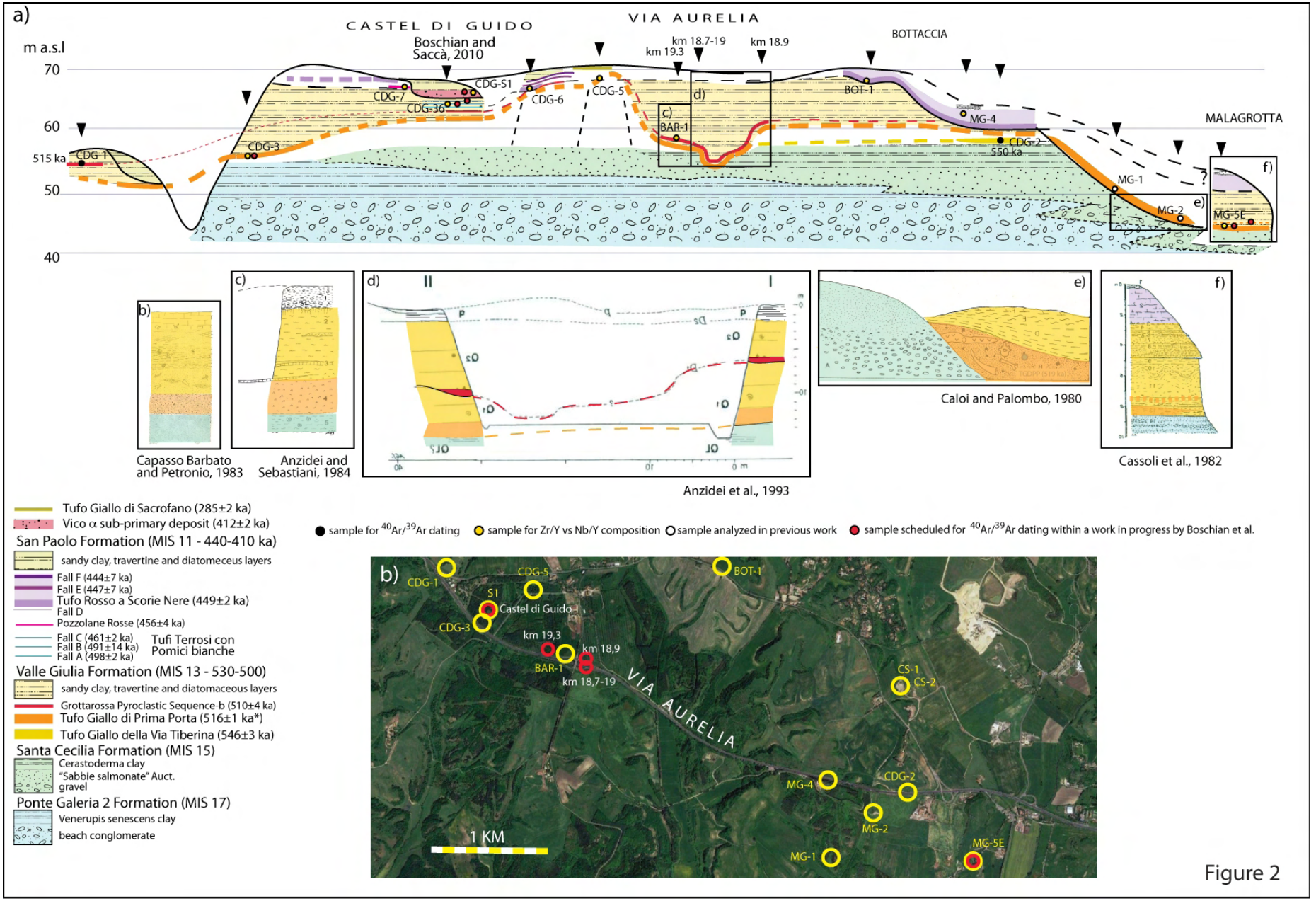
a)
CASTEL DI GUIDO
VIA AURELIA
BOTTACCIA
MALAGROTTA
m a.s.l
70
60
50
40
515 ka
550 ka
Boschian and Saccà, 2010
km 18,7-19
km 19.3
km 18.9
CDG-1
CDG-3
CDG-7
CDG-36
CDG-S1
CDG-6
CDG-5
BAR-1
BOT-1
MG-4
CDG-2
MG-1
MG-2
MG-5E
b)
c)
d)
e)
f)
Capasso Barbato and Petronio, 1983
Anzidei and Sebastiani, 1984
Anzidei et al., 1993
Caloi and Palombo, 1980
Cassoli et al., 1982
Tufo Giallo di Sacrofano (285±2 ka)
Vico α sub-primary deposit (412±2 ka)
San Paolo Formation (MIS 11 - 440-410 ka)
sandy clay, travertine and diatomeceus layers
Fall F (444±7 ka)
Fall E (447±7 ka)
Tufo Rosso a Scorie Nere (449±2 ka)
Fall D
Pozzolane Rosse (456±4 ka)
Fall C (461±2 ka)
Fall B (491±14 ka)
Fall A (498±2 ka)
Tufi Terrosi con Pomici bianche
Valle Giulia Formation (MIS 13 - 530-500)
sandy clay, travertine and diatomaceous layers
Grottarossa Pyroclastic Sequence-b (510±4 ka)
Tufo Giallo di Prima Porta (516±1 ka*)
Tufo Giallo della Via Tiberina (546±3 ka)
Santa Cecilia Formation (MIS 15)
Cerastoderma clay
"Sabbie salmonate" Auct.
gravel
Ponte Galeria 2 Formation (MIS 17)
Venerupis senescens clay
beach conglomerate
sample for 40Ar/39Ar dating
sample for Zr/Y vs Nb/Y composition
sample analyzed in previous work
sample scheduled for 40Ar/39Ar dating within a work in progress by Boschian et al.
b)
CDG-1
CDG-5
S1
Castel di Guido
CDG-3
km 19,3
km 18,9
BAR-1
km 18,7-19
BOT-1
VIA AURELIA
CS-1
CS-2
MG-4
CDG-2
MG-2
MG-1
MG-5E
1 KM

Figure 2

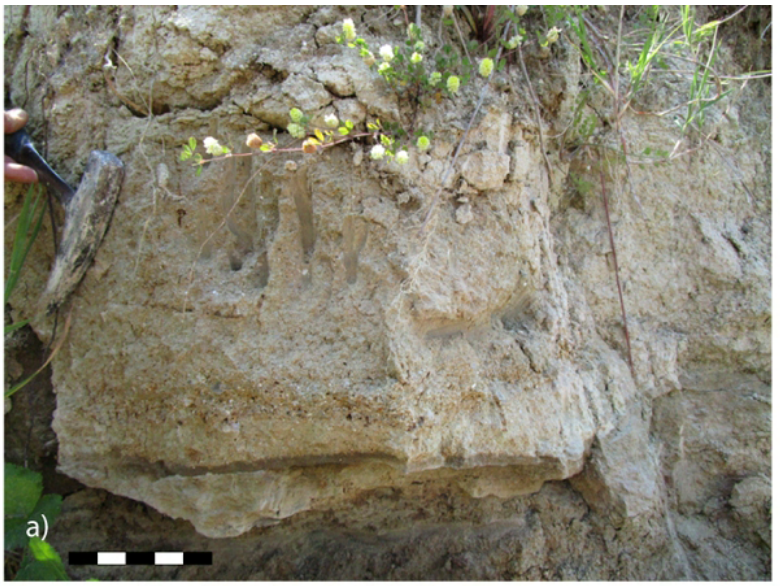

CDG 2 - Via Aurelia km 15.9 - Tufo Giallo della Via Tiberina

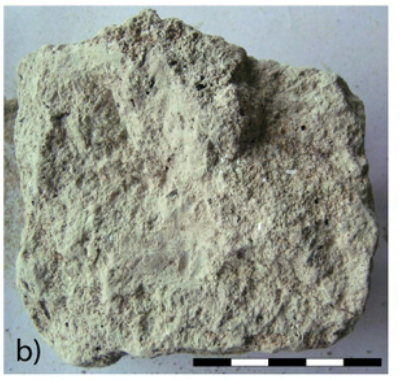

CS2- Casale Selce - Tufo Giallo di Prima Porta

CS3- Casale Selce - Tufo Giallo di Prima Porta

MG-5D- Malagrotta - Tufo Giallo di Prima Porta

MG1- Casal Bruciato -
Tufo Giallo di Prima Porta

NCR4 - Cava Rinaldi - Tufo Giallo di Prima Porta

MG2- Casal Bruciato - Tufo Giallo di Prima Porta

Via Aurelia km 19 - Tufo Giallo di Prima Porta

CDG3 - Tufo Giallo di Prima Porta

CDG1 - Tufo Giallo di Prima Porta

CDG5 - Tufo Giallo di Prima Porta

CDG8 - Grottarossa Pyroclastc Sequencea

CDG6 - Tufo Rosso a Scorie Nere

MG4 - "leucititic tuff"

BAR1 - Grottarossa
Pyroclastc Sequencea

Figure 3

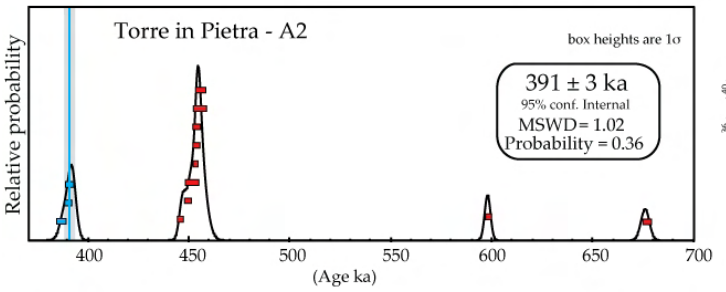
Torre in Pietra - A2
box heights are 1σ
391 ± 3 ka
95% conf. Internal
MSWD = 1.02
Probability = 0.36
Relative probability
(Age ka)

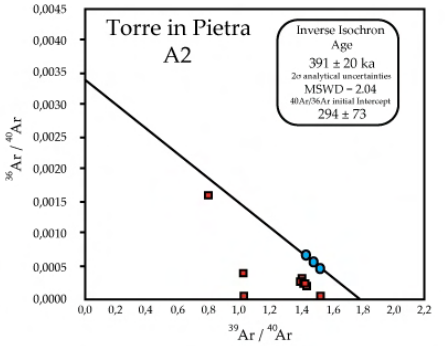
Torre in Pietra
A2
Inverse Isochron
Age
391 ± 20 ka
2σ analytical uncertainties
MSWD = 2.04
40Ar/36Ar initial Intercept
294 ± 73
36Ar / 40Ar
39Ar / 40Ar

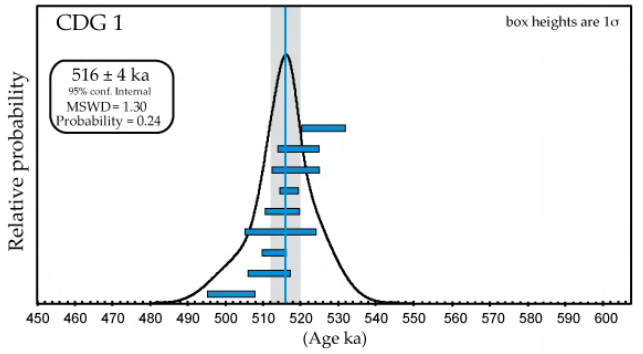
CDG 1
box heights are 1σ
516 ± 4 ka
95% conf. Internal
MSWD = 1.30
Probability = 0.24
Relative probability
(Age ka)

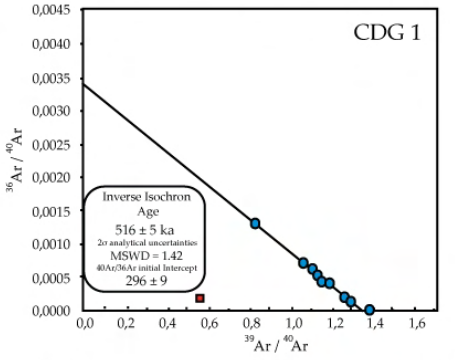
CDG 1
Inverse Isochron
Age
516 ± 5 ka
2σ analytical uncertainties
MSWD = 1.42
40Ar/36Ar initial Intercept
296 ± 9
36Ar / 40Ar
39Ar / 40Ar

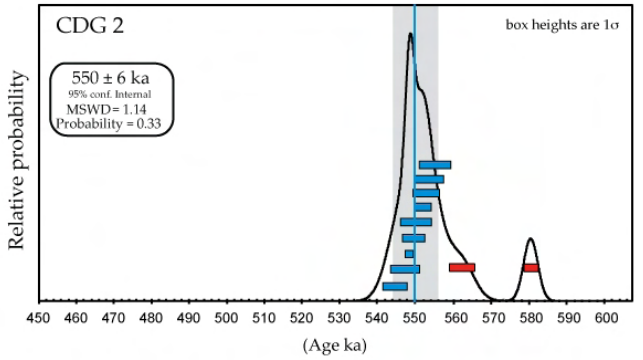
CDG 2
box heights are 1σ
550 ± 6 ka
95% conf. Internal
MSWD = 1.14
Probability = 0.33
Relative probability
(Age ka)

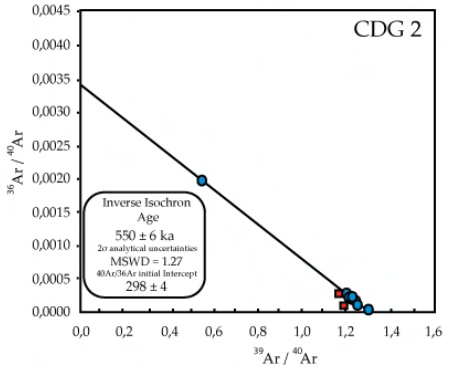
CDG 2
Inverse Isochron
Age
550 ± 6 ka
2σ analytical uncertainties
MSWD = 1.27
40Ar/36Ar initial Intercept
298 ± 4
36Ar / 40Ar
39Ar / 40Ar

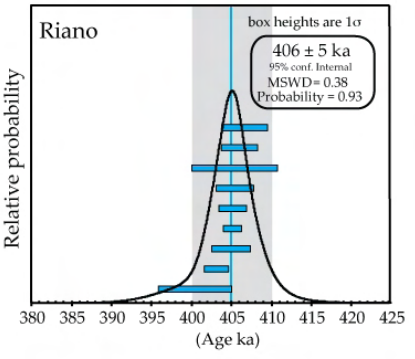
Riano
box heights are 1σ
406 ± 5 ka
95% conf. Internal
MSWD = 0.38
Probability = 0.93
Relative probability
(Age ka)

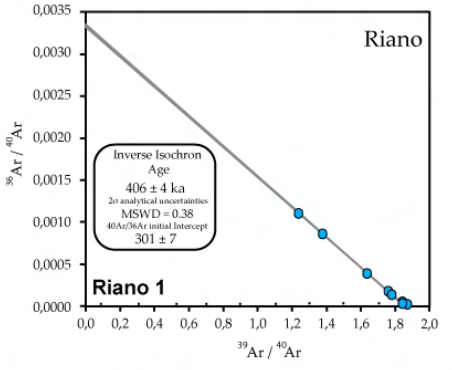
Riano
Inverse Isochron
Age
406 ± 4 ka
2σ analytical uncertainties
MSWD = 0.38
40Ar/36Ar initial Intercept
301 ± 7
Riano 1
36Ar / 40Ar
39Ar / 40Ar

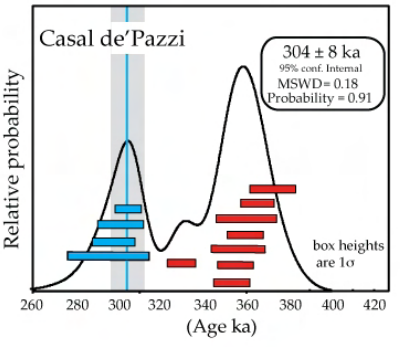
Casal de'Pazzi
304 ± 8 ka
95% conf. Internal
MSWD = 0.18
Probability = 0.91
box heights
are 1σ
Relative probability
(Age ka)

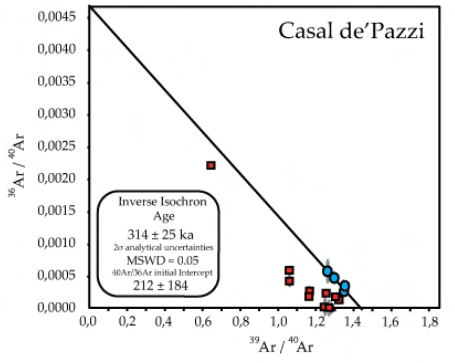
Casal de'Pazzi
Inverse Isochron
Age
314 ± 25 ka
2σ analytical uncertainties
MSWD = 0.05
40Ar/36Ar initial Intercept
212 ± 184
36Ar / 40Ar
39Ar / 40Ar

Figure 4

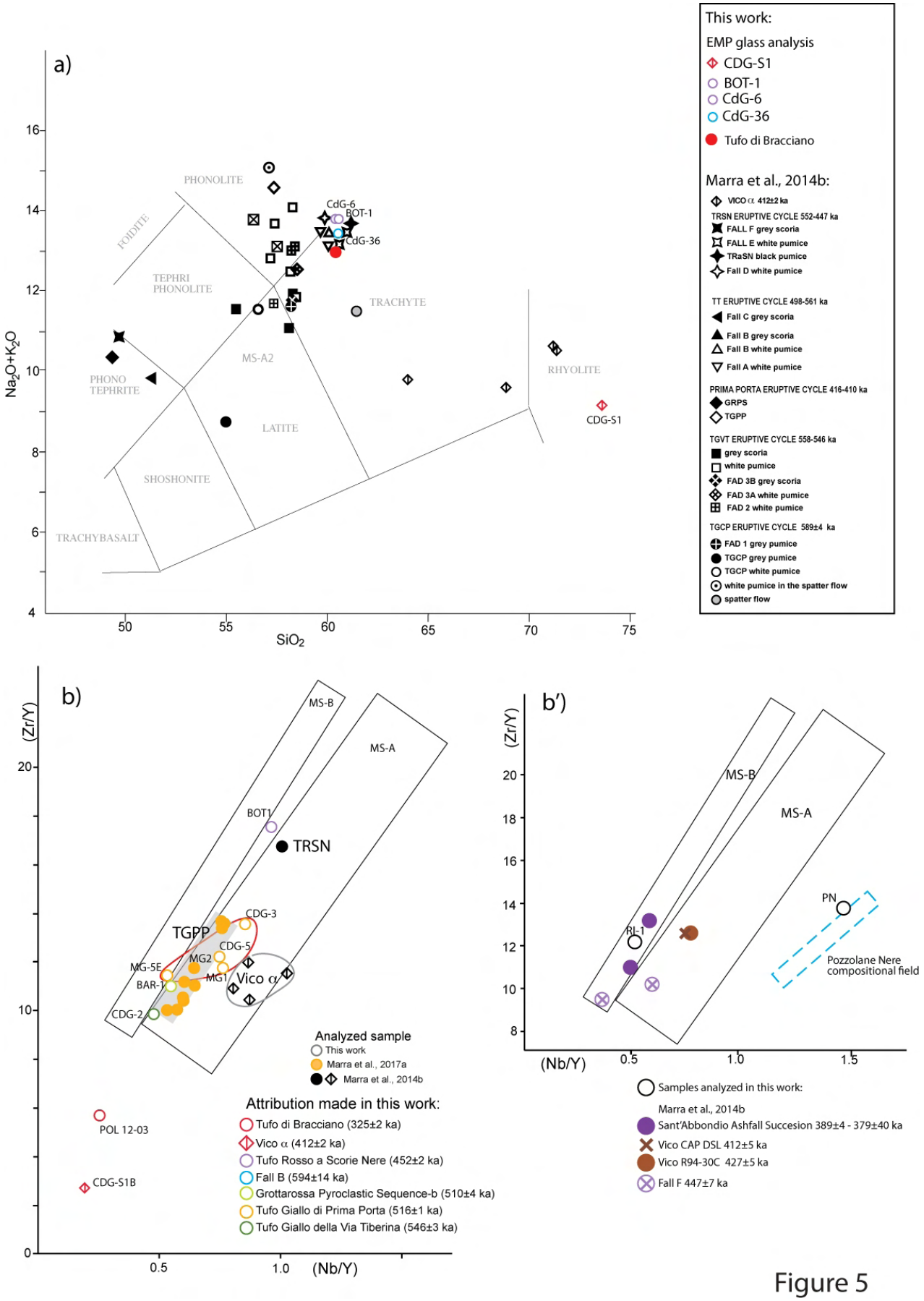
a)
PHONOLITE
FOIDITE
TEPHRI PHONOLITE
TRACHYTE
MS-A2
PHONO TEPHRITE
RHYOLITE
LATITE
SHOSHONITE
TRACHYBASALT
CdG-6
BOT-1
CdG-36
CDG-S1
Na2O+K2O
SiO2
This work:
EMP glass analysis
CDG-S1
BOT-1
CdG-6
CdG-36
Tufo di Bracciano
Marra et al., 2014b:
VICO α 412±2 ka
TRSN ERUPTIVE CYCLE 552-447 ka
FALL F grey scoria
FALL E white pumice
TRaSN black pumice
Fall D white pumice
TT ERUPTIVE CYCLE 498-561 ka
Fall C grey scoria
Fall B grey scoria
Fall B white pumice
Fall A white pumice
PRIMA PORTA ERUPTIVE CYCLE 416-410 ka
GRPS
TGPP
TGVT ERUPTIVE CYCLE 558-546 ka
grey scoria
white pumice
FAD 3B grey scoria
FAD 3A white pumice
FAD 2 white pumice
TGCP ERUPTIVE CYCLE 589±4 ka
FAD 1 grey pumice
TGCP grey pumice
TGCP white pumice
white pumice in the spatter flow
spatter flow
b)
(Zr/Y)
(Nb/Y)
MS-B
MS-A
BOT1
TRSN
TGPP
CDG-3
CDG-5
MG2
MG1
MG-5E
BAR-1
CDG-2
Vico α
Analyzed sample
This work
Marra et al., 2017a
Marra et al., 2014b
Attribution made in this work:
Tufo di Bracciano (325±2 ka)
Vico α (412±2 ka)
Tufo Rosso a Scorie Nere (452±2 ka)
Fall B (594±14 ka)
Grottarossa Pyroclastic Sequence-b (510±4 ka)
Tufo Giallo di Prima Porta (516±1 ka)
Tufo Giallo della Via Tiberina (546±3 ka)
POL 12-03
CDG-S1B
b')
(Zr/Y)
(Nb/Y)
MS-B
MS-A
PN
RL-1
Pozzolane Nere compositional field
Samples analyzed in this work:
Marra et al., 2014b
Sant'Abbondio Ashfall Succesion 389±4 - 379±40 ka
Vico CAP DSL 412±5 ka
Vico R94-30C 427±5 ka
Fall F 447±7 ka

Figure 5

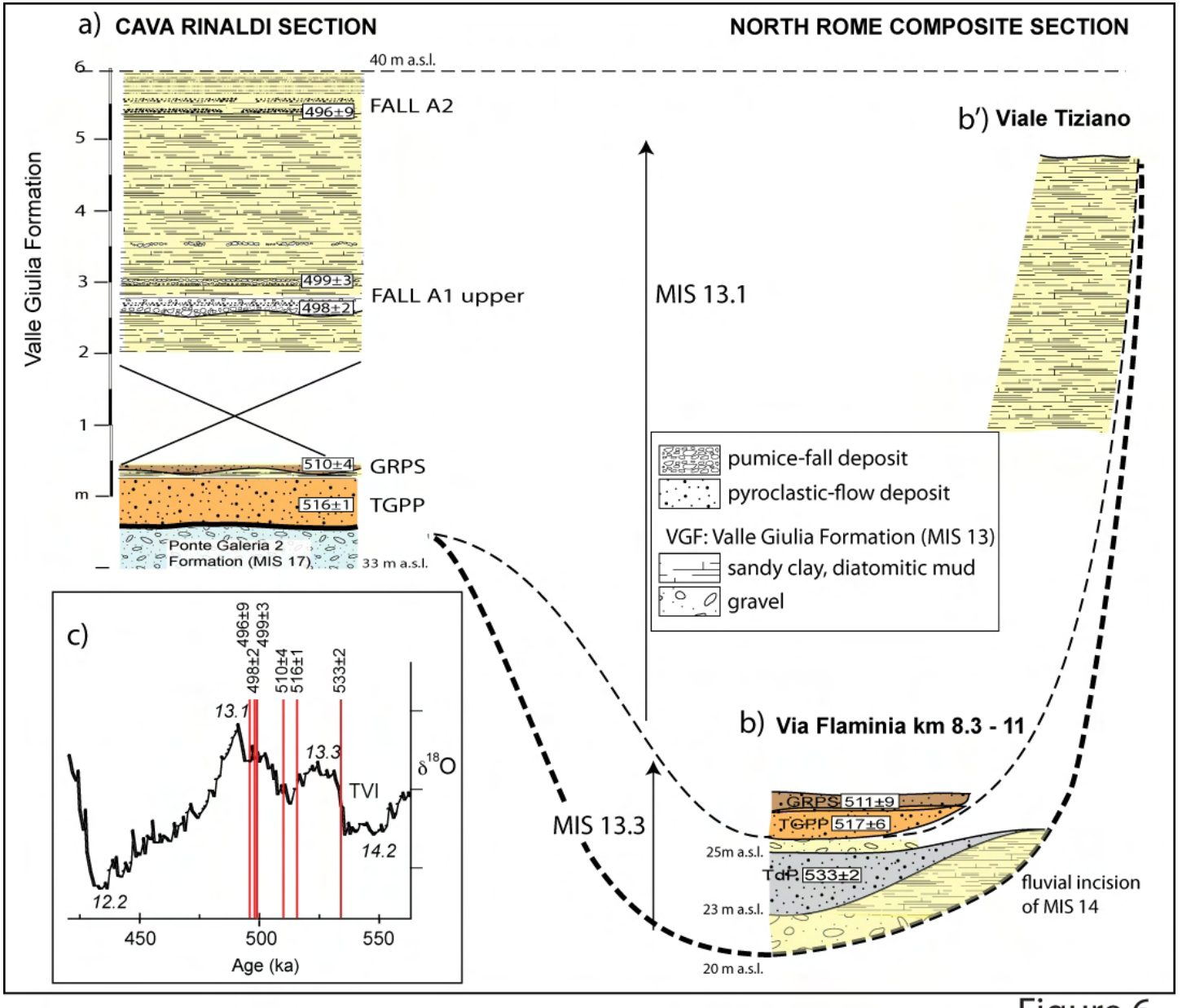
a) CAVA RINALDI SECTION
NORTH ROME COMPOSITE SECTION
40 m a.s.l.
Valle Giulia Formation
6
5
4
3
2
1
m
496±9
FALL A2
499±3
498±2
FALL A1 upper
510±4
GRPS
516±1
TGPP
Ponte Galeria 2
Formation (MIS 17)
33 m a.s.l.
b') Viale Tiziano
MIS 13.1
pumice-fall deposit
pyroclastic-flow deposit
VGF: Valle Giulia Formation (MIS 13)
sandy clay, diatomitic mud
gravel
b) Via Flaminia km 8.3 - 11
GRPS 511±9
TGPP 517±6
25m a.s.l.
TdP 533±2
23 m a.s.l.
fluvial incision
of MIS 14
MIS 13.3
20 m a.s.l.
c)
496±9
499±3
498±2
510±4
516±1
533±2
13.1
13.3
TVI
14.2
12.2
δ18O
450
500
550
Age (ka)

Figure 6

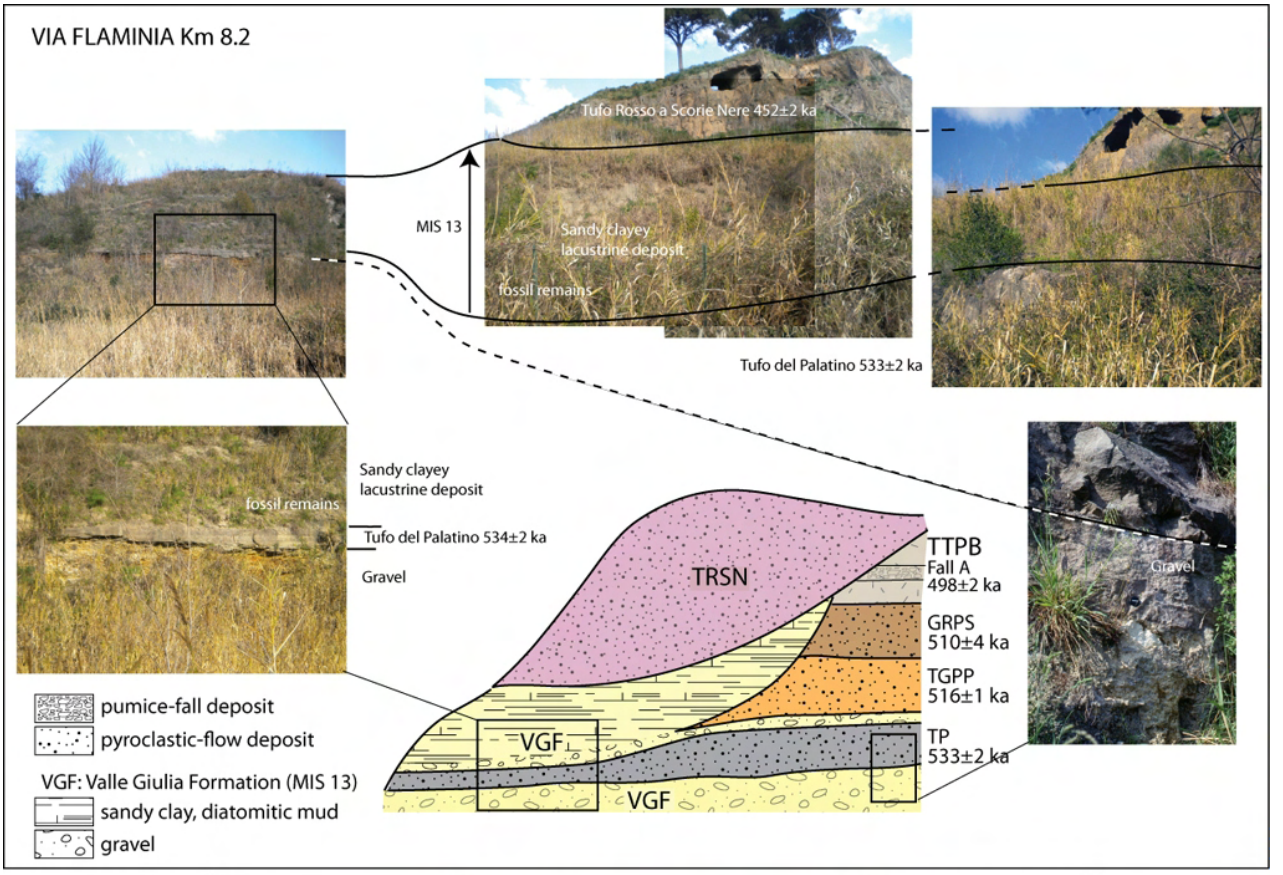
VIA FLAMINIA Km 8.2
Tufo Rosso a Scorie Nere 452±2 ka
MIS 13
Sandy clayey lacustrine deposit
fossil remains
Tufo del Palatino 533±2 ka
fossil remains
Sandy clayey lacustrine deposit
Tufo del Palatino 534±2 ka
Gravel
TRSN
TTPB Fall A 498±2 ka
GRPS 510±4 ka
TGPP 516±1 ka
TP 533±2 ka
VGF
VGF
Gravel
pumice-fall deposit
pyroclastic-flow deposit
VGF: Valle Giulia Formation (MIS 13)
sandy clay, diatomitic mud
gravel

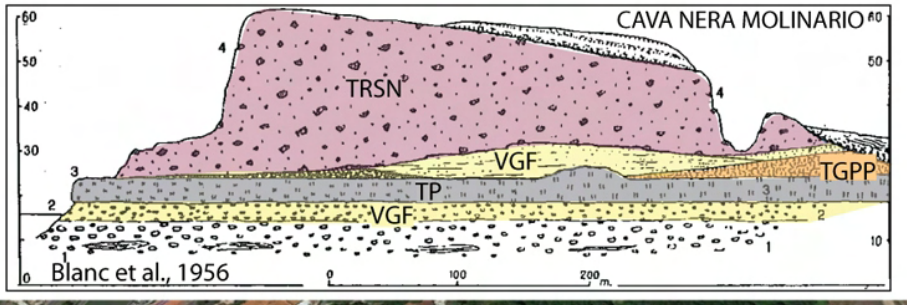
CAVA NERA MOLINARIO
TRSN
VGF
TP
VGF
TGPP
Blanc et al., 1956
0
100
200 m.


Tufo Rosso a Scorie Nere
Valle Giulia Formation
Cava Nera Molinario
TRSN
TRSN
Tufo del Palatino 530 ka
Valle Giulia Fm
TP
gravel
Via Flaminia, km 8.2

Figure 7

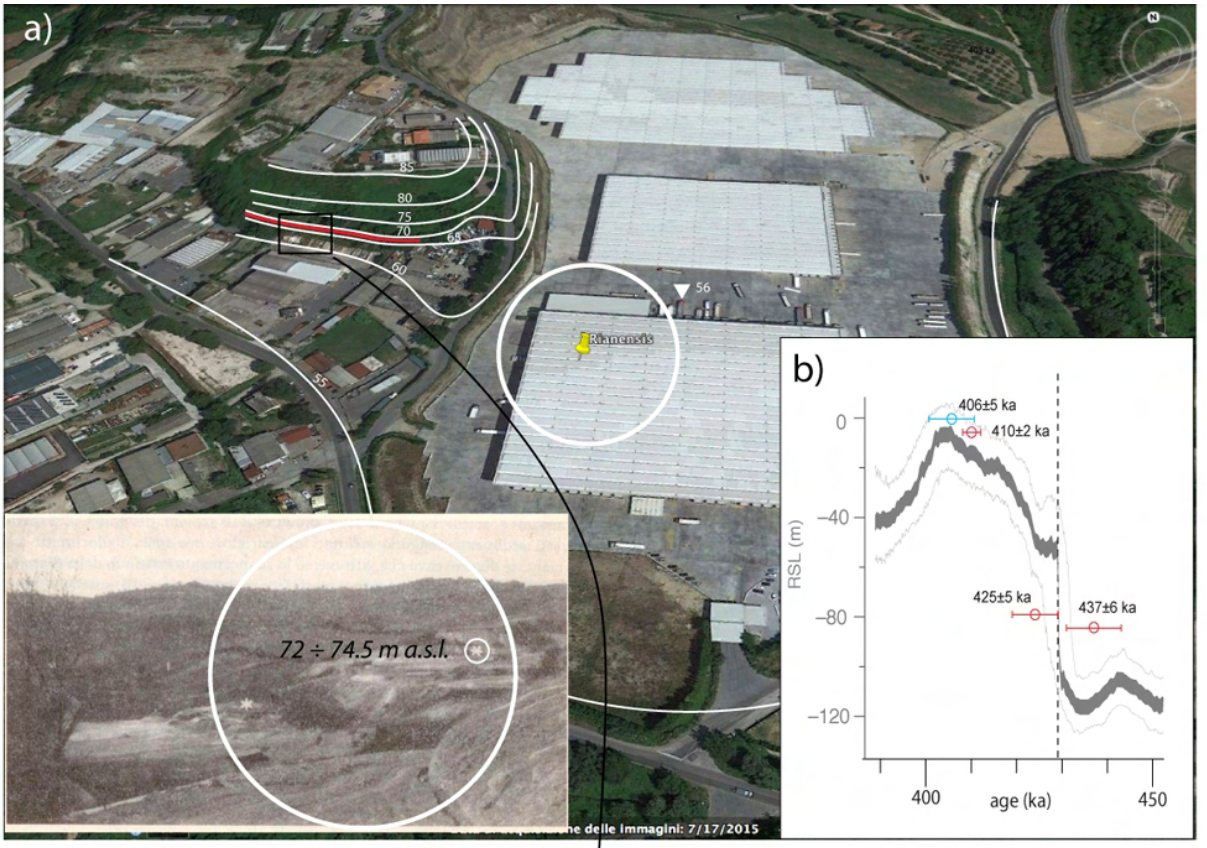
a)
85
80
75
70
65
60
55
56
Rianensis
72 ÷ 74.5 m a.s.l.
b)
406±5 ka
410±2 ka
425±5 ka
437±6 ka
RSL (m)
0
−40
−80
−120
400
age (ka)
450

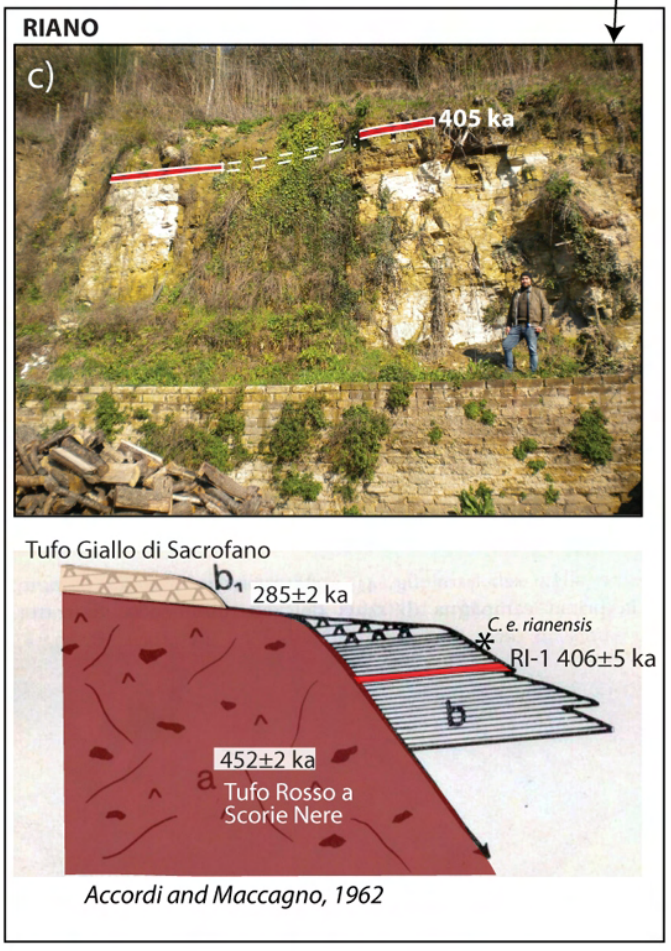
RIANO
c)
405 ka
Tufo Giallo di Sacrofano
b1
285±2 ka
C. e. rianensis
RI-1 406±5 ka
b
452±2 ka
a
Tufo Rosso a Scorie Nere
Accordi and Maccagno, 1962

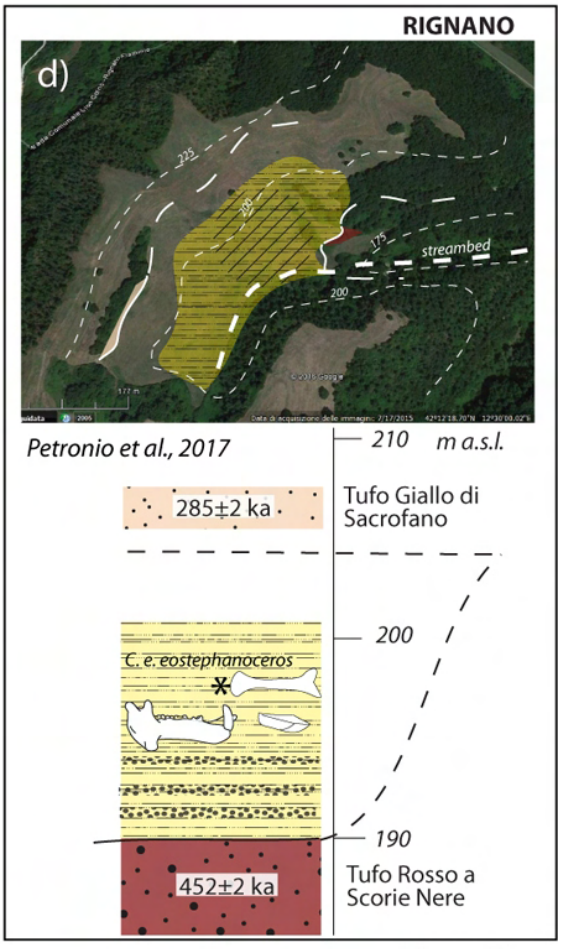
RIGNANO
d)
streambed
Petronio et al., 2017
210
m a.s.l.
285±2 ka
Tufo Giallo di Sacrofano
200
C. e. eostephanoceros
190
452±2 ka
Tufo Rosso a Scorie Nere

Figure 8

CASTEL DI GUIDO
Boschian and Saccà, 2010

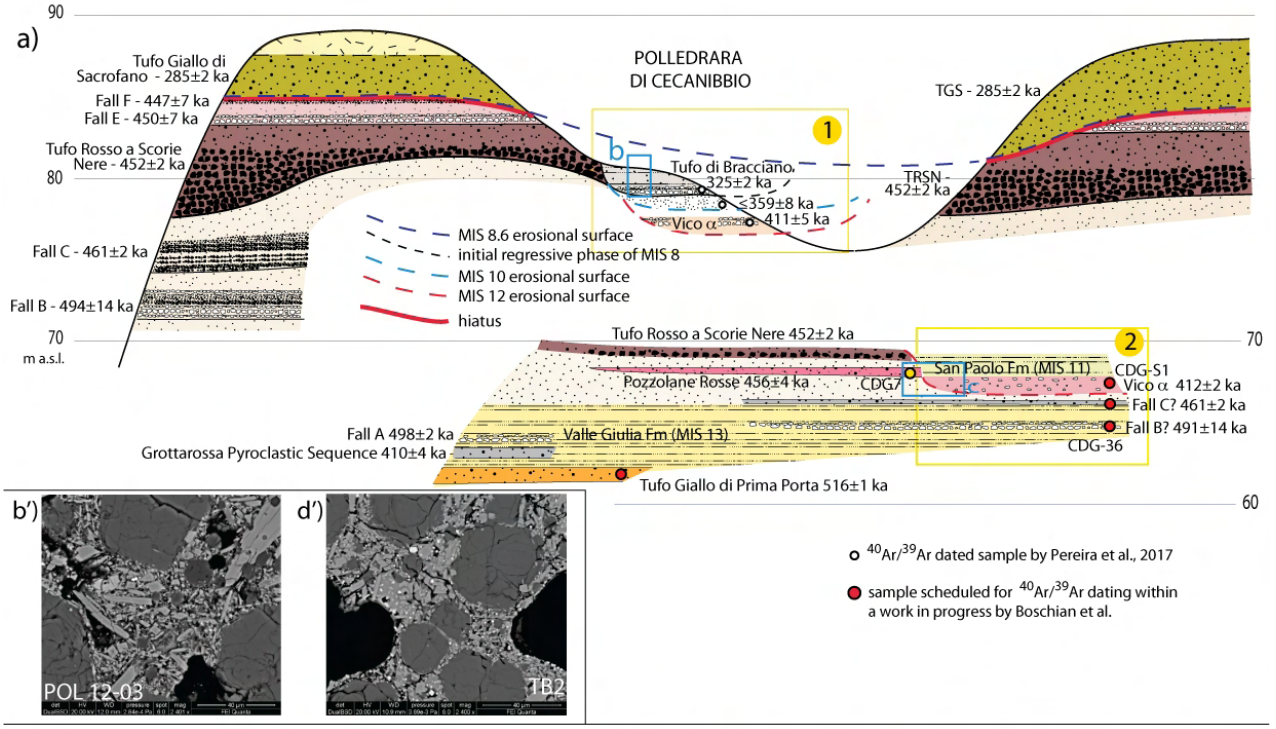

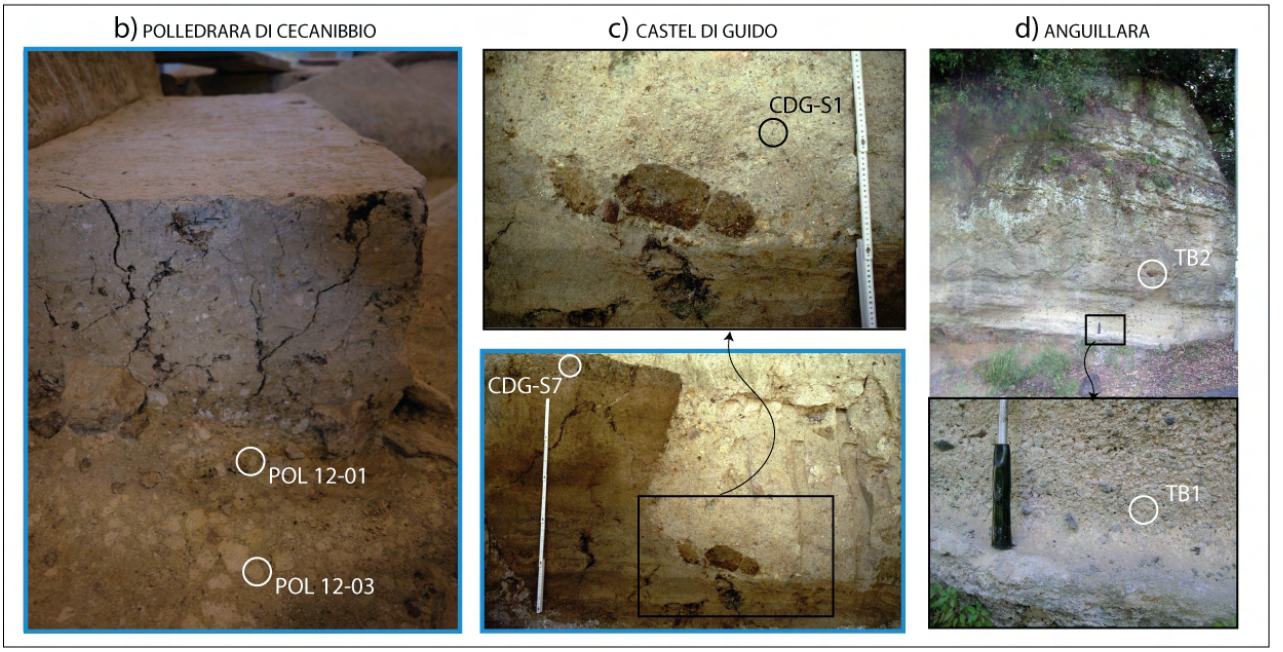

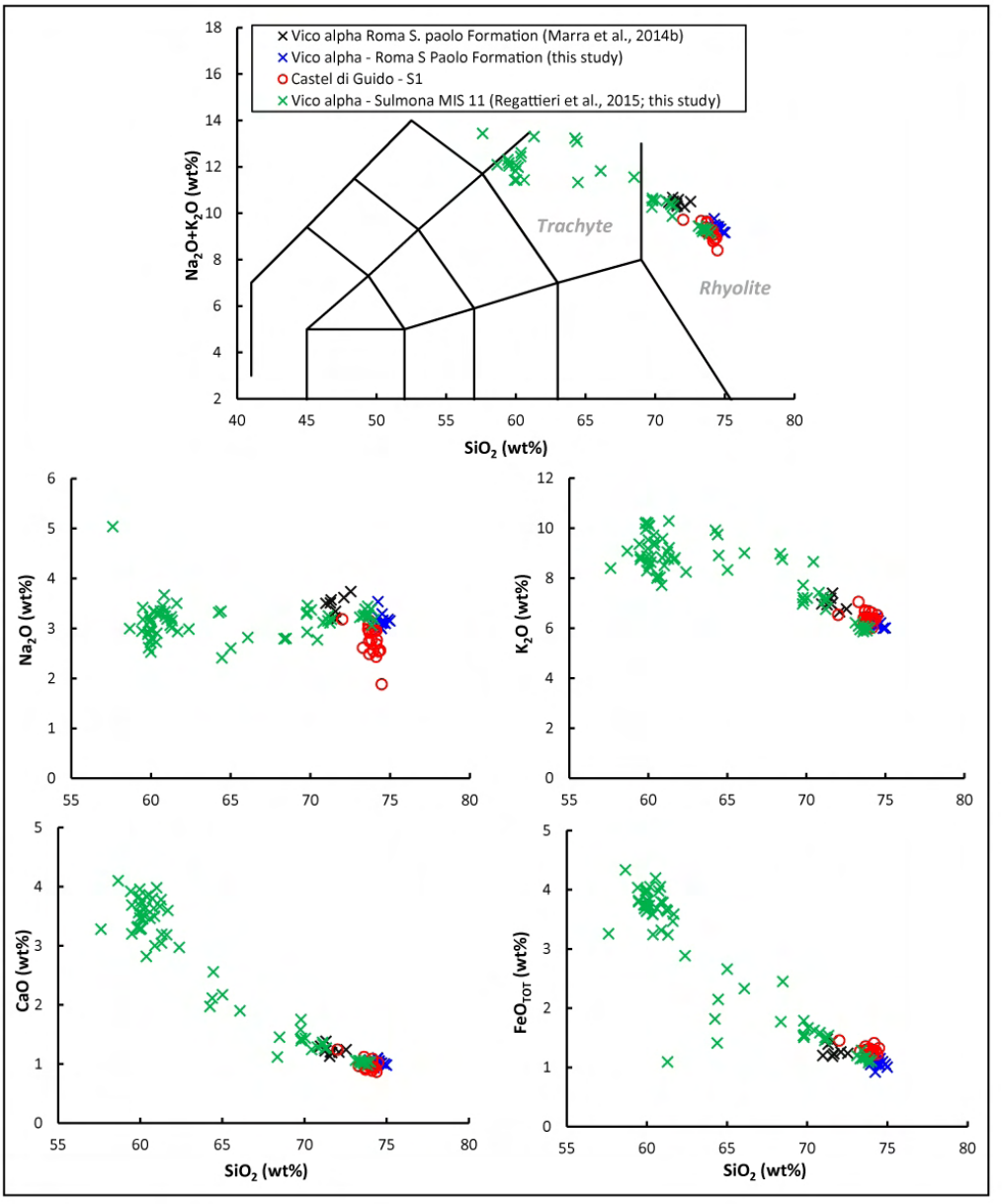
Vico alpha Roma S. paolo Formation (Marra et al., 2014b)
Vico alpha - Roma S Paolo Formation (this study)
Castel di Guido - S1
Vico alpha - Sulmona MIS 11 (Regattieri et al., 2015; this study)
Trachyte
Rhyolite
Na2O+K2O (wt%)
SiO2 (wt%)
Na2O (wt%)
K2O (wt%)
CaO (wt%)
FeOTOT (wt%)

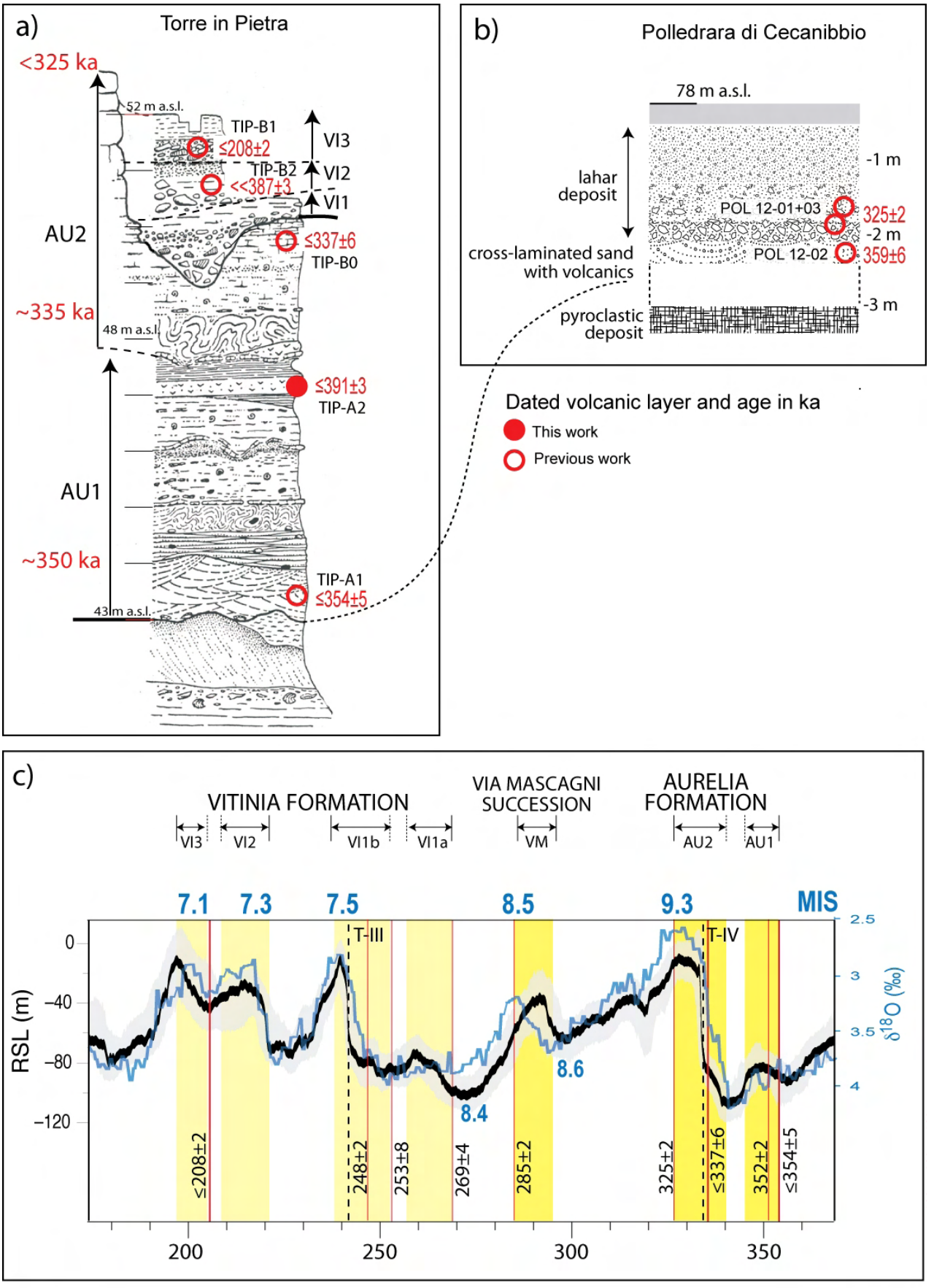
a)
Torre in Pietra
<325 ka
52 m a.s.l.
TIP-B1
≤208±2
TIP-B2
<<387±3
VI3
VI2
VI1
AU2
≤337±6
TIP-B0
~335 ka
48 m a.s.l.
≤391±3
TIP-A2
AU1
~350 ka
TIP-A1
≤354±5
43 m a.s.l.
b)
Polledrara di Cecanibbio
78 m a.s.l.
lahar deposit
-1 m
POL 12-01+03
325±2
-2 m
cross-laminated sand with volcanics
POL 12-02
359±6
-3 m
pyroclastic deposit
Dated volcanic layer and age in ka
This work
Previous work
c)
VITINIA FORMATION
VIA MASCAGNI SUCCESSION
AURELIA FORMATION
VI3
VI2
VI1b
VI1a
VM
AU2
AU1
7.1
7.3
7.5
8.5
9.3
MIS
T-III
T-IV
8.6
8.4
RSL (m)
0
−40
−80
−120
δ18O (‰)
2.5
3
3.5
4
≤208±2
248±2
253±8
269±4
285±2
325±2
≤337±6
352±2
≤354±5
200
250
300
350

Figure 11

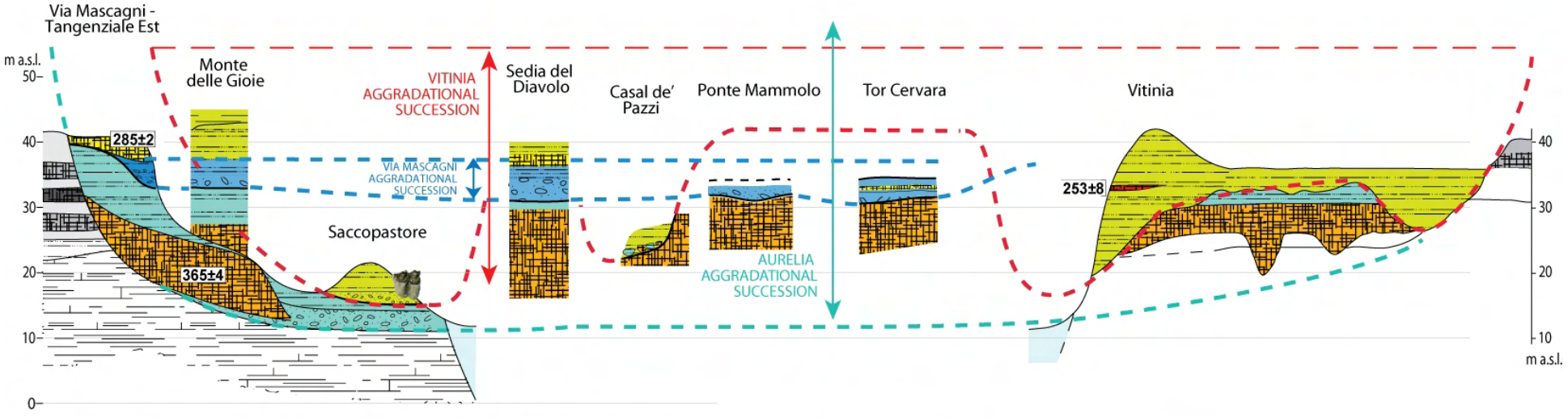

Aggradational succession

- MIS 1 — Modern Tiber Fm
- MIS 7 — Vitinia Fm
- MIS 8.5 — Via Mascagni succession
- MIS 9 — Aurelia Fm

Volcanic deposit

- Tufo Giallo di Sacrofano
- Tufo Lionato
- Older ash-fall and pyroclastic-flow deposits

Older aggradational successions

- clay
- sandy clay and travertine
- gravel
- marine clay Pliocene substrate

upper molar of *Dama dama tiberina*

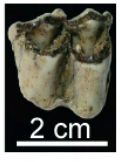

Figure 12

PREVIOUS ATTRIBUTION (Palombo, 2004, and references therein)	THIS WORK		
EARLY AURELIAN - TORRE IN PIETRA FU	FORMATION	MIS	AGE (ka)
Torre in Pietra lower level (1)	Aurelia Fm	9	355-335
Polledrara di Cecanibbio (2)	Aurelia Fm	9	325±2
Castel di Guido (Via Aurelia km 20)	San Paolo Fm	11	412±2
Riano Flaminio	San Paolo Fm	11	~406
Collina Barbattini, Via Aurelia km 18.9	Valle Giulia Fm	13	516-496
Via Aurelia km 19.3	Valle Giulia Fm	13	516-496
Malagrotta	Valle Giulia Fm	13	516±1
Cava Rinaldi upper level (3)	Valle Giulia Fm	13	516±1
Cretone (4)	Santa Cecilia Fm	15	>544±11 <585±4
Prati Fiscali	Via Mascagni succ.	8.5	~285
Sedia del Diavolo upper gravels (3)	Via Mascagni succ.	8.5	~285
Monte delle Gioie (3)	Via Mascagni succ.	8.5	~285
MIDDLE AURELIAN - VITINIA FU			
Vitinia upper level (5)	Vitinia Fm	7	~248
Torre in Pietra upper level (1)	Vitinia Fm	7.5	270-240
Casal de' Pazzi	Vitinia Fm	7	270-250
Cerveteri-Migliorie di San Paolo	Vitinia Fm	8.5/7	290-200
Via Flaminia km 8.2	Valle Giulia Fm	13	533±2
LATE AURELIAN			
Saccopastore (6)	Vitinia Fm	7	245-220

TABLE 1

TABLE 2
MIS 15 - SANTA CECILIA FORMATION - ISERNIA FU
Cretone *Palaeoloxodon antiquus*, *Bos primigenius*, *Dama* sp., *Cervus* sp.
MIS 13 - VALLE GIULIA FORMATION - FONTANA RANUCCIO FU
Cava Rinaldi *Ursus* sp, *Castor fiber*, *Bos primigenius*, *Elephas antiquus (=Palaeoloxodon antiquus)*, *Cervus* cf. *elaphus* (Ambrosetti, 1965). *Ursus spelaeus* (Capasso Barbato and Minieri,1987).
Via Aurelia km 18.7-19 (Collina Barbattini) and km 18.9 *Elephas antiquus (=Palaeoloxodon antiquus), Stephanorhinus* cf. *kirchbergensis, Hippopotamus sp.* (=cf. *Hippopotamus amphibius*), *Cervus (Dama)* cf. *clactonianus* (=*Dama clactoniana*), *Cervus (Dama)* cf. *dama* (=*Dama* sp.), *Cervus (Cervus) elaphus* (=*Cervus elaphus* ssp.), *Equus caballus* sp. (=*Equus ferus*), *Bos primigenius*, *Crocidura* cf. s*uaveolens, Rana* sp. (?*Rana dalmatina), Bufo viridis*, *Arvicola terrestris* (=*Arvicola* sp.), *Microtus arvalis vel Microtus agrestis* (Anzidei et al. 1993). From surface collection at Collina Barbattini: *Sus scrofa*, *Ursus* cf. *spelaeus, Panthera* cf. *spelaea, Equus ferus, Stephanorhinus* cf. *kirchbergensis*, Aves indet. (F. Perrone, unpublished Thesis).
Via Aurelia km 19.3 *Bos* sp., *Cervus* sp., *Elephas* sp. (Anzidei and Sebastiani, 1984). *Elephas* sp. *(?Palaeoloxodon antiquus)*, *Dicerorhinus hemitoechus (=Stephanorhinus hemitoechus)*, *Bos primigenius*, *Hippopotamus* cf. *antiquus*, *Dama* sp., *Cervus elaphus* ssp. (Capasso Barbato and Petronio, 1981).
Malagrotta *Elephas antiquus (=Palaeoloxodon antiquus)*, *Equus caballus (=Equus ferus)*, *Canis lupus*[1], *Dicerorhinus* cf. *hemitoechus (=Stephanorhinus* cf. *hemitoechus)*, *Sus scrofa*, *Hippopotamus* sp., *Cervus elaphus, Dama* cf. *clactoniana*, *Capreolus capreolus*, *Bos primigenius, Castor* sp., *Oryctolagus* sp (Caloi and Palombo, 1980). [1]attributed in this work to *Canis* sp.
MIS 11 - SAN PAOLO FORMATION - FONTANA RANUCCIO FU
Malagrotta Within the uppermost travertine layers occurring above the "leucititic tuff" at the top of the sedimentary succession of Malagrotta described by Cassoli et al. (1982): *Vulpes vulpes* (Capasso Barbato and Minieri, 1987).
Via Flaminia km 8.2 *Mammuthus chosaricus*, *Cervus elaphus rianensis*[2] (Kotsakis et al., 1979). [2]re-determined in this work as *Cervus elaphus* ssp.
Riano *Cervus elaphus rianensis* (Accordi and Maccagno, 1962). *Palaeoloxodon antiquus*, *Dama clactoniana* (Leonardi and Petronio, 1974).
Castel di Guido (Via Aurelia km 20) *Lepus* cf. *europeus*, *Canis lupus*, Canidae gen. e sp. indet., *Panthera leo*, *Elephas namadicus*, *Stephanorhinus* cf. *hundsheimensis*, *Equus caballus (=Equus ferus)*, *Hippopotamus* sp., *Cervus elaphus* cf. *rianensis*, *Bos primigenius* (Sala and Barbi, 1996). Recovered from surface collection in the surroundings of the area in the years preceding the excavations: *Elephas antiquus (=Palaeoloxodon antiquus)*, *Rhinoceros* sp., *Equus* sp., *Hippopotamus amphibius*, *Sus scrofa*, *Bos primigenius*, *Cervus elaphus*, *Dama* sp., *Capreolus capreolus*, *Felis leo spelaea*, *Canis lupus*, *Emys orbicularis* (in addition to undetermined remains of birds and fishes) Radmilli et al. (1979). *Canis lupus*, *Panthera spelaea* (Capasso Barbato and Minieri, 1987).
MIS 9 - AURELIA FORMATION - TORRE IN PIETRA FU
La Polledrara di Cecanibbio *Bos primigenius*, *Palaeoloxodon antiquus*, *Stephanorhinus* cf. *hemitoechus, Equus ferus, Macaca sylvanus*, *Lepus* sp., *Canis lupus*, *Vulpes vulpes*, *Meles meles*, *Sus scrofa*, *Cervus elaphus* ssp., *Felis silvestris*, *Bubalus murrensis* (Anzidei et al., 2012, and references therein). *Apodemus sylvaticus*, *Pliomys* cf. *episcopalis*, *Arvicola* sp., *Microtus (Iberomys)* cf. *breccensis* (Anzidei et al., 2004).
Torre in Pietra lower level *Glis glis, Oryctolagus cuniculus, Lepus* sp., *Palaeoloxodon antiquus*, *Equus ferus*, *Cervus elaphus rianensis*, *Bos primigenius*, *Canis lupus*, *Stephanorhinus hemitoechus*, *Sus scrofa*, *Megaloceros giganteus*, *Vulpes vulpes*, *Ursus spelaeus*, *Panthera spelaea* (Caloi and Palombo, 1978; Malatesta, 1978; Palombo 2004; Petronio et al., 2011).
Sedia del Diavolo ("lower level") *Meles meles, Palaeoloxodon antiquus, Stephanorhinus* cf. *hemitoechus, Dama sp. and Bos primigenius* (Caloi et al., 1980b) Two female skulls of *C. elaphus* recovered within the Tufo Lionato pyroclastic-flow deposit (365±a ka).
MIS 8.5 - VIA MASCAGNI SUCCESSION - VITINIA FU
Sedia del Diavolo ("upper gravel") *Canis* sp., *Stephanorhinus* sp., *Equus hydruntinus*, *Palaeoloxodon antiquus, Sus scrofa, Hippopotamus amphibius, Dama dama tiberina*, *Dama* cf. *clactoniana, Cervus elaphus* ssp. and *Bos primigenius* (Caloi et al., 1980b; Di Stefano et al., 1998)

Prati Fiscali *Panthera pardus, Stephanorhinus* sp.*., Stephanorhinus hemitoechus, Equus* sp.*., Equus hydruntinus, Hippopotamus* sp.*., Dama dama* ssp.*., Cervus elaphus* ssp.*., Bos primigenius, Palaeoloxodon antiquus* (Petronio et al., 2011). **Monte Sacro** *Ursus sp., Crocuta crocuta, Stehanorhinus sp., Equus* sp.*., Equus hydruntinus, Sus scrofa, Hippopotamus sp., Cervus elaphus* ssp.*., Bos primigenius, Palaeoloxodon antiquus*. (Petronio et al., 2011).
Batteria Nomentana *Dama dama tiberina* (Di Stefano and Petronio 1997; Di Stefano et al., 1998)
Ponte Mammolo *Canis lupus*, *Ursus spelaeus*, *Equus ferus*, *Megaloceros giganteus* and *Bos primigenius* (Biddittu et al., 1987).
Vigna San Carlo *Ursus* sp., *Stephanorhinus* sp., *Dama dama tiberina*, *Cervus elaphus* ssp., *Bos primigenius, Elephas antiquus (=Palaeoloxodon antiquus)* (Di Stefano et al., 1998).
MIS 8.5 - 7.0 - VITINIA FU
Cerveteri-Migliorie di San Paolo *Elephas* sp. (=*Palaeoloxodon antiquus*), *Equus caballus* cf. *piveteaui* (=*Equus ferus*), *Dicerorhinus* sp. (=*Stephanorhinus* sp.), *Dama dama* ssp.[(3)], *Cervus elaphus* ssp., *Bos primigenius* (Capasso Barbato et al., 1983). [(3)]re-determined as *D. d. tiberina* (Di Stefano and Petronio, 1997).
MIS 7 - VITINIA FORMATION - VITINIA FU
Vitinia Upper levels *Palaeoloxodon antiquus*, *Stephanorhinus hemitoechus*., *Cervus elaphus rianensis*, *Bos primigenius*, *Canis lupus*, *Vulpes vulpes*, *Dama dama tiberina* (Petronio et al., 2011).
Torre in Pietra upper level *Glis glis, Oryctolagus cuniculus, Lepus* sp.*., Palaeoloxodon antiquus*, *Equus ferus*, *Cervus elaphus rianensis*, *Bos primigenius*, *Canis lupus*, *Stephanorhinus hemitoechus*, *Sus scrofa*, *Megaloceros giganteus*, *Vulpes vulpes*, *Ursus spelaeus*, *Panthera spelaea, Castor fiber*, *Meles meles, Martes* sp., *Clethrionomys glareolus*, *Apodemus* sp., *Microtus arvalis-agrestis*, *Arvicola* sp., *Macaca sylvanus*, *Capreolus capreolus*, *Crocuta crocuta, Hippopotamus amphibius*, *Dama dama tiberina* (Caloi and Palombo, 1978; Malatesta, 1978; Palombo 2004; Petronio et al., 2011).
Saccopastore *Aquila heliaca*, *Panthera spelaea*, *Palaeoloxodon antiquus*, *Stephanorhinus* sp., *Equus ferus, Equus hydruntinus, Hippopotamus amphibius*, *Bos primigenius*, *Cervus elaphus* ssp., *Dama dama tiberina* (Salari et al., 2015; Marra et al., 2017b).
Casal de' Pazzi *Canis lupus, Crocuta crocuta, Palaeloxodon antiquus, Stephanorhinus sp., Equus ferus, Hippopotamus* cf. *amphibius, Sus scrofa, Cervus elaphus* ssp., *Dama dama* ssp., *Bos primigenius* (Caloi et al., 1988; Marra et al., 2017b).
MIS 5 - EPI-TYRRHENIAN FORMATION - MELPIGNANO FU
Fosso del Cupo *C. elaphus*, *B. primigenius, S. hemitoechus* (Ponzi, 1866-67). *Panthera spelaea*, *Vulpes vulpes*, *Sus scrofa*, *Equus hydruntinus*, *Dama dama dama* (Ceruleo et al., 2016).

Faunal lists reporting all the vertebrate taxa recovered at the investigated sites correlated with the MISs according to the chronostrotagraphic revision presented in this paper.

Names of the taxa are reported according to the cited literature, while updated and re-determined names are reported in brackets, when appropriate.

A review in the light of a new chronostratigraphic framework for the geologic sections and the faunal assemblages of Aurelian Mammal Age of Latium (Italy)

F. Marra[1], S. Nomade[2], A. Pereira[2,3,4,5], C. Petronio[6], L. Salari[6], G. Sottili[6], J.-J. Bahain[5], G. Boschian[7], G. Di Stefano[6], C. Falguéres[5], F. Florindo[1], M. Gaeta[6], B. Giaccio[8], M. Masotta[9]

1. Istituto Nazionale di Geofisica e Vulcanologia, Via di Vigna Murata 605, 00143 Roma, Italy

2. Laboratoire des Sciences du Climat et de L'Environnement, UMR8212, IPSL-CEA-CNRS-UVSQ and Université Paris-Saclay, Domaine du CNRS Bât. 12, Avenue de la Terrasse, 91198 Gif-Sur-Yvette, France.

3. Sezione di Scienze Preistoriche e Antropologiche, Dipartimento di Studi Umanistici, Università degli Studi di Ferrara, C.so Ercole d'Este I, 32, Ferrara, Italy

4. Ecole française de Rome, Piazza Farnese, IT-00186, Roma, Italy

5. Département Hommes et environnements, Muséum national d'Histoire naturelle, UMR 7194 du CNRS, 1 rue René Panhard, 75013 Paris, France.

6. Dipartimento di Scienze della Terra, Sapienza, Università di Roma, P.le Aldo Moro 5, 00185, Roma, Italy

7. Dipartimento di Biologia, Università di Pisa, 56126 Pisa, Italy

8. Istituto di Geologia Ambientale e Geoingegneria - C.N.R., Montelibretti (Rome), Italy

9. Dipartimento di Scienze della Terra, Università di Pisa, 56126 Pisa, Italy

Supplementary online material

Methods

$^{40}Ar/^{39}Ar$ analytical procedure

After crushing and sieving about thirty transparent potassic feldspars crystals, ranging size between 500 μm and 1 mm were handpicked. Crystals were next leached with an HF acid solution (7%) to remove remaining groundmass. These potassium feldspars were then loaded in aluminium disks and irradiated in the β1 tube of the Osiris reactor, CEA Saclay (France). Different irradiations were performed for these five samples: Casal de 'Pazzi sample was irradiated 180 min in irradiation number 77 (IRR 77), Torre in Pietra-A2 in IRR 85 for 60 min and CDG 1, CDG 2 and Riano in IRR 108 for 90 min. After irradiations, samples were separately transferred in a copper sample holder and put into a double vacuum Cleartran window. Crystals were next individually fused by a 25 Watt Synrad CO_2 laser (using 10 to 15 % of the nominal power, see analytical protocol from Nomade et al., 2011). Extracted gases were purified by two GP 110 getters (ZrAl). Argon isotopes (^{36}Ar, ^{37}Ar, ^{38}Ar, ^{39}Ar, ^{40}Ar) were measured using a VG 5400 mass spectrometer equipped with a single electron multiplier (Balzers 217 SEV SEN) coupled to an ion counter. Neutron J fluence for each sample was calculating using co-irradiated Alder Creek Sanidine (ACs-2) standard with an age of 1.193 Ma (Nomade et al., 2005) (IRR 77, *J = 0.00025180 ± 0.0000126*; IRR 85; *J = 0.00038530 ± 0.0000077*; IRR 108; *J = 0,00041040 ± 0.00000226*) and the total decay constant of Steiger and Jäger (1977). Several recent calibrations of the ACs-2 standard suggest a younger absolute age ranging from 1.186 to 1.189 Ma (Jicha et al., 2016; Niespolo et al., 2017). However, the difference implied (0.3-0.6%) for the final ages obtained is here negligible, well within the full-propagated reported uncertainties. Procedural blank measurements are performed after every three or four unknown. For typical 10 min static blank, typical backgrounds are about 2.0 to 3.0 x 10^{-17} and 5.0 to 6.0 x 10^{-19} moles for ^{40}Ar and ^{36}Ar respectively. The precision and accuracy of the mass discrimination correction was monitored by weekly measurements of air argon of various beam sizes (Nomade et al., 2010) and was calculated relative to a $^{40}Ar/^{36}Ar$ ratio of 298.56 (Lee et al., 2006).

Supplementary Tables 1-5 - Full geochronological data

Sample ID: TIP-A2 Lab# N1351-01/N1351-13 J = 0.00038530 ± 0.00000077
Sanidine Irradiation # 85 reactor OSIRIS
Flux standard ACS-2 1.194 Ma Single crystal total fusion

N	^{40}Ar (moles)	^{36}Ar V	±σ$_{36}$ V	^{37}Ar V	±σ$_{37}$ V	^{38}Ar V	±σ$_{38}$ V	^{39}Ar V	±σ$_{39}$ V	^{40}Ar V	±σ$_{40}$ V	D$^{(1)}$	±%σ$_D$	%^{40}Ar*	Age (ka)	±σ (ka)	K/Ca ± 1σ
N1351-01	7,334E-15	1,611E-06	2,352E+00	1,181E-04	7,446E-01	1,150E-04	2,447E-01	7,478E-03	8,596E-02	5,353E-03	9,052E-02	1,0128E+00	7,000E-02	9,133E+01	4,545E+02	1,201E+00	9,494E+00 7,116E-02
N1351-02	5,150E-15	1,121E-06	3,640E+00	1,317E-04	7,414E-01	7,966E-05	2,703E-01	5,306E-03	8,601E-02	3,759E-03	9,091E-02	1,0125E+00	7,000E-02	9,156E+01	4,508E+02	1,687E+00	6,045E+00 4,512E-02
N1351-03	3,189E-15	1,582E-06	1,699E+00	6,107E-05	1,033E+00	5,100E-05	2,819E-01	3,310E-03	9,911E-02	2,328E-03	8,222E-02	1,0123E+00	7,000E-02	8,019E+01	3,919E+02	1,760E+00	8,131E+00 8,437E-02
N1351-04	2,211E-15	9,630E-07	2,641E+00	4,130E-05	1,241E+00	3,642E-05	4,769E-01	2,385E-03	1,066E-01	1,614E-03	8,432E-02	1,0122E+00	7,000E-02	8,263E+01	3,885E+02	2,264E+00	8,663E+00 1,079E-01
N1351-05	3,644E-15	7,482E-07	4,442E+00	5,955E-05	8,879E-01	5,682E-05	4,171E-01	3,734E-03	1,064E-01	2,660E-03	1,016E-01	1,0124E+00	7,000E-02	9,191E+01	4,550E+02	1,957E+00	9,406E+00 8,411E-02
N1351-06	3,670E-15	4,324E-06	5,644E-01	3,770E-05	1,694E+00	3,376E-05	4,872E-01	2,137E-03	1,144E-01	2,679E-03	9,162E-02	1,0123E+00	7,000E-02	5,244E+01	4,570E+02	2,533E+00	8,501E+00 1,444E-01
N1351-07	2,221E-15	3,308E-07	1,089E+01	3,797E-05	1,610E+00	3,629E-05	4,771E-01	2,325E-03	1,221E-01	1,621E-03	1,125E-01	1,0122E+00	7,000E-02	9,421E+01	4,566E+02	3,278E+00	9,183E+00 1,483E-01
N1351-08	2,074E-15	6,431E-08	5,492E+01	3,417E-05	1,376E+00	3,498E-05	2,962E-01	2,300E-03	1,390E-01	1,514E-03	1,326E-01	1,0122E+00	7,000E-02	9,897E+01	4,528E+02	3,273E+00	1,010E+01 1,396E-01
N1351-09	3,038E-15	5,585E-07	3,992E+00	4,635E-05	1,219E+00	4,748E-05	4,267E-01	3,143E-03	1,450E-01	2,218E-03	1,614E-01	1,0123E+00	7,000E-02	9,277E+01	4,549E+02	1,785E+00	1,017E+01 1,249E-01
N1351-10	1,871E-15	6,705E-07	2,902E+00	2,955E-05	1,594E+00	3,130E-05	3,392E-01	2,072E-03	1,237E-01	1,366E-03	1,136E-01	1,0122E+00	7,000E-02	8,571E+01	3,926E+02	2,056E+00	1,052E+01 1,682E-01
N1351-11	4,195E-15	1,280E-06	1,416E+00	7,809E-05	1,942E+01	4,699E-05	3,318E-01	3,134E-03	1,062E-01	3,062E-03	5,091E-02	1,0103E+00	7,000E-02	8,806E+01	5,980E+02	1,441E+00	6,020E+00 1,169E+00
N1351-12	2,144E-15	5,281E-07	2,675E+00	2,913E-05	5,571E+01	3,343E-05	5,206E-01	2,200E-03	1,140E-01	1,565E-03	1,120E-01	1,0099E+00	7,000E-02	9,042E+01	4,470E+02	1,623E+00	1,133E+01 6,312E+00
N1351-13	4,680E-15	1,284E-07	1,512E+01	1,113E-04	5,404E+01	5,244E-05	6,176E-01	3,492E-03	1,221E-01	3,416E-03	1,108E-01	1,0103E+00	7,000E-02	9,943E+01	6,760E+02	2,080E+00	4,708E+00 2,544E+00

Results	40Ar*/39Ark ± 1σ	Age ± 1σ (Ka)	MSWD	39Ar(k) (n)	K/Ca ± 1σ
Weighted mean	0,5629 ± 0,0017 ± 0,30%	391,3 ± 1,4 ± 0,36%	1,02	0,39 3	8,6 ± 0,6
		Full External Error ± 4,0	1,21	Statistical T ratio	
		Analytical Error ± 1,2	1,0108		

Results	40(a)/36(a) ± 1σ	40(r)/39(k) ± 1σ	Age ± 1σ (Ka)	MSWD
Inverse Isochron	294,6857 ± 36,5042 ± 12,39%	0,5633 ± 0,0147 ± 2,61%	391,5 ± 10,2 ± 2,62%	2,04
			Full External Error ± 10,9	
			Analytical Error ± 10,2	

Statistics				
	Statistical F ratio	0,87	Convergence	0,0028754378
	Error Magnification	1,4288	Number of Iterations	3
	Number of Data Points	3	Calculated Line	Weighted York-2

Background corrections TIP-A2

N	^{36}Ar V	±σ36 V	^{37}Ar V	±σ37 V	^{38}Ar V	±σ38 V	^{39}Ar V	±σ39 V	^{40}Ar V	±σ40 V
N1351-01	2,733E-07	2,842E-08	1,450E-07	1,494E-08	8,187E-08	1,793E-08	1,627E-06	2,033E-07	1,305E-05	3,915E-07
N1351-02	2,733E-07	2,842E-08	1,450E-07	1,494E-08	8,187E-08	1,793E-08	1,627E-06	2,033E-07	1,305E-05	3,915E-07
N1351-03	2,252E-07	1,621E-08	1,079E-07	2,697E-08	1,420E-07	2,300E-08	1,028E-06	2,066E-07	1,147E-05	4,013E-07
N1351-04	2,252E-07	1,621E-08	1,079E-07	2,697E-08	1,420E-07	2,300E-08	1,028E-06	2,066E-07	1,147E-05	4,013E-07
N1351-05	2,252E-07	1,621E-08	1,079E-07	2,697E-08	1,420E-07	2,300E-08	1,028E-06	2,066E-07	1,147E-05	4,013E-07
N1351-06	2,252E-07	1,621E-08	1,079E-07	2,697E-08	1,420E-07	2,300E-08	1,028E-06	2,066E-07	1,147E-05	4,013E-07
N1351-07	1,433E-07	3,138E-08	9,170E-08	2,072E-08	3,497E-08	2,658E-08	1,206E-07	1,193E-07	7,046E-06	3,453E-07
N1351-08	1,433E-07	3,138E-08	9,170E-08	2,072E-08	3,497E-08	2,658E-08	1,206E-07	1,193E-07	7,046E-06	3,453E-07
N1351-09	1,538E-07	1,323E-08	2,580E-08	2,554E-08	2,634E-08	2,344E-08	1,339E-06	1,326E-06	8,123E-06	3,493E-07
N1351-10	1,538E-07	1,323E-08	2,580E-08	2,554E-08	2,634E-08	2,344E-08	1,339E-06	1,326E-06	8,123E-06	3,493E-07
N1351-11	8,053E-08	7,409E-09	5,493E-08	2,104E-08	6,756E-08	7,432E-09	2,589E-07	7,094E-08	9,559E-06	2,677E-07
N1351-12	8,053E-08	7,409E-09	5,493E-08	2,104E-08	6,756E-08	7,432E-09	2,589E-07	7,094E-08	9,559E-06	2,677E-07
N1351-13	1,008E-07	1,381E-08	6,580E-08	2,106E-08	3,491E-08	1,990E-08	4,310E-07	1,552E-07	8,745E-06	3,585E-07

Table S1

Sample ID: CDG 1	Lab# N1480-01/N1480-10	J = 0.00038260 ± 0.00000027																
Sanidine		Irradiation #108		reactor	OSIRIS													
Flux standard ACS-2	1.194 Ma	Single crystal total fusion																
N	^{40}Ar	^{36}Ar	±σ$_{36}$	^{37}Ar	±σ$_{37}$	^{38}Ar	±σ$_{38}$	^{39}Ar	±σ$_{39}$	^{40}Ar	±σ$_{40}$	D$^{(1)}$	±%σ$_D$	%^{40}Ar*	Age	±σ	K/Ca	± 1σ
	(moles)	V	V	V	V	V	V	V	V	V	V				(ka)	(ka)		
N1480-01	3,691E-15	3,520E-06	9,168E-01	3,744E-05	1,012E+01	3,139E-05	5,978E-01	2,214E-03	1,222E-01	2,694E-03	9,893E-02	1,0093E+00	7,000E-02	6,111E+01	5,131E+02	3,182E+00	2,543E+01	2,573E+00
N1480-02	1,461E-15	2,608E-08	1,192E+02	2,993E-05	1,014E+01	2,338E-05	1,244E+00	1,461E-03	1,749E-01	1,066E-03	8,803E-01	1,0087E+00	7,000E-02	9,955E+01	5,016E+02	6,300E+00	2,099E+01	2,129E+00
N1480-03	1,118E-15	5,164E-07	4,204E+00	2,236E-05	1,019E+01	1,468E-05	7,140E-01	8,960E-04	2,407E-01	8,162E-04	3,513E-01	1,0086E+00	7,000E-02	8,139E+01	5,117E+02	5,600E+00	1,723E+01	1,756E+00
N1480-04	1,206E-15	3,661E-07	5,820E+00	1,856E-05	1,022E+01	2,076E-05	4,375E-01	1,035E-03	1,568E-01	8,800E-04	2,282E-01	1,0087E+00	7,000E-02	8,783E+01	5,153E+02	4,522E+00	2,398E+01	2,451E+00
N1480-06	1,286E-15	4,153E-07	7,013E+00	1,857E-05	1,022E+01	1,718E-05	9,310E-01	1,071E-03	1,842E-01	9,384E-04	1,961E-01	1,0087E+00	7,000E-02	8,698E+01	5,261E+02	5,811E+00	2,480E+01	2,535E+00
N1480-07	2,507E-15	2,647E-07	1,000E+01	2,612E-05	1,016E+01	3,623E-05	3,548E-01	2,340E-03	9,903E-02	1,830E-03	1,064E-01	1,0090E+00	7,000E-02	9,581E+01	5,170E+02	2,458E+00	3,852E+01	3,914E+00
N1480-08	1,004E-15	1,525E-07	1,723E+01	1,889E-05	1,022E+01	1,519E-05	1,111E+00	9,170E-04	2,792E-01	7,329E-04	2,764E-01	1,0086E+00	7,000E-02	9,406E+01	5,188E+02	6,268E+00	2,087E+01	2,134E+00
N1480-09	9,174E-16	4,911E-07	6,206E+00	1,891E-05	1,022E+01	1,155E-05	8,158E-01	7,040E-04	2,988E-01	6,696E-04	4,139E-01	1,0086E+00	7,000E-02	7,840E+01	5,147E+02	9,453E+00	1,601E+01	1,637E+00
N1480-10	9,604E-16	3,786E-07	5,244E+00	1,893E-05	1,022E+01	1,299E-05	5,945E-01	7,838E-04	1,751E-01	7,010E-04	2,314E-01	1,0086E+00	7,000E-02	8,416E+01	5,195E+02	5,490E+00	1,781E+01	1,821E+00

Results	40Ar*/39Ark	± 1σ	Age (Ka)	± 1σ	MSWD	39Ar(k) (n)	K/Ca	± 1σ
Weighted mean	0,8222	± 0,0012	515,6	± 1,7	1,30	0,24	20,4	± 1,6
		± 0,15%		± 0,33%		9		
			Full External Error	± 6,6	99,00	Statistical T ratio		
			Analytical Error	± 1,7	1,1412			

Results	40(a)/36(a)	± 1σ	40(r)/39(k)	± 1σ	Age (Ka)	± 1σ	MSWD
Inverse Isochron	296,2480	± 4,3944	0,7484	± 0,0034	516,5	± 2,4	1,42
		± 1,48%		± 0,46%		± 0,46%	
Full External Error						± 6,8	
Analytical Error						± 2,4	

Statistics				
	Statistical F ratio	1,12	Convergence	0,0000677750
	Error Magnification	1,1896	Number of Iterations	3
	Number of Data Points	9	Calculated Line	Weighted York-2

Background corrections CDG 1

N	^{36}Ar	±σ36	^{37}Ar	±σ37	^{38}Ar	±σ38	^{39}Ar	±σ39	^{40}Ar	±σ40
	V	V	V	V	V	V	V	V	V	V
N1480-01	2,126E-07	2,147E-08	1,000E-08	1,000E-09	1,956E-07	3,012E-08	9,876E-07	1,383E-07	4,597E-05	1,011E-06
N1480-02	2,126E-07	2,147E-08	1,000E-08	1,000E-09	1,956E-07	3,012E-08	9,876E-07	1,383E-07	4,597E-05	1,011E-06
N1480-03	1,773E-07	1,363E-08	1,000E-08	1,000E-09	5,825E-08	2,901E-08	1,907E-07	1,087E-07	3,415E-05	5,908E-07
N1480-04	1,773E-07	1,363E-08	1,000E-08	1,000E-09	5,825E-08	2,901E-08	1,907E-07	1,087E-07	3,415E-05	5,908E-07
N1480-06	1,777E-07	2,203E-08	1,000E-08	1,000E-09	2,274E-08	2,272E-08	3,811E-07	1,166E-07	3,540E-05	5,593E-07
N1480-07	1,777E-07	2,203E-08	1,000E-08	1,000E-09	2,274E-08	2,272E-08	3,811E-07	1,166E-07	3,540E-05	5,593E-07
N1480-08	1,279E-07	2,366E-08	1,000E-08	1,000E-09	1,384E-08	7,778E-09	1,517E-07	1,168E-07	3,607E-05	3,246E-07
N1480-09	1,279E-07	2,366E-08	1,000E-08	1,000E-09	1,384E-08	7,778E-09	1,517E-07	1,168E-07	3,607E-05	3,246E-07
N1480-10	1,099E-07	1,692E-08	1,000E-08	1,000E-09	1,841E-08	1,839E-08	1,888E-07	1,050E-07	3,528E-05	6,809E-07

Table S2

Sample ID: CDG 2 Lab# N1486-01/N1486-11 J = 0.00035160 ± 0.00000035
Sanidine Irradiation #108 reactor OSIRIS
Flux standard ACS-2 1.194 Ma Single crystal total fusion

N	^{40}Ar (moles)	^{36}Ar V	±σ$_{36}$ V	^{37}Ar V	±σ$_{37}$ V	^{38}Ar V	±σ$_{38}$ V	^{39}Ar V	±σ$_{39}$ V	^{40}Ar V	±σ$_{40}$ V	D[1]	±%σ$_D$	%^{40}Ar*	Age (ka)	±σ (ka)	K/Ca	± 1σ
N1486-01	1,972E-15	2,952E-07	6,996E+00	2,175E-05	5,140E+00	2,914E-05	4,257E-01	1,758E-03	1,304E-01	1,439E-03	2,292E-01	1,0088E+00	7,000E-02	9,403E+01	5,501E+02	2,933E+00	3,476E+01	1,787E+00
N1486-02	3,106E-15	2,289E-07	9,902E+00	2,173E-05	5,140E+00	4,279E-05	5,123E-01	2,844E-03	1,567E-01	2,267E-03	1,751E-01	1,0091E+00	7,000E-02	9,706E+01	5,527E+02	2,154E+00	5,629E+01	2,894E+00
N1486-03	3,069E-15	2,389E-07	8,774E+00	2,173E-05	5,140E+00	4,267E-05	5,603E-01	2,668E-03	1,143E-01	2,240E-03	9,539E-02	1,0091E+00	7,000E-02	9,690E+01	5,813E+02	1,893E+00	5,279E+01	2,714E+00
N1486-04	6,325E-15	1,026E-06	2,115E+00	6,591E-05	5,068E+00	9,055E-05	3,593E-01	5,618E-03	1,063E-01	4,617E-03	7,178E-02	1,0099E+00	7,000E-02	9,350E+01	5,490E+02	1,099E+00	3,665E+01	1,858E+00
N1486-05	4,370E-15	6,261E-06	4,308E-01	3,057E-05	5,108E+00	2,968E-05	6,092E-01	1,726E-03	1,304E-01	3,190E-03	1,340E-01	1,0094E+00	7,000E-02	4,150E+01	5,479E+02	3,841E+00	2,429E+01	1,241E+00
N1486-06	2,020E-15	3,619E-07	7,778E+00	3,062E-05	5,108E+00	2,773E-05	7,969E-01	1,768E-03	1,063E-01	1,474E-03	9,878E-02	1,0088E+00	7,000E-02	9,288E+01	5,535E+02	3,498E+00	2,482E+01	1,268E+00
N1486-07	1,751E-15	4,066E-08	6,010E+01	3,250E-05	5,109E+00	2,542E-05	4,605E-01	1,664E-03	9,223E-02	1,278E-03	7,434E-02	1,0088E+00	7,000E-02	9,930E+01	5,452E+02	3,201E+00	2,201E+01	1,125E+00
N1486-08	1,874E-15	2,862E-07	1,080E+01	3,250E-05	5,109E+00	2,763E-05	6,819E-01	1,653E-03	1,932E-01	1,368E-03	9,687E-02	1,0088E+00	7,000E-02	9,400E+01	5,558E+02	4,172E+00	2,186E+01	1,118E+00
N1486-09	1,512E-15	1,610E-07	1,603E+01	3,251E-05	5,109E+00	2,254E-05	6,853E-01	1,374E-03	1,141E-01	1,104E-03	1,191E-01	1,0087E+00	7,000E-02	9,595E+01	5,508E+02	4,115E+00	1,817E+01	9,285E-01
N1486-10	2,967E-15	6,229E-07	6,076E+00	3,247E-05	5,109E+00	4,091E-05	2,767E-01	2,517E-03	1,304E-01	2,166E-03	1,032E-01	1,0091E+00	7,000E-02	9,156E+01	5,630E+02	3,353E+00	3,332E+01	1,703E+00
N1486-11	2,257E-15	2,510E-07	1,424E+01	3,249E-05	5,109E+00	3,301E-05	5,562E-01	2,032E-03	1,390E-01	1,648E-03	1,083E-01	1,0089E+00	7,000E-02	9,565E+01	5,543E+02	3,883E+00	2,688E+01	1,374E+00

Results	40Ar*/39Ark	± 1σ	Age (Ka)	± 1σ	MSWD	39Ar(k) (n)	K/Ca	± 1σ
Weighted mean	0,7699	± 0,0012	550,1	± 2,9	1,14	0,53	24,6	± 2,5
		± 0,15%		± 0,52%		9		
			Full External Error	± 7,3	0,99	Statistical T ratio		
			Analytical Error	± 0,8				

Results	40(a)/36(a)	± 1σ	40(r)/39(k)	± 1σ	Age (Ka)	± 1σ	MSWD
Inverse Isochron	297,7071	± 1,7733	0,7701	± 0,0014	550,2	± 2,9	1,27
		± 0,60%		± 0,18%		± 0,53%	
					Full External Error	± 7,4	
					Analytical Error	± 1,0	

Statistics				
	Statistical F ratio	1,12	Convergence	1,772E-03
	Error Magnification	1,1254	Number of Iterations	3
	Number of Data Points	9	Calculated Line	Weighted York-2

Background corrections CDG 2

N	^{36}Ar V	±σ$_{36}$ V	^{37}Ar V	±σ$_{37}$ V	^{38}Ar V	±σ$_{38}$ V	^{39}Ar V	±σ$_{39}$ V	^{40}Ar V	±σ$_{40}$ V
N1486-01	1,447E-07	1,505E-08	1,000E-08	1,000E-09	6,077E-08	3,822E-08	8,670E-08	8,661E-08	3,394E-05	6,109E-07
N1486-02	1,403E-07	1,726E-08	1,000E-08	1,000E-09	2,173E-08	2,171E-08	7,540E-07	2,277E-07	4,208E-05	5,891E-07
N1486-03	1,403E-07	1,726E-08	1,000E-08	1,000E-09	2,173E-08	2,171E-08	7,540E-07	2,277E-07	4,208E-05	5,891E-07
N1486-04	1,403E-07	1,726E-08	1,000E-08	1,000E-09	2,173E-08	2,171E-08	7,540E-07	2,277E-07	4,208E-05	5,891E-07
N1486-05	1,703E-07	1,759E-08	1,000E-08	1,000E-09	4,179E-08	1,492E-08	6,934E-07	6,858E-08	3,904E-05	8,003E-07
N1486-06	9,790E-08	1,792E-08	1,000E-08	1,000E-09	2,211E-08	2,209E-08	1,222E-07	8,285E-08	3,058E-05	5,352E-07
N1486-07	1,268E-07	2,320E-08	1,000E-08	1,000E-09	2,211E-08	2,209E-08	1,222E-07	8,285E-08	3,058E-05	5,352E-07
N1486-08	1,268E-07	2,092E-08	1,000E-08	1,000E-09	3,151E-08	2,634E-08	9,785E-08	8,268E-08	3,226E-05	4,097E-07
N1486-09	1,268E-07	2,092E-08	1,000E-08	1,000E-09	3,151E-08	2,634E-08	9,785E-08	8,268E-08	3,226E-05	4,097E-07
N1486-10	1,268E-07	2,092E-08	1,000E-08	1,000E-09	3,151E-08	2,634E-08	9,785E-08	8,268E-08	3,226E-05	4,097E-07
N1486-11	1,638E-07	3,325E-08	1,000E-08	1,000E-09	6,927E-08	2,958E-08	2,531E-07	1,288E-07	3,342E-05	5,982E-07

Table S3

Sample ID: CdP	Lab# N-1460-01/1460-12	J = 0.00025180 ± 0.00000126		
Sanidine	Irradiation #77	reactor	OSIRIS	
Flux standard ACS-2	1.194 Ma	Single crystal total fusion		

N	^{40}Ar	^{36}Ar	$\pm\sigma_{36}$	^{37}Ar	$\pm\sigma_{37}$	^{38}Ar	$\pm\sigma_{38}$	^{39}Ar	$\pm\sigma_{39}$	^{40}Ar	$\pm\sigma_{40}$	D[1]	$\pm\%\sigma_D$	$\%^{40}Ar^*$	Age	$\pm\sigma$	K/Ca	$\pm 1\sigma$
N1460-01	1,833E-15	4,258E-07	3,530E+00	1,159E-05	1,673E+03	2,673E-05	6,861E-01	1,801E-03	1,721E-01	1,338E-03	1,458E-01	1,0114E+00	1,000E-01	9,068E+01	3,060E+02	5,656E+00	2,330E+01	3,900E+02
N1460-02	1,534E-15	2,576E-07	4,467E+00	1,932E-05	1,004E+03	2,085E-05	7,180E-01	1,303E-03	1,889E-01	1,120E-03	2,295E-01	1,0114E+00	1,000E-01	9,346E+01	3,647E+02	7,766E+00	1,012E+01	1,016E+02
N1460-03	1,159E-15	4,266E-07	4,905E+00	9,663E-06	2,008E+03	1,680E-05	5,017E-01	1,094E-03	1,723E-01	8,462E-04	2,539E-01	1,0113E+00	1,000E-01	8,519E+01	2,992E+02	9,460E+00	1,699E+01	3,411E+02
N1460-04	1,255E-15	4,154E-07	3,039E+00	1,160E-05	1,673E+03	1,543E-05	7,525E-01	9,707E-04	2,603E-01	9,163E-04	2,558E-01	1,0113E+00	1,000E-01	8,672E+01	3,718E+02	1,044E+01	1,256E+01	2,101E+02
N1460-05	1,475E-15	3,094E-07	6,052E+00	1,256E-05	1,545E+03	1,923E-05	5,695E-01	1,250E-03	2,238E-01	1,077E-03	1,825E-01	1,0114E+00	1,000E-01	9,165E+01	3,586E+02	8,241E+00	1,492E+01	2,305E+02
N1460-06	1,635E-15	7,166E-07	2,898E+00	8,695E-06	2,231E+03	1,993E-05	3,561E-01	1,258E-03	2,149E-01	1,194E-03	1,807E-01	1,0114E+00	1,000E-01	8,227E+01	3,545E+02	8,246E+00	2,171E+01	4,843E+02
N1460-07	1,008E-15	2,646E-07	4,574E+00	9,664E-06	2,008E+03	1,309E-05	7,142E-01	9,883E-04	1,643E-01	7,356E-04	1,641E-01	1,0113E+00	1,000E-01	8,940E+01	3,023E+02	1,017E+01	1,534E+01	3,081E+02
N1460-08	7,923E-16	3,529E-08	4,066E+01	1,450E-05	1,339E+03	1,230E-05	3,540E-01	7,207E-04	1,893E-01	5,783E-04	3,210E-01	1,0112E+00	1,000E-01	9,867E+01	3,597E+02	1,405E+01	7,456E+00	9,983E+01
N1460-09	5,851E-16	2,588E-07	5,295E+00	4,833E-06	4,016E+03	9,572E-06	7,502E-01	5,380E-04	1,804E-01	4,271E-04	2,386E-01	1,0112E+00	1,000E-01	8,228E+01	2,967E+02	1,873E+01	1,670E+01	6,706E+02
N1460-10	1,312E-15	3,212E-08	5,291E+01	9,662E-06	2,008E+03	1,965E-05	8,837E-01	1,225E-03	1,345E-01	9,580E-04	1,487E-01	1,0113E+00	1,000E-01	9,927E+01	3,526E+02	8,319E+00	1,902E+01	3,820E+02
N1460-11	8,713E-16	2,563E-08	5,051E+01	9,665E-06	2,008E+03	1,372E-05	8,261E-01	8,055E-04	1,414E-01	6,360E-04	1,368E-01	1,0112E+00	1,000E-01	9,918E+01	3,557E+02	1,249E+01	1,250E+01	2,511E+02
N1460-12	1,646E-15	2,256E-07	8,835E+00	2,898E-05	6,694E+02	2,443E-05	5,392E-01	1,566E-03	1,414E-01	1,202E-03	1,064E-01	1,0114E+00	1,000E-01	9,479E+01	3,303E+02	6,573E+00	8,108E+00	5,428E+01

Results	40Ar*/39Ark	$\pm 1\sigma$	Age (Ka)	$\pm 1\sigma$	MSWD	39Ar(k) (n)	K/Ca	$\pm 1\sigma$
Weighted mean	0,6681	± 0,0094 ± 1,41%	303,5	± 4,5 ± 1,49%	0,18	24,27 4	17,8	± 189,2
			Full External Error	± 5,9	1,10	Statistical T ratio		
			Analytical Error	± 4,3	1,0000			

Results	40(a)/36(a)	$\pm 1\sigma$		$\pm 1\sigma$	Age (Ka)	$\pm 1\sigma$	MSWD
Inverse Isochron	212,1086	± 91,6709 ± 43,22%	0,6921	± 0,0261 ± 3,77%	314,4	± 12,0 ± 3,80%	0,05
					Full External Error	± 12,6	
					Analytical Error	± 11,9	

Statistics				
	Statistical F ratio	1,05	Convergence	0,0001416069
	Error Magnification	1,0000	Number of Iterations	3
	Number of Data Points	4	Calculated Line	Weighted York-2

Background corrections CdP

N	^{36}Ar V	$\pm\sigma36$ V	^{37}Ar V	$\pm\sigma37$ V	^{38}Ar V	$\pm\sigma38$ V	^{39}Ar V	$\pm\sigma39$ V	^{40}Ar V	$\pm\sigma40$ V
N1460-01	1,835E-07	8,349E-09	1,420E-08	1,420E-12	4,836E-08	2,244E-08	6,110E-07	1,136E-07	4,221E-05	2,659E-07
N1460-02	1,835E-07	8,349E-09	1,420E-08	1,420E-12	4,836E-08	2,244E-08	6,110E-07	1,136E-07	4,221E-05	2,659E-07
N1460-03	1,835E-07	8,349E-09	1,420E-08	1,420E-12	4,836E-08	2,244E-08	6,110E-07	1,136E-07	4,221E-05	2,659E-07
N1460-04	1,531E-07	1,018E-08	1,420E-08	1,420E-12	2,647E-08	1,228E-08	3,188E-07	1,100E-07	3,348E-05	5,457E-07
N1460-05	1,531E-07	1,018E-08	1,420E-08	1,420E-12	2,647E-08	1,022E-08	3,188E-07	1,100E-07	3,348E-05	5,457E-07
N1460-06	1,531E-07	1,018E-08	1,420E-08	1,420E-12	2,647E-08	1,022E-08	3,188E-07	1,100E-07	3,348E-05	5,457E-07
N1460-07	1,531E-07	1,018E-08	1,420E-08	1,420E-12	2,647E-08	1,022E-08	3,188E-07	1,100E-07	3,348E-05	5,457E-07
N1460-08	1,531E-07	1,018E-08	1,420E-08	1,420E-12	2,647E-08	1,022E-08	3,188E-07	1,100E-07	3,348E-05	5,457E-07
N1460-09	1,639E-07	5,851E-09	1,420E-08	1,420E-12	6,061E-09	6,055E-09	4,006E-08	4,002E-08	2,931E-05	3,459E-07
N1460-10	1,639E-07	5,851E-09	1,420E-08	1,420E-12	6,061E-09	6,055E-09	4,006E-08	4,002E-08	2,931E-05	3,459E-07
N1460-11	1,639E-07	5,851E-09	1,420E-08	1,420E-12	6,061E-09	6,055E-09	4,006E-08	4,002E-08	2,931E-05	3,459E-07
N1460-12	1,639E-07	5,851E-09	1,420E-08	1,420E-12	6,061E-09	6,055E-09	4,006E-08	4,002E-08	2,931E-05	3,459E-07

Table S4

Sample ID: Riano	Lab# N-1490-01/1490-09	J = 0.00041040 ± 0.00000226	
Sanidine	Irradiation # 108	reactor	OSIRIS
Flux standard ACS-2	1.194 Ma	Single crystal total fusion	

N	^{40}Ar (moles)	^{36}Ar V	±σ$_{36}$ V	^{37}Ar V	±σ$_{37}$ V	^{38}Ar V	±σ$_{38}$ V	^{39}Ar V	±σ$_{39}$ V	^{40}Ar V	±σ$_{40}$ V	D$^{(1)}$	±%σ$_D$	%^{40}Ar*	Age (ka)	±σ (ka)	K/Ca ± 1σ	
N1490-01	2,128E-15	2,877E-07	6,407E+00	3,176E-05	2,068E+01	4,845E-05	4,354E-01	2,727E-03	1,477E-01	1,553E-03	1,240E-01	1,0090E+00	7,000E-02	9,471E+01	4,066E+02	1,735E+00	3,692E+01	7,637E+00
N1490-02	4,093E-15	3,332E-06	1,120E+00	3,172E-05	2,068E+01	6,378E-05	3,415E-01	3,703E-03	1,304E-01	2,987E-03	1,121E-01	1,0095E+00	7,000E-02	6,682E+01	4,064E+02	2,434E+00	5,020E+01	1,038E+01
N1490-03	1,491E-15	9,435E-07	1,854E+00	3,179E-05	2,068E+01	2,011E-05	7,012E-01	1,496E-03	1,840E-01	1,089E-03	1,490E-01	1,0087E+00	7,000E-02	7,439E+01	4,081E+02	2,883E+00	2,024E+01	4,186E+00
N1490-04	1,912E-15	3,745E-08	1,375E+02	2,776E-05	2,079E+01	3,890E-05	4,542E-01	2,601E-03	1,839E-01	1,395E-03	1,966E-01	1,0089E+00	7,000E-02	9,938E+01	4,019E+02	4,592E+00	4,030E+01	8,376E+00
N1490-05	1,810E-15	5,454E-08	1,039E+02	3,177E-05	2,068E+01	3,873E-05	4,542E-01	2,424E-03	2,025E-01	1,321E-03	1,872E-01	1,0089E+00	7,000E-02	9,901E+01	4,069E+02	5,386E+00	3,280E+01	6,785E+00
N1490-06	4,675E-15	1,824E-07	2,190E+01	6,574E-05	2,034E+01	9,994E-05	2,292E-01	6,270E-03	8,062E-02	3,413E-03	9,378E-02	1,0096E+00	7,000E-02	9,859E+01	4,046E+02	1,534E+00	4,101E+01	8,341E+00
N1490-07	4,840E-15	4,868E-07	5,820E+00	4,903E-05	2,045E+01	9,632E-05	2,963E-01	6,288E-03	8,603E-02	3,533E-03	8,375E-02	1,0097E+00	7,000E-02	9,600E+01	4,066E+02	1,143E+00	5,515E+01	1,128E+01
N1490-08	3,427E-15	1,094E-07	4,032E+01	9,924E-05	2,023E+01	7,364E-05	4,247E-01	4,594E-03	1,304E-01	2,501E-03	1,539E-01	1,0093E+00	7,000E-02	9,912E+01	4,069E+02	2,344E+00	1,990E+01	4,026E+00
N1490-09	3,025E-15	8,865E-07	3,862E+00	3,238E-05	2,068E+01	5,572E-05	5,979E-01	3,602E-03	1,140E-01	2,208E-03	1,151E-01	1,0092E+00	7,000E-02	8,815E+01	4,075E+02	2,261E+00	4,783E+01	9,894E+00

Results	40Ar*/39Ark ± 1σ	Age ± 1σ (Ka)	MSWD	39Ar(k) (n)	K/Ca ± 1σ
Weighted mean	0,5389 ± 0,0009 ± 0,16%	406,3 ± 2,3 ± 0,57%	0,38	100,00 9	29,4 ± 4,0
		Full External Error ± 5,5	0,99	Statistical T ratio	
		Analytical Error ± 0,7	1,0000		

Results	40(a)/36(a) ± 1σ	± 1σ	Age ± 1σ (Ka)	MSWD
Inverse Isochron	300,7981 ± 3,5867 ± 1,19%	0,5386 ± 0,0011 ± 0,20%	406,0 ± 2,4 ± 0,58%	0,38
Full External Error			± 5,5	
Analytical Error			± 0,8	

Statistics				
	Statistical F ratio	1,12	Convergence	0,0006042070
	Error Magnification	1,0000	Number of Iterations	3
	Number of Data Points	9	Calculated Line	Weighted York-2

Background corrections Riano

N	^{36}Ar V	±σ36 V	^{37}Ar V	±σ37 V	^{38}Ar V	±σ38 V	^{39}Ar V	±σ39 V	^{40}Ar V	±σ40 V
N1490-01	1,041E-07	8,640E-09	1,282E-08	2,564E-09	6,905E-08	1,823E-08	7,846E-07	1,232E-07	2,787E-05	3,344E-07
N1490-02	7,228E-08	2,515E-09	1,282E-08	2,564E-09	3,024E-08	1,872E-08	4,287E-07	1,305E-07	3,558E-05	3,914E-07
N1490-03	7,228E-08	2,515E-09	1,282E-08	2,564E-09	3,024E-08	1,872E-08	4,287E-07	1,305E-07	3,558E-05	3,914E-07
N1490-04	1,108E-07	5,152E-08	1,282E-08	2,564E-09	8,729E-08	1,222E-08	7,731E-07	7,576E-08	2,492E-05	4,959E-07
N1490-05	1,108E-07	5,152E-08	1,282E-08	2,564E-09	8,729E-08	1,222E-08	7,731E-07	7,576E-08	2,492E-05	4,959E-07
N1490-06	1,430E-07	1,959E-08	1,282E-08	2,564E-09	2,730E-08	2,340E-08	2,224E-06	2,602E-07	4,250E-05	7,565E-07
N1490-07	1,430E-07	1,959E-08	1,282E-08	2,564E-09	2,730E-08	2,340E-08	2,224E-06	2,602E-07	4,250E-05	7,565E-07
N1490-08	1,122E-07	2,492E-08	1,282E-08	2,564E-09	5,086E-08	1,744E-08	2,088E-06	8,707E-08	2,961E-05	6,337E-07
N1490-09	1,122E-07	2,492E-08	1,282E-08	2,564E-09	5,086E-08	1,744E-08	2,088E-06	8,707E-08	2,961E-05	6,337E-07

Table S5

Microprobe analyses

Microchemical analyses of six samples have been obtained at the Istituto Nazionale di Geofisica e Vulcanologia (INGV) in Rome (Italy) using a JEOL-JXA8200 electron probe microanalyser equipped with five spectrometers. Glasses were analysed using 15 kV accelerating voltage and 10 nA beam current, with a defocused electron beam of 5 μm and a counting time of 10 s on background and 20 s on peak. The following standards were adopted: jadeite (Si and Na), labradorite (Al and Ca), forsterite (Mg), andradite (Fe), rutile (Ti), orthoclase (K), barite (Ba), apatite (P) and spessartine (Mn). Sodium and potassium were analysed first to prevent alkali migration effects. The precision of the microprobe was measured through the analysis of well-characterized synthetic oxides and minerals. Data quality was ensured by analysing standard materials as unknowns. Based on counting statistics, analytical precision was better than 5% for all cations.

Sample POL 12-03 is part of the same material sampled under authorization by *Soprintendenza del Lazio e dell'Etruria Meridionale* for the $^{40}Ar/^{39}Ar$ dating at La Polledrara by Pereira et al. (2017).

Supplementary Table 6 - EMP glass analyses

SAMPLE	Comment	SiO2	TiO2	Al2O3	FeO	MnO	MgO	CaO	Na2O	K2O	P2O5	Total
BOT-1	bot1-gl1	59,03	0,44	18,95	2,48	0,17	0,36	2,66	3,62	9,99	0,07	97,78
	bot1-gl2	59,12	0,43	18,71	2,51	0,09	0,32	2,46	3,54	9,96	0,12	97,26
	bot1-gl3	58,67	0,48	18,97	2,65	0,17	0,37	2,60	3,44	9,83	0,05	97,23
	bot1-gl4	59,82	0,49	18,80	2,43	0,21	0,40	2,56	3,68	9,87	0,11	98,37
	bot1-gl5	59,06	0,56	18,63	2,54	0,18	0,36	2,52	3,70	9,97	0,08	97,60
	bot1-gl6	58,81	0,41	19,09	2,59	0,14	0,38	2,30	3,66	9,97	0,07	97,43
	bot1-gl7	59,35	0,46	18,94	2,28	0,05	0,34	2,59	3,58	9,75	0,06	97,40
	bot1-gl8	59,12	0,48	18,91	2,53	0,15	0,39	2,28	3,65	10,02	0,11	97,64
	bot1-gl9	58,80	0,44	19,22	2,60	0,15	0,40	2,37	3,84	9,91	0,05	97,80
	bot1-gl10	59,06	0,53	18,74	2,73	0,19	0,29	2,63	3,71	9,94	0,06	97,89
	bot1-gl11	59,17	0,57	19,20	2,70	0,15	0,43	2,66	3,73	9,78	0,14	98,54
	bot1-gl12	59,12	0,42	19,18	2,59	0,12	0,42	2,49	3,78	9,86	0,08	98,06
	bot1-gl13	59,45	0,50	19,12	2,66	0,15	0,36	2,61	3,59	10,11	0,00	98,55
	bot1-gl14	59,14	0,50	18,85	2,38	0,15	0,40	2,52	3,62	9,85	0,02	97,43
	bot1-gl15	59,79	0,38	18,84	2,76	0,14	0,39	2,58	3,61	9,78	0,07	98,34
	bot1-gl16	58,84	0,41	18,73	2,41	0,15	0,35	2,40	3,60	9,98	0,08	96,96
	bot1-gl17	58,82	0,51	19,00	2,52	0,11	0,40	2,48	3,65	9,88	0,02	97,40
	bot1-gl18	58,14	0,57	18,37	2,52	0,11	0,40	2,73	3,45	9,57	0,14	96,00
	bot1-gl19	59,45	0,52	18,97	2,45	0,16	0,32	2,60	3,56	9,94	0,07	98,05
	bot1-gl20	58,72	0,36	19,22	2,61	0,10	0,36	2,73	3,34	9,63	0,03	97,11
	bot1-gl21	58,31	0,51	18,70	2,64	0,18	0,45	2,35	3,44	10,12	0,04	96,74
	bot1-gl22	58,25	0,52	18,64	2,45	0,11	0,44	2,43	3,59	9,62	0,01	96,06
	bot1-gl23	59,37	0,40	19,17	2,74	0,20	0,35	2,49	3,65	9,98	0,04	98,40
	bot1-gl24	59,20	0,41	18,70	2,68	0,08	0,45	2,49	3,52	9,93	0,05	97,50
	bot1-gl25	59,47	0,37	19,03	2,41	0,14	0,37	2,52	3,58	9,92	0,06	97,87
	bot1-gl26	58,76	0,45	19,06	2,72	0,13	0,36	2,55	3,44	9,74	0,02	97,22
	bot1-gl27	59,50	0,41	19,02	2,70	0,08	0,36	2,52	3,58	10,12	0,03	98,31
	bot1-gl28	59,49	0,33	19,21	2,32	0,11	0,44	2,48	3,59	9,94	0,01	97,91
	bot1-gl29	59,30	0,44	18,56	2,56	0,16	0,40	2,66	3,57	9,84	0,08	97,57
	bot1-gl30	59,05	0,53	18,80	2,30	0,18	0,34	2,36	3,42	9,68	0,04	96,70
	bot1-gl31	59,43	0,48	18,99	2,50	0,14	0,41	2,59	3,67	9,89	0,05	98,15
	bot1-gl32	59,89	0,57	19,12	2,56	0,16	0,38	2,50	3,73	9,64	0,08	98,63
	bot1-gl33	59,22	0,41	18,88	2,53	0,21	0,40	2,23	3,69	10,17	0,07	97,81
	bot1-gl34	59,60	0,49	19,08	2,65	0,13	0,39	2,52	3,65	10,04	0,09	98,63
	bot1-gl35	60,29	0,37	18,94	2,67	0,17	0,39	2,48	3,72	9,85	0,04	98,92
	bot1-gl36	58,29	0,48	18,72	2,31	0,16	0,33	2,67	3,49	9,99	0,01	96,45
	bot1-gl37	59,40	0,45	19,00	2,71	0,10	0,40	2,44	3,55	9,81	0,09	97,94
	bot1-gl38	59,33	0,37	18,85	2,29	0,12	0,44	2,38	3,85	9,82	0,05	97,51
	bot1-gl39	58,81	0,49	19,00	2,67	0,09	0,38	2,35	3,54	9,79	0,01	97,14
	bot1-gl40	58,72	0,44	18,62	2,18	0,13	0,36	2,79	3,65	9,77	0,03	96,70
	Average	***59,13***	***0,46***	***18,91***	***2,54***	***0,14***	***0,38***	***2,51***	***3,61***	***9,88***	***0,06***	***97,62***
	St.Dev	***0,46***	***0,06***	***0,21***	***0,15***	***0,04***	***0,04***	***0,13***	***0,11***	***0,14***	***0,04***	***0,70***

SAMPLE	Comment	SiO2	TiO2	Al2O3	FeO	MnO	MgO	CaO	Na2O	K2O	P2O5	Total
CDG-36	cdg-gl1	58,52	0,45	18,51	2,83	0,18	0,46	2,61	3,60	9,91	0,02	97,09
	cdg-gl2	58,79	0,40	18,26	2,29	0,15	0,35	2,35	3,60	9,79	0,05	96,02
	cdg-gl3	59,34	0,51	18,87	2,44	0,10	0,37	2,49	3,63	10,02	0,04	97,81
	cdg-gl4	58,97	0,45	18,69	2,36	0,18	0,37	2,55	3,32	9,67	0,08	96,65
	cdg-gl5	59,67	0,38	18,81	2,65	0,16	0,37	2,53	3,59	9,87	0,06	98,09
	cdg-gl7	59,25	0,51	19,11	2,64	0,14	0,35	2,66	3,58	9,82	0,07	98,14
	cdg-gl8	60,35	0,34	18,91	2,41	0,17	0,38	2,40	3,73	9,71	0,05	98,44
	cdg-gl9	58,11	0,36	18,62	2,61	0,08	0,35	2,57	3,73	10,00	0,01	96,44
	cdg-gl10	59,13	0,43	19,10	2,62	0,10	0,39	2,45	3,81	9,62	0,06	97,71
	cdg-gl11	59,28	0,52	18,90	2,62	0,07	0,37	2,44	3,60	9,88	0,03	97,71
	cdg-gl12	59,20	0,52	18,64	2,52	0,09	0,31	2,71	3,53	10,06	0,01	97,60
	cdg-gl13	59,08	0,51	18,93	2,70	0,12	0,42	2,61	3,75	9,76	0,06	97,94
	cdg-gl14	58,48	0,45	18,54	3,07	0,14	0,38	2,32	3,71	9,89	0,04	97,03
	cdg-gl15	59,03	0,34	19,02	2,53	0,11	0,41	2,60	3,52	10,08	0,10	97,74
	cdg-gl16	58,78	0,45	18,44	2,67	0,13	0,43	2,61	3,68	9,91	0,08	97,18
	cdg-gl17	58,70	0,53	18,79	2,51	0,14	0,31	2,63	3,69	10,13	0,04	97,47
	cdg-gl18	59,67	0,38	18,80	2,60	0,12	0,35	2,60	3,83	9,92	0,09	98,37
	cdg-gl19	58,41	0,48	18,78	2,73	0,19	0,42	2,88	3,42	9,93	0,08	97,32
	cdg-gl20	59,05	0,36	18,48	2,35	0,10	0,40	2,46	3,59	10,08	0,06	96,93
	cdg-gl21	58,78	0,44	18,79	2,60	0,18	0,41	2,47	3,28	9,94	0,03	96,92
	cdg-gl22	58,62	0,48	18,73	2,62	0,12	0,38	2,51	3,53	10,19	0,04	97,21
	cdg-gl23	59,18	0,47	19,26	2,60	0,11	0,41	2,44	3,64	9,98	0,06	98,15
	cdg-gl24	59,08	0,38	18,60	2,47	0,11	0,39	2,42	3,40	10,20	0,04	97,10
	cdg-gl25	59,34	0,41	18,90	2,66	0,10	0,39	2,64	3,67	9,81	0,06	97,98
	cdg-gl26	58,13	0,33	18,50	2,60	0,08	0,31	2,47	3,66	9,94	0,04	96,07
	cdg-gl27	59,57	0,47	18,89	2,66	0,15	0,43	2,67	3,74	9,51	0,09	98,18
	cdg-gl28	58,81	0,47	18,77	2,47	0,12	0,41	2,51	3,72	9,72	0,05	97,05
	cdg-gl29	59,01	0,57	18,89	2,59	0,15	0,37	2,41	3,78	9,86	0,01	97,64
	cdg-gl30	59,31	0,58	19,06	2,65	0,16	0,35	2,51	3,67	9,86	0,02	98,17
	cdg-gl31	58,57	0,47	18,71	2,42	0,10	0,36	2,56	3,41	9,74	0,06	96,39
	cdg-gl32	58,62	0,41	18,55	3,14	0,09	0,48	2,92	3,49	9,68	0,12	97,50
	cdg-gl33	59,34	0,43	18,73	2,38	0,12	0,37	2,48	3,51	10,08	0,07	97,50
	cdg-gl34	59,31	0,40	18,76	2,49	0,18	0,38	2,44	3,69	9,98	0,09	97,72
	cdg-gl35	58,33	0,54	18,62	2,70	0,14	0,45	2,85	3,66	9,41	0,07	96,77
	cdg-gl36	59,59	0,31	18,87	2,57	0,14	0,36	2,42	3,63	9,73	0,07	97,70
	cdg-gl37	59,21	0,28	18,82	2,40	0,12	0,42	2,59	3,65	9,84	0,04	97,36
	cdg-gl38	59,28	0,52	18,65	2,48	0,13	0,48	2,55	3,81	10,07	0,07	98,04
	cdg-gl39	59,20	0,40	18,96	2,63	0,08	0,41	2,32	3,57	9,47	0,01	97,05
	cdg-gl40	58,24	0,47	18,74	2,62	0,14	0,40	2,54	3,61	9,65	0,04	96,45
	cdg-gl41	59,30	0,43	18,94	2,62	0,10	0,33	2,57	3,61	9,73	0,08	97,71
	Average	***59,02***	***0,44***	***18,77***	***2,59***	***0,13***	***0,39***	***2,54***	***3,62***	***9,86***	***0,06***	***97,41***
	St.Dev	***0,47***	***0,07***	***0,20***	***0,17***	***0,03***	***0,04***	***0,14***	***0,13***	***0,19***	***0,03***	***0,63***

SAMPLE	Comment	SiO2	TiO2	Al2O3	FeO	MnO	MgO	CaO	Na2O	K2O	P2O5	Total
CDG-S1	cdg-s1-gl1	70,18	0,08	13,91	1,22	0,11	0,06	0,92	2,50	6,75	0,01	95,75
	cdg-s1-gl3	68,77	0,19	14,59	1,39	0,05	0,05	1,18	3,04	6,24	0,01	95,51
	cdg-s1-gl4	71,15	-	13,77	1,18	0,05	0,02	0,91	2,84	6,05	0,00	95,97
	cdg-s1-gl5	70,58	0,12	13,55	1,16	0,08	0,07	0,85	2,81	6,03	0,00	95,24
	cdg-s1-gl6	70,03	0,16	13,77	1,15	0,14	0,06	0,87	3,00	5,83	0,00	95,01
	cdg-s1-gl7	71,00	0,08	13,82	1,27	0,10	0,06	1,00	2,83	5,93	0,00	96,10
	cdg-s1-gl10	71,59	0,11	13,82	1,27	0,15	0,11	0,98	1,81	6,27	0,02	96,13
	cdg-s1-gl11	69,81	0,12	13,44	1,20	0,13	0,06	0,89	2,76	6,31	0,00	94,72
	cdg-s1-gl12	70,59	0,21	13,71	1,25	0,12	0,11	0,95	2,63	6,17	0,05	95,79
	cdg-s1-gl13	70,93	0,23	13,57	1,23	0,07	0,06	0,87	2,82	6,45	0,00	96,23
	cdg-s1-gl14	71,65	0,05	13,82	1,22	0,17	0,07	0,92	2,85	6,02	0,00	96,78
	cdg-s1-gl15	70,15	0,18	13,62	1,29	0,14	0,09	0,96	2,93	5,91	0,00	95,26
	cdg-s1-gl16	69,81	0,09	13,61	1,22	0,04	0,02	1,06	2,83	6,08	0,06	94,82
	cdg-s1-gl17	69,95	0,15	13,56	1,33	0,06	0,07	0,89	2,61	5,68	0,00	94,31
	cdg-s1-gl18	69,69	0,20	13,34	1,20	0,11	0,07	0,87	2,38	5,94	0,01	93,82
	cdg-s1-gl19	70,02	0,11	13,65	1,18	0,00	0,05	0,94	2,41	6,32	0,01	94,69
	cdg-s1-gl20	70,13	0,13	13,36	1,21	0,06	0,09	1,03	2,54	6,04	0,01	94,60
	cdg-s1-gl21	69,43	0,04	13,37	1,17	0,09	0,11	0,97	2,28	6,20	0,00	93,66
	cdg-s1-gl22	69,65	0,13	13,74	1,21	0,14	0,06	0,87	2,35	6,30	0,06	94,51
	cdg-s1-gl25	70,06	0,08	13,50	1,16	0,07	0,05	0,82	2,41	6,01	0,04	94,19
	Average	***70,26***	***0,13***	***13,68***	***1,23***	***0,09***	***0,07***	***0,94***	***2,63***	***6,13***	***0,01***	***95,15***
	St.Dev	***0,73***	***0,05***	***0,27***	***0,06***	***0,04***	***0,03***	***0,09***	***0,30***	***0,24***	***0,02***	***0,86***

Sample		SiO_2	TiO_2	Al_2O_3	FeO*	MgO	MnO	CaO	Na_2O	K_2O	P_2O_5	Total
CDG 36	gl_1	56,01	0,40	17,08	3,07	0,63	0,13	2,70	2,55	9,27	0,14	91,98
	gl_2	56,30	0,43	16,98	3,21	0,72	0,15	3,03	2,78	9,75	0,09	93,44
	gl_4	57,81	0,52	17,29	3,14	0,60	0,15	3,18	2,55	9,80	0,19	95,23
	gl_5	57,34	0,44	16,71	3,23	0,60	0,15	2,96	2,78	9,40	0,16	93,77
	gl_7	55,73	0,44	16,73	3,06	0,62	0,14	3,10	2,73	9,60	0,07	92,22
	gl_9	56,65	0,36	17,06	2,76	0,46	0,13	2,53	2,86	10,27	0,09	93,16
	gl_11	57,12	0,52	17,22	2,82	0,62	0,15	2,90	2,84	10,02	0,13	94,32
	gl_12	56,06	0,44	17,02	3,13	0,66	0,12	2,88	3,07	9,98	0,10	93,46
	gl_14	56,95	0,50	17,07	2,98	0,59	0,07	2,74	2,91	9,90	0,11	93,82
	gl_16	55,95	0,45	16,63	3,13	0,52	0,10	2,79	1,89	9,64	0,12	91,22
	gl_19	57,50	0,53	17,16	2,93	0,44	0,12	2,53	2,71	9,84	0,08	93,84
	gl_20	57,06	0,55	17,41	2,93	0,59	0,18	2,70	2,70	10,07	0,12	94,31
	gl_21	57,48	0,47	17,07	2,87	0,39	0,09	2,54	2,99	9,84	0,10	93,83
	gl_22	56,27	0,39	16,97	3,11	0,55	0,13	2,86	2,87	9,63	0,06	92,84
	gl_23	55,69	0,51	16,62	2,90	0,56	0,11	3,00	2,36	9,20	0,03	90,98
	gl_24	55,58	0,59	16,85	3,38	0,56	0,09	2,75	2,63	9,20	0,07	91,69
	AVE	***56,59***	***0,47***	***16,99***	***3,04***	***0,57***	***0,12***	***2,82***	***2,70***	***9,71***	***0,10***	***93,13***
	std	***0,73***	***0,06***	***0,23***	***0,17***	***0,09***	***0,03***	***0,20***	***0,28***	***0,32***	***0,04***	***1,21***

Trace-element analyses

Ten bulk samples collected at the investigated geologic sections were analyzed for major and trace element composition during four different laboratory runs at Activation Laboratories, Canada by Lithium Metaborate/Tetraborate Fusion ICP-MS. The fused samples were diluted and analyzed by Perkin Elmer Sciex ELAN 6000, 6100 or 9000 ICP/MS. Three blanks and five controls (three before the sample group and two after) were analyzed for each group of samples. Wet chemical techniques were used to measure the loss on ignition (LOI) at 900°C. International rock standards have been used for calibration and the precision is better than 5% for Rb and Sr, 10% for Ni, Zr, Nb, Ba, Ce, and La, and 15% for the other elements.
Full data are reported in Supplementary Dataset #1.

Reference list:

Jicha, Brian R., Singer, B.S., Sobol P. (2016). Re-evaluation of the ages of 40Ar/39Ar sanidine standards and supereruptions in the western U.S. using a Noblesse multi-collector mass spectrometer. Chemical Geology 431, 54-66.

Lee, J.Y., Marti, K., Severinghaus, J.P., Kawamura, K., Hee-–Soo, Y., Lee, J.B., Kim, J.S., 2006. A redetermination of the isotopic abundances of atmospheric Ar. Geochimica et Cosmochimica Acta 70, 4507-4512. doi:10.1016/j.gca.2006.06.1563.

Niespolo E., Rutt. D., Deino A.L., Renne P.R., (2017). Intercalibration and age of the Alder Creek sanidine 40Ar/39Ar standard. Quaternary Geochronology, 39, 205-213.

Nomade, S., Renne, P.R., Vogel, N., Deino, A.L., Sharp, W.D., Becker, T.A., Jaouni, A.R., Mundil, R., (2005). Alder Creek sanidine (ACs-2), A Quaternary 40Ar/39Ar dating standard tied to the Cobb Mountain geomagnetic event. Chemical Geology 218, 315–338.

Nomade S., Gauthier A., Guillou H., Pastre J-F., (2010). 40Ar/39Ar temporal framework for the Alleret maar lacustrine sequence (French Massif-Central): Volcanological and paleoclimatic implications. Quaternary Geochronology 5, 20-27.

Nomade S., Muttoni G., Guillou H., Robin E., Scardia G., (2011) First 40Ar/39Ar age of the Ceprano man (central Italy). Quaternary Geochronology 6, 453-457.

Pereira, A., Nomade, S., Falguères, C., Bahain, J-J., Tombret, O., Garcia, T., Voinchet, P., Bulgarelli, A.G., Anzidei, P., 2017. 40Ar/39Ar and ESR/U-series data for the La Polledrara di Cecanibbio archaeological site (Lazio, Italy). Journal of Archaeological Science: Reports, in press.

Steiger, R.H., Jäger, E., (1977). Subcommission on geochronology: convention on the use of decay constants in geo- and cosmochronology. Earth and Planetary Science Letters 36, 359-362